

UNIVERSIDAD DE BARCELONA

FACULTAD DE MEDICINA

DEPARTAMENTO DE OBSTETRICIA Y GINECOLOGÍA, PEDIATRÍA,  
RADIOLOGÍA Y MEDICINA FÍSICA

PROGRAMA DE DOCTORADO DE RADIOLOGÍA DIAGNÓSTICA Y  
TERAPEÚTICA. BIENIO 1997-1999.

**ESPECTROSCOPIA POR RESONANCIA MAGNÉTICA  
DE PROTÓN EN EL DIAGNÓSTICO DE TUMORES  
CEREBRALES**

PARA OPTAR AL TÍTULO DE DOCTOR EN MEDICINA Y CIRUGÍA

D. CARLOS MAJÓS TORRÓ

DIRECTORES:

DR. JAUME GILI PLANAS

DR. JULI ALONSO FARRÉ

DR. JOSEP MARÍA MERCADER SOBREQUÉS



## **AGRADECIMIENTOS**

Querría expresar mi agradecimiento a todas las personas que me han ayudado a elaborar esta tesis.

Al personal del “Hospital Universitari de Bellvitge” que de alguna manera se ha visto implicado en esta tesis, y en particular al personal del “Institut del Diagnòstic per la Imatge” (IDI), porque un trabajo como el actual requiere de la colaboración, muchas veces imperceptible e inconsciente, de multitud de profesionales empleados en los más diversos campos. En especial al Dr Carlos Aguilera y a la Dra Marta Serrallonga, jefe de servicio y compañera del IDI, respectivamente, que han compartido conmigo el día a día de este trabajo aportando buenas dosis de ilusión y apoyo, y al Dr Juan José Acebes, jefe del servicio de neurocirugía, por haber confiado en la espectroscopia, en muchas ocasiones más que uno mismo, y haber alimentado la importancia de este estudio.

Al personal del departamento de Bioquímica de la Universidad Autónoma de Barcelona por haber compartido sus amplios conocimientos y por su imprescindible ayuda para entender el terreno en que estaba trabajando. En especial al Dr. Carles Arús, por su rigor científico y por guiarme en el campo del trabajo científico universitario y la colaboración interdisciplinaria nacional e internacional.

A los directores de esta tesis (Doctores Jaume Gili, Juli Alonso i Josep María Mercader). Por orientarme en un campo a veces difícil y confuso, por su alta perspectiva y por apoyar en todo momento la evolución de la investigación.

A todos los que me han ayudado y que no he sido capaz de recordar en estos agradecimientos. Por el doble mérito de ayudarme pasando desapercibidos.

En especial a Maica y a Júlia, por compartir el día a día, por sus dosis de ilusión y apoyo, por su imprescindible ayuda, por sus sabios consejos (sobretodo de Maica, claro) y por hacer que merezca la pena.

También a mis padres, porque han tenido mucho que ver en todo esto.

## **ABREVIATURAS**

AA.	Astrocitoma Anaplásico
ABG.	Astrocitoma de Bajo Grado
Ac.	Acetato
Ala.	Alanina
AP.	Anatomía patológica
B.	Campo magnético
B <sub>ext.</sub>	Campo magnético externo
B <sub>local.</sub>	Campo magnético local
Cho.	Colina
Cr.	Creatina
ERM.	Espectroscopia por Resonancia Magnética
ERM <sup>1</sup> H.	Espectroscopia por Resonancia Magnética de Protón
FID.	“Free Induction Decay”
f <sub>p</sub> .	Frecuencia de precesión
Glu.	Glucosa
Glx.	Glutamina-glutamato
Gly.	Glicina
IRM.	Imagen por Resonancia Magnética
Lact.	Lactato
LDA.	“Linear Discriminant Analysis”
Lip.	Lípidos
Lip 0.9.	Componente de los lípidos debido al grupo metil
Lip 1.3.	Componente de los lípidos debido al grupo metíleno
ml.	Myo-inositol
NAA.	N-acetil aspartato
NACC.	Compuestos que contienen el grupo N-acetilo
ppm.	partes por millón
PRESS.	“Point Resolved Spectroscopic Sequence”
RM.	Resonancia Magnética
sl.	Escilo-inositol
SNC.	Sistema Nervioso Central
Succ.	Succinato
Tau.	Taurina
TE.	Tiempo de eco
TF.	Transformada de Fourier
TNEP.	Tumores Neuroectodérmicos Primitivos
TR.	Tiempo de repetición
TSP.	3-trimetilsilil[2,2,3,3- <sup>2</sup> H]propionato sódico
σ.	Constante de apantallamiento
γ.	Constante giromagnética

## **ÍNDICE DE MATERIAS**

1. Introducción	1
1.1. Bases biofísicas y bioquímicas de la ERM $^1\text{H}$	3
1.1.1. Biofísica	4
1.1.1.1. Bases biofísicas. Ley de Larmor. Constante de apantallamiento. Desplazamiento químico	4
1.1.1.2. Resumiendo las bases físicas	10
1.1.1.3. Algunos aspectos adicionales a tener en cuenta	10
1.1.1.3.1. Selección del área a estudiar	10
1.1.1.3.2. Homogeneización del área a estudiar	10
1.1.1.3.3. Supresión de la señal del agua	12
1.1.1.3.4. Obtención del espectro del voxel seleccionado. Constitución del espectro	12
1.1.1.3.5. Influencia del tiempo de eco sobre el espectro	14
1.1.1.3.6. Secuencias de voxel único frente a secuencias multivoxel	17
1.1.1.4. Procesamiento de los espectros de esta tesis	18
1.1.2. Metabolitos presentes en los espectros de tumores	18
1.2. ERM $^1\text{H}$ en el estudio de tumores cerebrales	23
1.2.1. Antecedentes	23
1.2.2. Interés de la ERM $^1\text{H}$ en el diagnóstico de tumores cerebrales	23
1.2.3. Limitaciones en la correlación entre ERM $^1\text{H}$ y anatomía patológica	24
1.2.4. Diferenciación parénquima cerebral normal / tumor	28
1.2.5. Tumores gliales. Diferenciación del grado tumoral	31
1.2.5.1. Incremento de los compuestos derivados de la colina con el grado tumoral	31

1.2.5.2. Papel del lactato en la gradación de tumores	32
1.2.5.3. Papel de los lípidos en la gradación de tumores	33
1.2.5.4. Papel del Myo-Inositol y la glicina en la gradación de tumores	33
1.2.6. Meningiomas	36
1.2.6.1. N-Acetyl Aspartato y otros compuestos N-acetilados en meningiomas	37
1.2.6.2. Compuestos derivados de la colina y creatina-fosfocreatina en meningiomas	37
1.2.6.3. Lactato y alanina en meningiomas	38
1.2.6.4. Glutamina y glutamato en meningiomas	39
1.2.7. Metástasis	39
1.2.8. Tumor Neuroectodérmico Primitivo	42
 2. Hipótesis de trabajo. Objetivos	43
2.1. Hipótesis de trabajo. Interés de la tesis	45
2.2. Objetivos generales	47
2.3. Objetivos específicos	48
 3. Material y métodos	51
3.1. Pacientes	53
3.2. Espectroscopia por Resonancia Magnética de Protón	54
3.3. Análisis estadístico	56
3.4. Método para la clasificación de los tumores	57
3.5. Comprobación de resultados	58
 4. Trabajos publicados	59
4.1. Trabajo 1: Proton Magnetic Resonance Spectroscopy ( $^1\text{H}$ MRS) of human brain tumours: assessment of differences between tumour types and its applicability in brain tumour categorization.	

Majós C, Alonso J, Aguilera C, Serrallonga M, Pérez-Martín J, Acebes JJ, Arús C, Gili J. Eur Radiol 2003; 13: 582-591	61
4.2. Trabajo 2: Adult primitive neuroectodermal tumor: Proton MR Spectroscopic findings with possible application for differential diagnosis. Majós C, Alonso J, Aguilera C, Serrallonga M, Acebes JJ, Arús C, Gili J. Radiology 2002; 225: 556-566	73
4.3. Trabajo 3: Utility of proton MR spectroscopy in the diagnosis of radiologically atypical intracranial meningiomas. Majós C, Alonso J, Aguilera C, Serrallonga M, Coll S, Acebes JJ, Arús C, Gili J. Neuroradiology 2003; 45: 129-136	87
<b>5. Resumen de los trabajos y discusión global</b>	<b>97</b>
5.1. Aspectos de los apartados de material y métodos de los artículos de trascendencia para valorar los resultados	99
5.2. Discusión global de los tres artículos	103
<b>6. Conclusiones</b>	<b>109</b>
6.1. Conclusiones generales	111
6.2. Conclusiones específicas	111
<b>7. Bibliografía</b>	<b>115</b>



## **1. INTRODUCCIÓN**



En este apartado se analizan las bases físicas de la Espectroscopia por Resonancia Magnética de Protón (ERM  $^1\text{H}$ ) (apartado 1.1.) y los antecedentes de la ERM  $^1\text{H}$  aplicada al diagnóstico de los tumores cerebrales más frecuentes (apartado 1.2.). Se muestran, a título ilustrativo, espectros promedio procedentes de la base de datos de ERM  $^1\text{H}$  del centro del “Institut de Diagnòstic per la Imatge (IDI)” del Hospital Universitario de Bellvitge. Para la obtención de estos espectros se ha utilizado una secuencia PRESS de voxel único con los siguientes parámetros: TR, 2000 ms; TE, 30-32 y/o 136 ms; amplitud de banda, 1000 Hz; número de puntos en el espectro, 512.

### **1.1. Bases biofísicas y bioquímicas de la ERM $^1\text{H}$**

Con el descubrimiento del fenómeno de la resonancia magnética (RM) se inició la utilización de la espectroscopia por resonancia magnética (ERM) en el campo de la química. En la actualidad, la ERM se utiliza de forma rutinaria para el análisis estructural de los compuestos químicos. Con los avances tecnológicos, la ERM se extendió al campo de la bioquímica como técnica de análisis estructural de macromoléculas y de las interacciones entre moléculas. Hoy en día, estos estudios se pueden realizar en órganos o tejidos de animales y personas “*in vivo*”, con la posibilidad de estudiar de forma directa algunos procesos metabólicos sin interferir en ellos.

Existe un alto número de núcleos atómicos que presentan el fenómeno de resonancia magnética nuclear. La información que se obtiene de cada uno de ellos es diferente. Con mucho, el núcleo más utilizado en el estudio del cerebro ha sido el protón.

### **1.1.1. Biofísica**

#### **1.1.1.1. Bases biofísicas. Ley de Larmor. Constante de apantallamiento. Desplazamiento químico.**

Tanto la obtención de imágenes por RM (IRM) como la ERM se basan en la propiedad que presentan ciertos núcleos atómicos para absorber selectivamente la energía de radiofrecuencia cuando se someten a un campo magnético (fenómeno de resonancia). El exceso energético que se deriva de este fenómeno es liberado por los núcleos mediante un proceso de relajación nuclear. La frecuencia a la que se produce este proceso, frecuencia de precesión ( $f_p$ ) (figura 1), es directamente proporcional al valor del campo magnético efectivo ( $B$ ) que percibe el núcleo, según viene definido por la ley de Larmor:

- (a)  $f_p = \gamma \cdot B / 2\pi$ , donde  $\gamma$  es la constante giromagnética del núcleo considerado y  $B$  es el campo magnético efectivo.

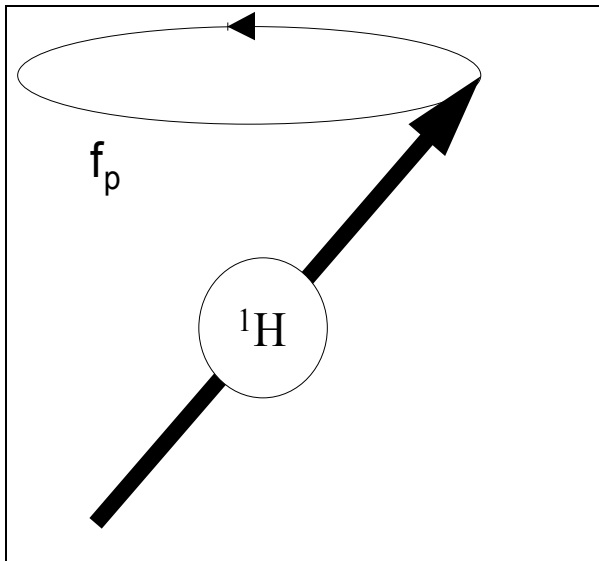


Figura 1. Imagen de un protón en que se ilustra el movimiento de precesión

El campo magnético efectivo ( $B$ ) viene determinado por un campo magnético externo ( $B_{ext}$ ), constituido a su vez por el campo magnético producido por el imán y los gradientes, y un campo magnético “interno”, denominado campo magnético local ( $B_{local}$ ), que está inducido por cargas en movimiento que forman parte de las diferentes moléculas.

$$(b) \quad B = B_{ext} + B_{local}$$

El  $B_{local}$  siempre se opone al campo magnético externo, por lo que ejerce un efecto de pantalla. Su efecto es que el núcleo perciba un campo magnético inferior al campo magnético externo. El  $B_{local}$  es proporcional al campo magnético externo a través de una constante que recibe el nombre de constante de apantallamiento ( $\sigma$ ).

$$(c) \quad B_{local} = -\sigma \cdot B_{ext}$$

En consecuencia:

$$(d) \quad B = B_{\text{ext}} (1 - \sigma)$$

Aplicando la fórmula (d) en (a) obtenemos:

$$(e) \quad f_p = \gamma \cdot B_{\text{ext}} (1 - \sigma) / 2 \pi$$

Dado que  $\gamma$  es la constante giromagnética, constante para cada núcleo considerado, y el campo magnético externo ( $B_{\text{ext}}$ ) será constante para cada experimento, tenemos que la  $f_p$  dependerá, en último término, de la constante de apantallamiento ( $\sigma$ ). Esta constante no dependerá únicamente del núcleo considerado, sino que será característica para la estructura electrónica de su entorno y en consecuencia será característica de la molécula en que esté presente. No será igual la  $\sigma$  del núcleo  $^1\text{H}$  presente en el grupo metil del lactato (figura 2) o de la colina (figura 3). En el caso de la colina, el grupo metil se encuentra adyacente a un átomo de N, que es más electronegativo que el átomo de C que se encuentra adyacente al grupo metil del lactato. El átomo de N, debido a su electronegatividad ejercerá cierta atracción sobre los electrones del grupo metil adyacente. Éste se encontrará más desposeído de su nube electrónica y, por lo tanto, menos apantallado. En consecuencia, la frecuencia de resonancia del grupo metil de la colina estará desplazada a valores más altos que el grupo metil del lactato (figura 4).

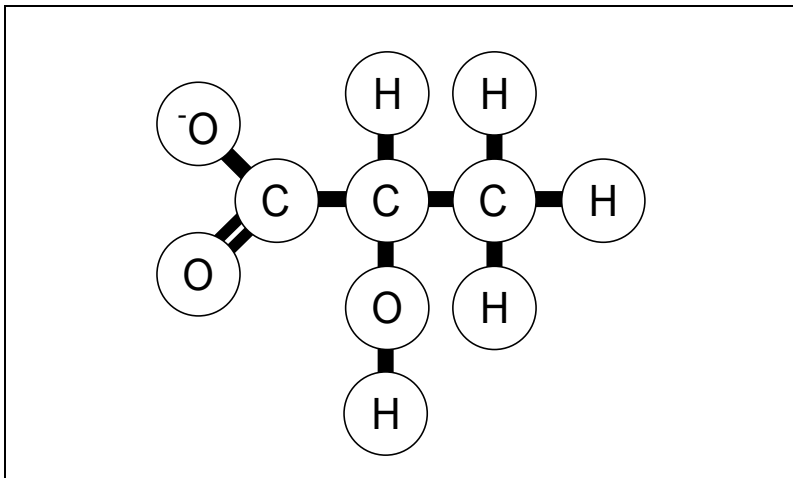


Figura 2. Estructura molecular del lactato.

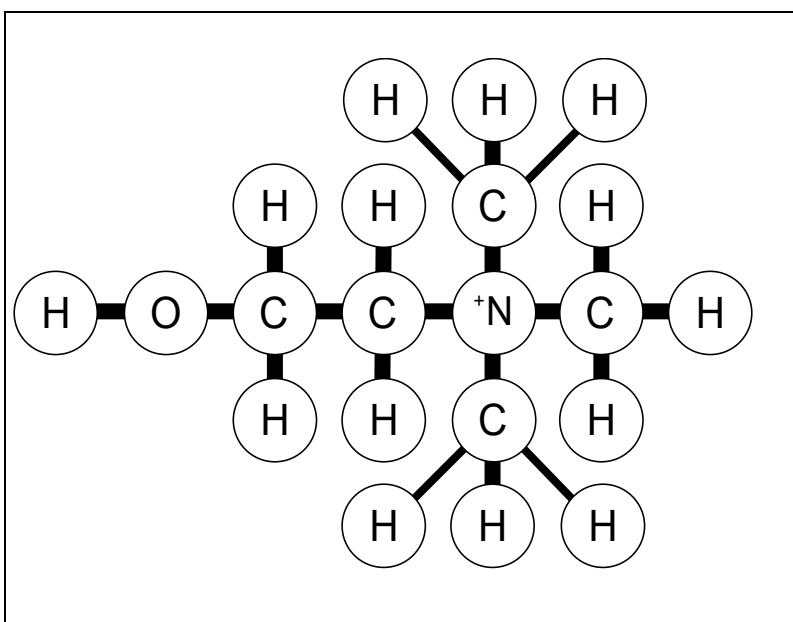


Figura 3. Estructura molecular de la colina. Los protones de sus grupos metil sufren menor apantallamiento que los del lactato por la mayor electronegatividad del N central.

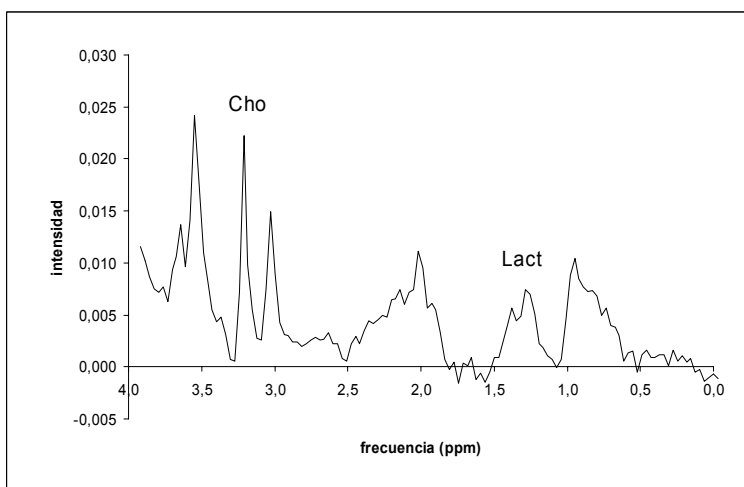


Figura 4. Espectro en el que se identifica la diferente posición de un  $^1\text{H}$  incluido en un grupo metil del lactato (Lact) respecto otro incluido en la molécula de colina (Cho).

En una representación del espectro en el dominio de la frecuencia, los valores del eje x vendrán en unidades de Hz. Una forma más frecuente de representarlo es en unidades de desplazamiento químico ( $\delta$ ). El desplazamiento químico del radical “A” respecto a un radical de referencia “R” viene definido por la ecuación:

$$(f) \quad \delta = (f_{pA} - f_{pR})/f_{pR}$$

El valor de esta variable es muy pequeño, y por ello se expresa multiplicado por  $10^6$ , en unidades de partes por millón (o ppm). Esta variable no tiene dimensión. La principal ventaja respecto a la valoración en Hz es que el desplazamiento químico no depende del campo magnético, únicamente depende de la constante de apantallamiento. Así pues, el desplazamiento químico identifica el compuesto en el que se encuentra el núcleo, de manera que la escala de desplazamiento químico permite la identificación de los diferentes compuestos presentes en la muestra analizada.

En la práctica para cada núcleo existen una serie de compuestos de referencia a partir de los cuales se tabula la posición de los demás. En la ERM  $^1\text{H}$ , una de las referencias más utilizadas históricamente en el terreno de la bioquímica es el 3-trimetilsilil[2,2,3,3- $^2\text{H}$ ]propionato sódico (TSP). Este compuesto no se encuentra en los organismos vivos, pero se ha respetado como referencia para los estudios ERM  $^1\text{H}$  realizados “in vivo”. A la posición de resonancia de este compuesto se le asigna el valor de 0 ppm y su  $f_p$  se utiliza

como  $f_{pR}$ . La tabla 1 muestra los valores de desplazamiento químico respecto al TSP (considerado como compuesto de referencia) para los compuestos más frecuentemente encontrados en estudios cerebrales.

Tabla 1. Metabolitos detectables en el cerebro normal y en los tumores cerebrales, junto con su posición en el espectro

Metabolito	Abreviatura	Localización (ppm)	Multiplicidad
Lactato	Lact	1,35	Doblete
Alanina	Ala	1,47	Doblete
Acetato	Ac	1,92	Singlete
N-acetil aspartato	NAA	2,02	Singlete
Glutamato	Glx	2,10	Multiplete
Glutamina	Glx	2,14	Multiplete
Glutamato	Glx	2,35	Triplete
Succinato	Succ	2,42	Singlete
Glutamina	Glx	2,46	Triplete
N-acetil aspartato	NAA	2,50	Doblete de dobletes
Creatina	Cr	3,03	Singlete
Colina	Cho	3,20	Singlete
<i>Scyllo</i> -inositol	sl	3,35	Singlete
Taurina	Tau	3,43	Triplete
Colina	Cho	3,52	Triplete
<i>Myo</i> -inositol	ml	3,55	Doblete de dobletes
Glicina	Gly	3,56	Singlete
Glutamato	Glx	3,77	Triplete
Glutamina	Glx	3,78	Triplete
Alanina	Ala	3,79	Cuadriplete
Creatina	Cr	3,93	Singlete

### **1.1.1.2. Resumiendo las bases físicas**

Resumiendo, cada átomo devuelve la energía con que ha sido excitado a una frecuencia determinada (frecuencia de precesión o  $f_p$ ) que no depende únicamente del átomo estudiado, sino también del compuesto en que se encuentra. En base a este fenómeno, la ERM  $^1H$  identifica los diferentes compuestos químicos según la frecuencia a que precesan.

### **1.1.1.3. Algunos aspectos adicionales a tener en cuenta**

#### **1.1.1.3.1. Selección del área a estudiar**

Para realizar un estudio de ERM  $^1H$  “in vivo” tendremos que identificar en un primer momento el área que queremos estudiar y posicionar en ella el “voxel” que nos indica el volumen específico que vamos a estudiar. Para ello realizaremos secuencias de IRM que nos proporcionarán imágenes de referencia (figura 5).

#### **1.1.1.3.2. Homogeneización del área a estudiar**

Constituye un paso de especial importancia en la preparación previa a la obtención del espectro. Consiste en modificar los gradientes de manera que el

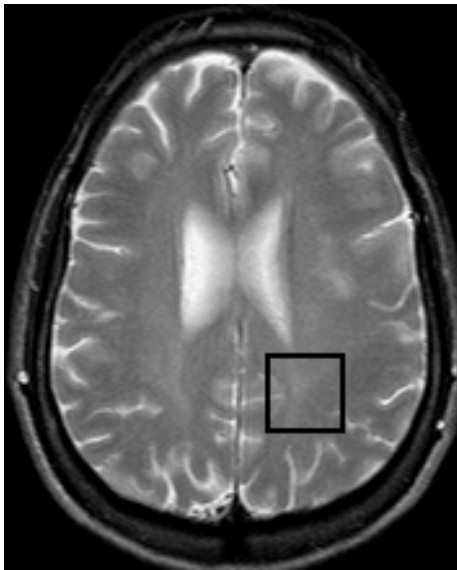


Figura 5. Imagen de IRM en que se muestra el posicionamiento del voxel. En este caso se encuentra localizado en sustancia blanca normal parietal izquierda

campo magnético externo al que están sometidos los diferentes compuestos sea lo más similar posible. En la fórmula " $f_p = \gamma \cdot B_{ext} \cdot (1-\sigma) / 2\pi$ ", si conseguimos que todas las moléculas estén sometidas a un  $B_{ext}$  idéntico, o muy similar, las diferencias de precesión entre ellas serán debidas únicamente al apantallamiento, o lo que es lo mismo, a su entorno eléctrico. Si el campo magnético no es homogéneo, el  $B_{ext}$  en una localización "A" será diferente del  $B_{ext}$  en una localización "B", y parte de las diferencias en las frecuencias de precesión entre protones de moléculas localizadas en los puntos "A" y "B" serán debidas a la diferencia del  $B_{ext}$  y no únicamente a diferencias del apantallamiento. Esto dificultaría o, en casos extremos, impediría la identificación del compuesto dado que puede llegar a producir un solapamiento de las resonancias del espectro.

#### **1.1.1.3.3. Supresión de la señal del agua**

Es otro de los pasos de preparación. Es necesario debido a que el agua es el compuesto más abundante en el parénquima cerebral con mucha diferencia. Su concentración es aproximadamente entre  $10^4$  y  $10^5$  veces la del resto de compuestos, de manera que nos los enmascararía. Existen diferentes métodos para suprimir la señal del agua. En los estudios de esta tesis se ha utilizado un método que consiste en enviar un pulso de radiofrecuencia a la frecuencia de resonancia específica del agua, que satura y reduce al máximo su señal. La figura 6 muestra dos registros obtenidos con los mismos parámetros en un voluntario sano sin (a) y con (b) supresión de agua.

#### **1.1.1.3.4. Obtención del espectro del voxel seleccionado. Constitución del espectro**

Para obtener la señal del voxel el aparato de resonancia envía una serie de pulsos que excitan selectivamente los  $^1\text{H}$  del área de interés seleccionada, y recibe la señal enviada por los mismos al relajarse, por medio de una antena receptora. Este proceso se repite un número de veces determinado y el resultado final será el promedio de la señal obtenida con todos los pulsos. Con ello, se obtiene una gráfica que nos muestra la evolución de la señal (corriente eléctrica) respecto al tiempo (figura 7), denominada FID (“free induction decay”).

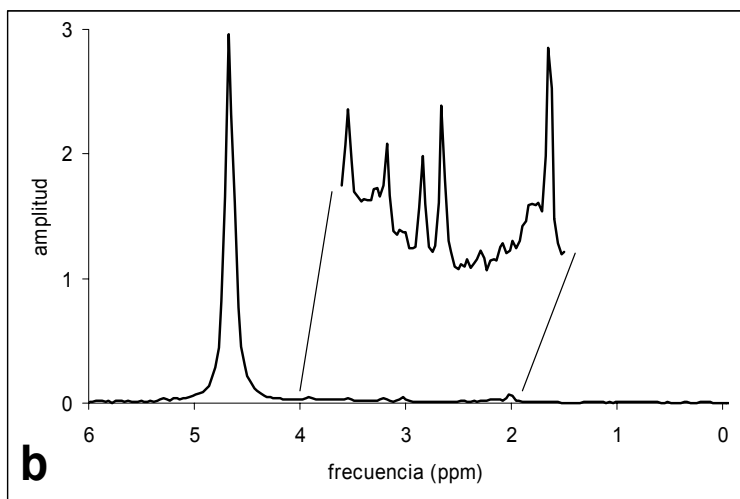
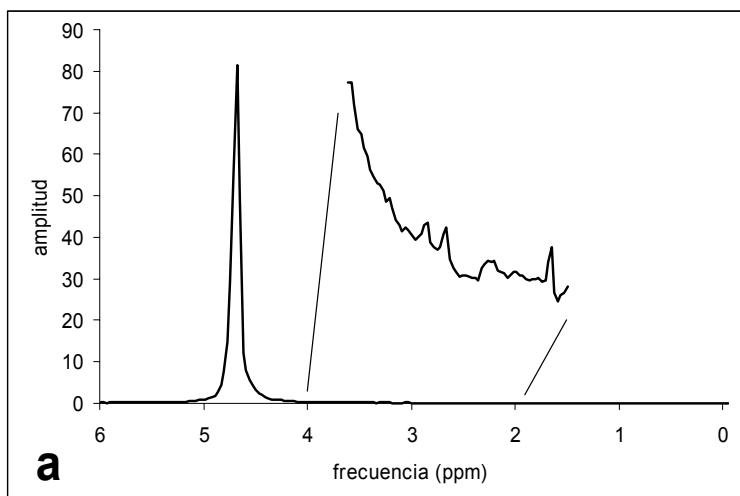


Figura 6. Espectro obtenido en parénquima normal sin (a) y con (b) supresión de agua. Ampliada se muestra el área comprendida entre 4 y 2 ppm. Nótese una mejor resolución de los picos en el espectro con supresión de agua, así como mejor relación señal/ruido y menor repercusión de la cola del pico de agua sobre el área de interés.

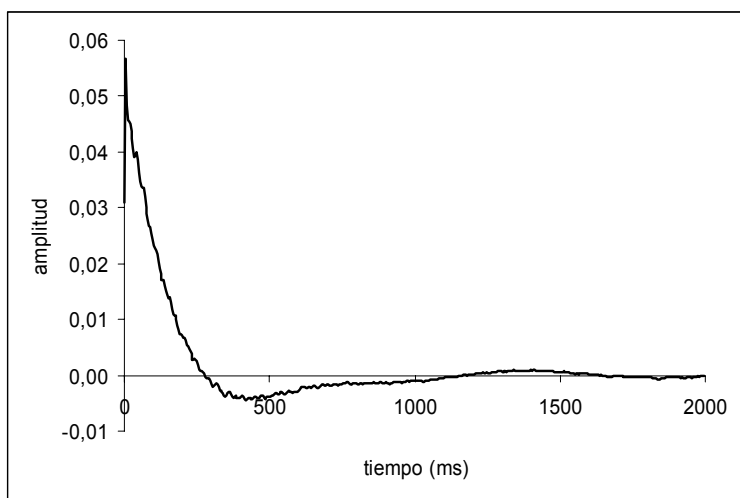


Figura 7. FID del espectro mostrado en la figura 6b. La gráfica muestra la intensidad de la señal obtenida en relación al tiempo

La información que nos ofrece la FID está constituida por la suma de las sinusoides de relajación de los múltiples protones incluidos en el voxel (figura 8). Mediante el procesado y análisis de la FID se pretende evaluar el número de sinusoides que la componen y la amplitud de cada uno.

La amplitud de la sinusoide está relacionada con la concentración de núcleos y la frecuencia de cada una de ellas viene determinada por el campo magnético efectivo que recibe cada uno de los componentes (que dependerá de su constante de apantallamiento, ver apartado 1.1.1.1.).

#### **1.1.1.3.5. Influencia del tiempo de eco sobre el espectro**

Para optimizar la adquisición del espectro se pueden variar diferentes parámetros. La modificación de estos parámetros influirá no sólo en la apariencia del espectro, sino también en la información que puede ser extraída. Uno de los más relevantes es el tiempo de eco (TE). En la actualidad, el TE usado “in vivo” por la mayoría de grupos varía entre 18 ms y 288 ms. A este respecto, se habla de estudios con TE corto o largo, utilizando la mayoría de estudios con TE corto un TE entre 18 y 45 ms, y los estudios con TE largo entre 120 y 288 ms. Se han aducido diferentes argumentos a favor y en contra de cada opción. Un TE largo permite observar un número reducido de metabolitos con menor distorsión de la línea de base. El resultado es un espectro más sencillo de procesar, analizar e interpretar. Con TE de alrededor

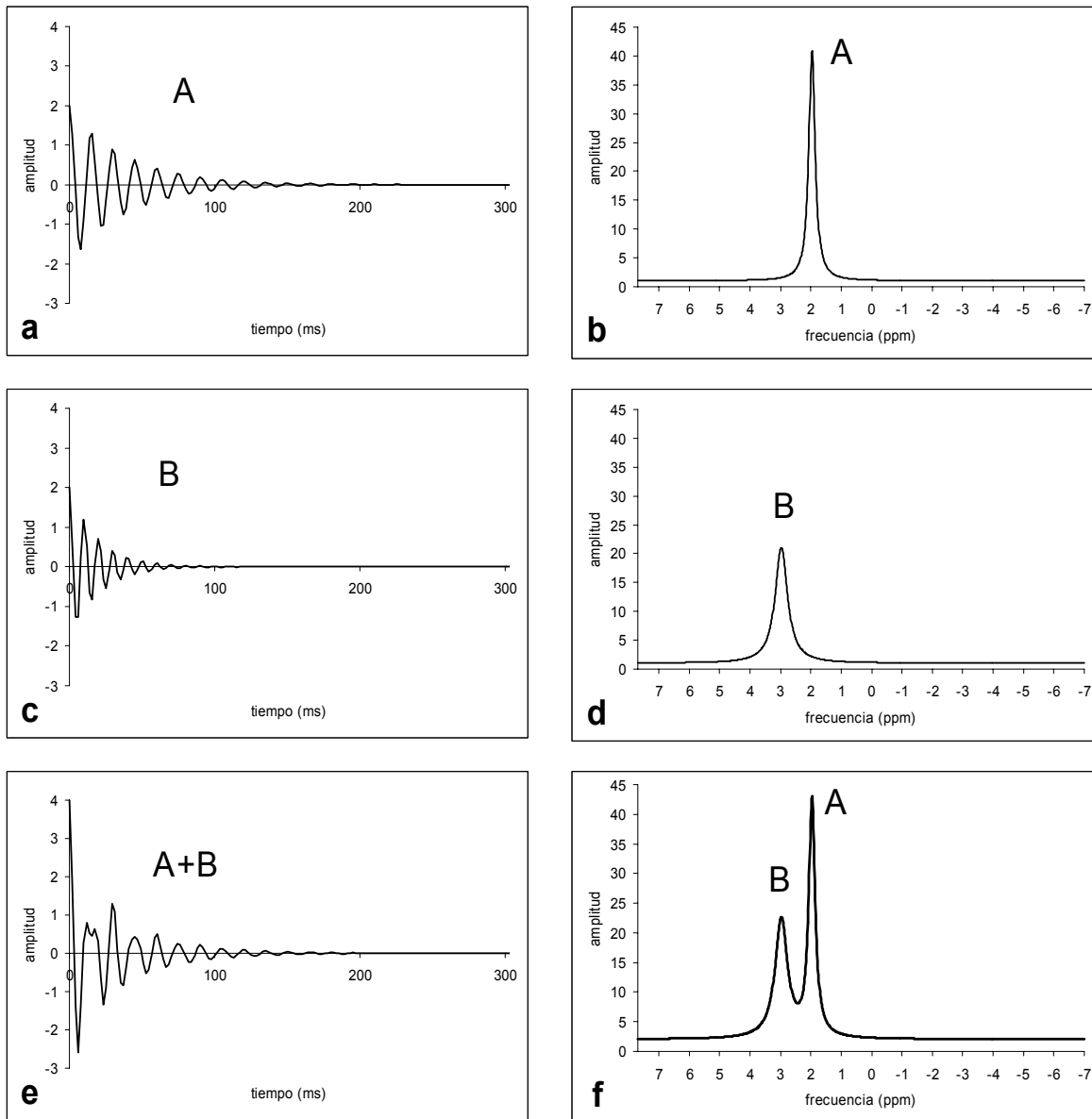


Figura 8. Proceso de formación del espectro. Espectros obtenidos mediante un programa específico que permite simular espectros (programa jMRUI). La figura 8e muestra una FID que sería la resultante de la suma de las FIDs mostradas en 8a y 8c. Al realizar la transformada de Fourier (TF) de esta FID obtenemos la figura 8f, que nos da una representación del espectro según la cantidad de señal a cada frecuencia y su intensidad relativa. La figura 8f sería también el resultado de la suma de las figuras 8b (TF de 8a) y 8d (TF de 8c). Ésta nos permite identificar mejor la presencia de dos compuestos (A y B) y sus intensidades que la figura 8e.

de 136 ms los dobletes de alanina y lactato se encuentran invertidos, siendo más sencillo diferenciarlos de lípidos y otras macromoléculas. Por otro lado, en TE corto son visibles un mayor número de resonancias debido a que la señal de compuestos con fuerte modulación puede perderse a TE largo. De esta manera, es necesario un TE corto para mejor valoración de algunos compuestos como por ejemplo lípidos, *myo*-inositol, glutamina o glutamato. La influencia del TE en la clasificación de tumores cerebrales “*in vivo*” no ha sido estudiada en profundidad, y no existe una decisión unánime sobre el TE a ser utilizado con este fin.

En los trabajos de esta tesis se ha utilizado secuencias con TE largo (136 ms) porque:

- producen mejor diferenciación entre lactato, alanina y lípidos
- probablemente existe un significado diferente en la observación de lípidos a TE largo respecto a TE corto
- la cuantificación es más sencilla y por lo tanto se ha considerado que los resultados deberían ser más reproducibles
- el hecho de ser más sencillo de analizar, cuantificar e interpretar puede condicionar una aplicación más satisfactoria en la práctica clínica.

#### **1.1.1.3.6. Secuencias de voxel único frente a secuencias multivoxel.**

Dentro de las técnicas de espectroscopia, se puede elegir entre secuencias de voxel único y secuencias multivoxel. Las secuencias multivoxel presentan la ventaja de poder estudiar en una misma sesión las características metabólicas de múltiples voxels. En una primera valoración, esto las haría de elección en cualquier situación. No obstante, presentan una serie de inconvenientes a tener en cuenta para estudiar tumores cerebrales. En primer lugar, cuanto mayor es el área a estudiar, mayores son las dificultades técnicas para obtener un registro de calidad. A efectos prácticos, la calidad del registro será menor, tanto en relación señal/ruido, como en homogeneidad del campo y definición de los picos. En segundo lugar, el tiempo de adquisición es mayor en las secuencias multivoxel. En tercer lugar, el método de localización que utilizan estas secuencias es menos preciso que en secuencias de voxel único, con pérdida de señal por el método utilizado, y contaminación desde voxels vecinos. Por último, el procesamiento de los registros es más largo y está menos automatizado. En la práctica, cuando la región a estudiar está claramente definida será de elección la realización de secuencias de voxel único por su mayor calidad y rapidez en cuanto a obtención y procesado. Cuando se desea valorar diferentes regiones a la vez o el área a estudiar no está claramente definida (seguimiento de tumores cerebrales post-tratamiento, guía para biopsia estereotáctica por ERM) serán de elección las secuencias multivoxel al obtener una mejor valoración espacial.

En esta tesis se han utilizado secuencias de voxel único por su mayor rapidez, su más sencillo análisis y la mejor calidad del espectro obtenido. Se ha considerado que estos factores harían estas secuencias de más fácil introducción en la práctica clínica. No obstante, el conocimiento obtenido usando este tipo de secuencias debería ser extrapolable a secuencias multivoxel.

#### **1.1.1.4. Procesamiento de los espectros de esta tesis**

Para el análisis de los espectros de esta tesis se ha realizado una cuantificación de intensidad considerando áreas reconstruidas usando el programa MRUI (1), accesible a través de <http://www.carbon.uab.es/mrui>. Este programa calcula la intensidad de cada resonancia en el dominio del tiempo. Para ello es necesario introducir previamente la posición y amplitud aproximada de la resonancia a estudio.

#### **1.1.2. Metabolitos presentes en los espectros de tumores**

Una vez obtenido y procesado el espectro, se puede relacionar cada resonancia en el espectro con un metabolito en el tejido, y la cantidad de este compuesto se puede valorar según el área de la resonancia. A continuación se describe la información que aportan diferentes metabolitos que se pueden

observar en un espectro de protón de tumores y que han sido utilizados en el análisis de los espectros:

- 0,9 y 1,3 ppm- Lípidos (Lip)- Originan resonancias relativamente anchas que son debidas a los grupos metil y metileno, respectivamente, de la cadena de ácidos grasos. Pueden originar otras señales menores entre 2-2,5 y 5-6 ppm. Se han relacionado con la presencia de necrosis (2) y se proponen como criterio de malignidad, sobre todo si aparecen en espectros registrados con un TE largo.
- 1,35 ppm- Lactato (Lact)- Proporciona información sobre el grado de metabolismo aerobio-anaerobio de la región. En condiciones normales no se detecta en el parénquima cerebral. Su presencia indica que la respiración oxidativa normal en el metabolismo celular se encuentra alterada y que los carbohidratos están siendo catabolizados por la vía anaerobia. Esta situación se da en lesiones altamente celulares y metabólicas que han crecido por encima de lo que su aporte vascular les permite. También se encuentra en lesiones quísticas o necróticas debido a la dificultad de lavado del lactato. Aumenta en lesiones de alto grado, pero su correlación con el grado tumoral (3) o con el metabolismo tumoral valorado por PET (4) no es buena.
- 1,47 ppm- Alanina (Ala)- Es un aminoácido no esencial que ha sido detectado en meningiomas.

- 2,02 ppm- N-Acetyl Aspartato (NAA) y otros compuestos N-acetilados (NACC)- Es la resonancia más intensa que se observa en la ERM  $^1\text{H}$  del parénquima sano. Diversos estudios sugieren que estos compuestos están presentes de manera específica en la neurona del cerebro de personas adultas, y que sería un marcador específico neuronal (5, 6, 7). Una disminución de NAA se ha observado en enfermedades que presentan pérdida de neuronas o axones (demencia, placas antiguas de EM, isquemia, Esclerosis Mesial, tumores -especialmente cuando son de origen extraaxial-). Una segunda resonancia de los NACC, menos prominente, se puede encontrar en 2,50 ppm. Respecto a esta especificidad de NAA y NACC como marcador neuronal, hay que tener en cuenta la presencia de cierto componente de Glx en esta región del espectro, con lo cual, en determinadas situaciones no hay que confundir la presencia de resonancia en 2,02 ppm con presencia de NAA, lo que nos podría llevar a descartar erróneamente algún diagnóstico o a atribuir la presencia de esta resonancia a contaminación externa.
- 2,1-2,4 ppm- Glutamina y glutamato (Glx)- Originan también una serie de señales en la región 3,6-3,8. Se valoran mejor a TE corto. Son difíciles de separar a un campo magnético de 1,5 T. Parece existir dos “pools” de glutamina y glutamato, relacionados con el componente neuronal y el glial. El compuesto que presenta mayor correlación con los procesos patológicos es la glutamina. Diversos estudios sugieren considerar la glutamina como

marcador glial. No obstante, Glx aumentado es un prominente hallazgo de los meningiomas.

- 3,03 ppm- Creatina y fosfocreatina (Cr)- Presentan una segunda resonancia en 3,90 ppm. Están relacionadas con la capacidad energética del cerebro, y se han considerado marcadores de los sistemas dependientes de energía en las células del SNC. Es la resonancia con menor variabilidad del cerebro y se ha utilizado a modo de referencia interna, normalizando los valores de NAA y Cho como ratios de estas resonancias respecto a la Cr (NAA/Cr, Cho/Cr). No obstante, disminuye en tumores cerebrales, ya sea por existencia de un bajo nivel energético o, en el caso de tumores secundarios, por originarse de células que no contienen este compuesto (8, 9, 10, 11).
- 3,20 ppm- Derivados de la colina (Cho)- Esta resonancia presenta contribuciones de diferentes metabolitos como son colina libre, fosforilcolina, glicerofosforilcolina y fosfatidilcolina. Refleja metabolismo de recambio celular y está aumentada en procesos que producen hipercelularidad. Aunque se ha relacionado con la mielina (se considera que el origen de estos metabolitos sería a partir de productos de destrucción de la mielina), su concentración en sustancia blanca es solo ligeramente más alta que en la sustancia gris. Se ha observado que varía tanto en procesos locales como sistémicos, con lo que también existiría cierta contribución extracerebral, probablemente hepática, en la concentración y composición del pico de colina. Se ha correlacionado los niveles de colina in vivo con el

potencial de proliferación tumoral, determinado por el análisis inmunohistoquímico de biopsias utilizando Ki-67 para gliomas (12, 13). Esto daría soporte a la idea de que la Cho se correlaciona directamente con malignidad. No obstante, debe notarse que los meningiomas pueden mostrar niveles de Cho superiores a los gliomas de mayor grado.

- 3,55 ppm- Myo-inositol (ml)- Es un azúcar que forma parte de un tipo de lípidos, fosfatidilinositol y de un grupo de mensajeros, los inositol polifosfatos. Se le otorga un papel como osmolito y se ha sugerido como marcador de astrocitos. Se encuentra aumentado en astrocitomas de bajo grado y disminuido o ausente en tumores no gliales. Un aumento en la señal de ml se ha descrito como característico de hemangiopericitomas frente a meningiomas, los cuales presentan ml bajo o ausente.
- 3,56 ppm- Glicina (Gly)- Su señal se superpone a la del ml. Se ha descrito aumentada en los glioblastomas multiformes.

Para terminar este apartado se quiere subrayar que la correlación resonancia-metabolito no es exacta. Diferentes protones en un mismo compuesto pueden presentar resonancias en diferentes localizaciones del espectro (ver tabla 1). De igual modo,  $^1\text{H}$  procedentes de diferentes compuestos se pueden superponer en un mismo área del espectro, de manera que la correlación directa entre resonancia y metabolito requiere de ulteriores

estudios “in vitro”. Un ejemplo lo tendríamos en los compuestos ml y Gly. Esto constituye una limitación que se debe tener en cuenta al analizar un espectro.

## **1.2. ERM $^1\text{H}$ en el estudio de tumores cerebrales**

### **1.2.1. Antecedentes**

Con el desarrollo de técnicas de ERM  $^1\text{H}$  apropiadas para su utilización “in vivo”, la información bioquímica que aporta la ERM  $^1\text{H}$  se ha ido combinando, cada día con mayor frecuencia, a la información morfológica que aporta la IRM. La accesibilidad actual de paquetes de software de espectroscopia ha incrementado su uso en situaciones clínicas cotidianas. En la actualidad, se pueden obtener estudios ERM  $^1\text{H}$  en la mayoría de equipos de resonancia con una duración cada vez más ajustada. Por lo tanto, los estudios de ERM  $^1\text{H}$  pueden ser añadidos en los estudios de RM convencional sin grandes inconvenientes. Uno de los terrenos en que la ERM  $^1\text{H}$  ha ido ganando más terreno ha sido el del diagnóstico de tumores cerebrales.

### **1.2.2. Interés de la ERM $^1\text{H}$ en el diagnóstico de tumores cerebrales**

Para un manejo óptimo de los pacientes afectos de tumor cerebral, es necesario disponer de un diagnóstico lo más exacto posible. La IRM puede

proporcionar un diagnóstico inicial de las masas cerebrales con una exactitud diagnóstica de entre 30 y 90% dependiendo del tipo de tumor (14, 15). La anatomía patológica (AP) sigue siendo considerada el “gold standard” para determinar el diagnóstico definitivo, por lo que la biopsia del tumor sigue siendo necesaria. No obstante, la mortalidad descrita en la realización de biopsias es del 1,7% (16). En un estudio de 550 pacientes a los que se practicó biopsia estereotáctica, Yu y colaboradores (14) encontraron que un 8% presentaban procesos inflamatorios o abscesos, un 2,2% presentaban otro tipo de lesiones, un 3,4% fueron biopsias no diagnósticas, y un 8% padecieron complicaciones. Un método no invasivo, como lo es la ERM  $^1\text{H}$ , que permitiera predecir con exactitud el tipo de lesiones, podría evitar biopsias en procesos no tumorales o tumores poco accesibles que serían tributarios de radio-quimioterapia más que de resección quirúrgica.

### **1.2.3. Limitaciones en la correlación entre ERM $^1\text{H}$ y anatomía patológica.**

Dado que la AP es la referencia para el diagnóstico de los tumores cerebrales, los resultados de la ERM  $^1\text{H}$  se tendrán en cuenta según su correlación con la AP. Cualquier dificultad en establecer esta correlación correctamente, sea derivada de la AP o de la ERM  $^1\text{H}$ , redundará negativamente en los resultados atribuidos a la ERM  $^1\text{H}$ . Estas limitaciones explicarán también parte de las discrepancias entre estudios, según la técnica utilizada para la ERM  $^1\text{H}$  (posicionamiento del voxel, imágenes de referencia

pre o postcontraste, técnica de voxel único o multivoxel) y para la AP (biopsia estereotáctica, resección parcial, resección total). Existen varias limitaciones a considerar:

1. Los tumores pueden ser muy heterogéneos y su espectro puede contener información de múltiples compartimentos de tejido (17): células tumorales viables, áreas de necrosis, áreas quísticas, tejido normal (infiltrado). Cada compartimento aporta un tipo determinado de información que condiciona la clasificación, por lo que debe tenerse muy en cuenta en base a que componente se ha elaborado cada clasificador antes de aplicarlo.
2. Células de diferente grado tumoral pueden coincidir en un mismo tumor (18). El espectro de un voxel de determinado volumen ( $1 \text{ cm}^3 - 8 \text{ cm}^3$ ) nos proporcionará el espectro promedio de ese volumen, mientras que el diagnóstico AP considerará el mayor grado detectado en la muestra, aunque represente únicamente una pequeña proporción del voxel (figura 9).
3. El diagnóstico histopatológico de una pequeña muestra del tumor obtenida por estereotaxia puede no ser representativa de la totalidad del tumor (figura 10). No se trata de una limitación de la ERM  $^1\text{H}$  sino de la técnica quirúrgica y/o la AP pero condicionarán un diagnóstico por ERM  $^1\text{H}$  diferente del anatomopatológico, que será considerado incorrecto.

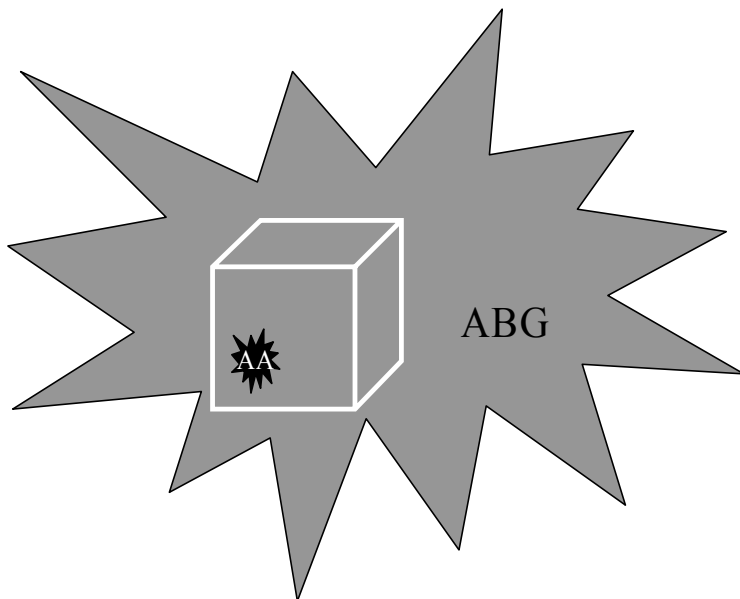


Figura 9. El espectro proporciona una valoración promediada del contenido total del voxel. En el caso ilustrado el espectro será propio de astrocitoma de bajo grado (ABG), infravalorando el grado del tumor (limitación 2). AA, astrocitoma anaplásico.

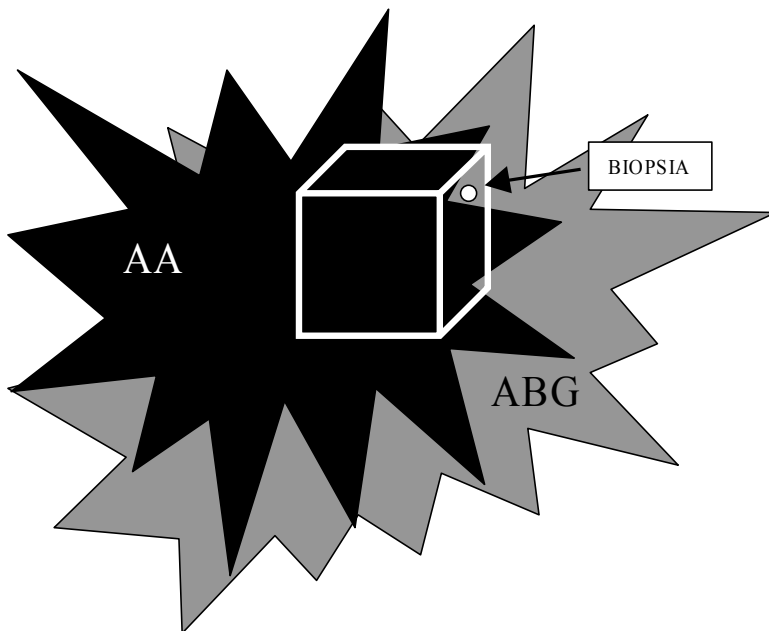


Figura 10. La muestra obtenida por estereotaxia puede no dar una valoración exacta del grado tumoral. En el caso ilustrado el espectro será de astrocitoma anaplásico (AA), mientras el diagnóstico de la biopsia será de astrocitoma de bajo grado (ABG) (limitación 3). El diagnóstico por ERM  $^1\text{H}$  será considerado incorrecto al no coincidir con la anatomía patológica.

4. Lo mismo sucede con la muestra obtenida del voxel seleccionado para la realización de ERM  $^1\text{H}$ . El espectro obtenido puede no correlacionarse con el diagnóstico AP por no haber estudiado el área de mayor grado. Se trata de una limitación propia de las técnicas de voxel único que queda minimizada en las técnicas multivoxel, en que la totalidad del tumor queda incluida en el estudio (19, 20, 21) (figura 11).

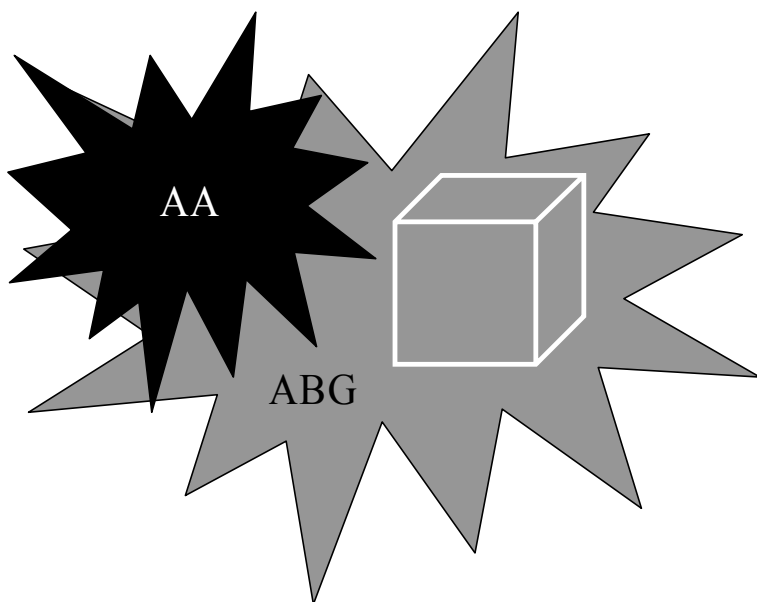


Figura 11. La muestra incluida en el voxel para espectroscopia puede no ser demostrativa del mayor grado tumoral (limitación 4). AA, astrocitoma anaplásico; ABG, astrocitoma de bajo grado.

5. Una última limitación viene derivada también de la AP. Algunos estudios han demostrado discrepancias en el diagnóstico emitido por diferentes anatomicopatólogos sobre una misma muestra (22). Estas discrepancias revertirán en los resultados obtenidos para la ERM  $^1\text{H}$ .

A pesar de estas limitaciones, hay patrones de espectroscopia que se han demostrado característicos de determinados tipos tumorales, y diferentes técnicas estadísticas se han mostrado capaces de relacionar determinados patrones de ERM  $^1\text{H}$  con determinados grupos tumorales (8, 19, 20, 23, 24, 25, 26).

#### **1.2.4. Diferenciación parénquima cerebral normal / tumor**

La ERM se ha demostrado útil para distinguir entre parénquima cerebral normal y tumores cerebrales (5, 27, 28, 29). Las principales características descritas en los tumores cerebrales son: descenso de NACC (30), descenso de Cr, aumento de Cho, aumento de Gly/ml (30), presencia de Lact, aumento de Glx (31) y presencia de resonancia de lípidos en diferentes proporciones (5, 17, 30, 32, 33, 34, 35, 36, 37, 38). El descenso de NACC expresaría la reducción o ausencia de neuronas y axones en la mayoría de tumores, más marcada en tumores extraaxiales. La disminución de Cr es un hallazgo inconstante en tumores, que se ha asociado a un status de baja energía, o al origen celular de tumores metastásicos en células que no contienen Cr. La elevación de Cho es un hallazgo muy prevalente en tumores. Se ha justificado por la proliferación de las membranas celulares. El lactato aparecería a partir de su acumulación en áreas quísticas y necróticas, o a partir de sobreproducción en tumores con una alta ratio de glicolisis y activación de la vía anaerobia. De su origen se justifica

que su distribución en el tumor sea heterogénea. Los lípidos se han asociado a áreas de necrosis.

Un aspecto de mayor dificultad es la distinción entre tumor y proceso patológico no tumoral (procesos inflamatorio-infecciosos, infarto subagudo, Esclerosis Múltiple). La figura 12 muestra dos lesiones de aspecto tumoral en que la ERM  $^1\text{H}$  aportó información útil para su diferenciación.

De todos modos, el papel de estos metabolitos en el diagnóstico de una lesión como tumoral debe ser valorado con cautela. En un estudio realizado con 241 pacientes con sospecha de neoplasia, 6 de los que mostraron un patrón de ERM  $^1\text{H}$  tumoral resultaron corresponder a astrogliosis reactiva en la AP (39). En este estudio se sugirió que el aumento de Cho en estos casos podría ser debido a proliferación de elementos celulares del sistema inmune y astroglía. A pesar de que los cambios espectroscópicos asociados a gliosis son una moderada elevación de Gly/ml y Cho, con moderada reducción de NACC, una gliosis reactiva severa puede llevar a cambios que pueden ser confundidos con un tumor de bajo grado (30, 40). Más allá de la semana de evolución, algunas lesiones isquémicas se pueden confundir con tumores por ERM  $^1\text{H}$  (9). Un tercer motivo de falso positivo pueden ser algunas formas pseudotumorales de EM (41, 42, 43).

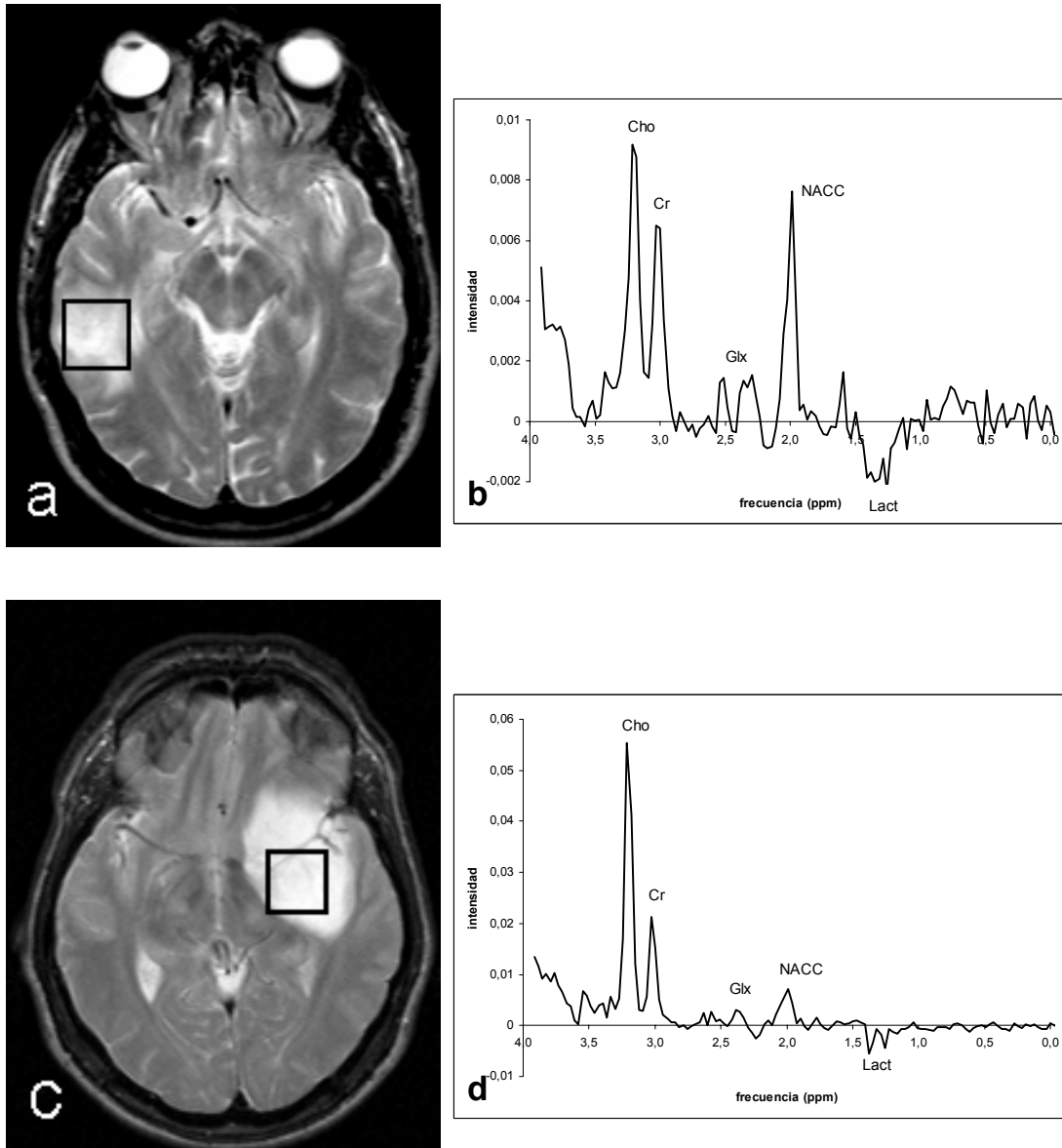


Figura 12. La figura muestra dos imágenes de aspecto tumoral (a y c) y los espectros respectivos obtenidos a TE de 136 ms (b y d). En el primer espectro (b) se aprecia discreta reducción de la resonancia de NACC con mínimo aumento de la ratio Cho/Cr. Este patrón no permite sugerir un origen tumoral. En el segundo caso el espectro (d) es más claramente tumoral, con marcada reducción de NACC y marcado aumento de la ratio Cho/Cr. En el primer caso la anatomía patológica no detectó tumor, y la evolución de las imágenes confirmó una lesión pseudotumoral. En el segundo caso el estudio histológico confirmó la presencia de un astrocitoma de bajo grado.

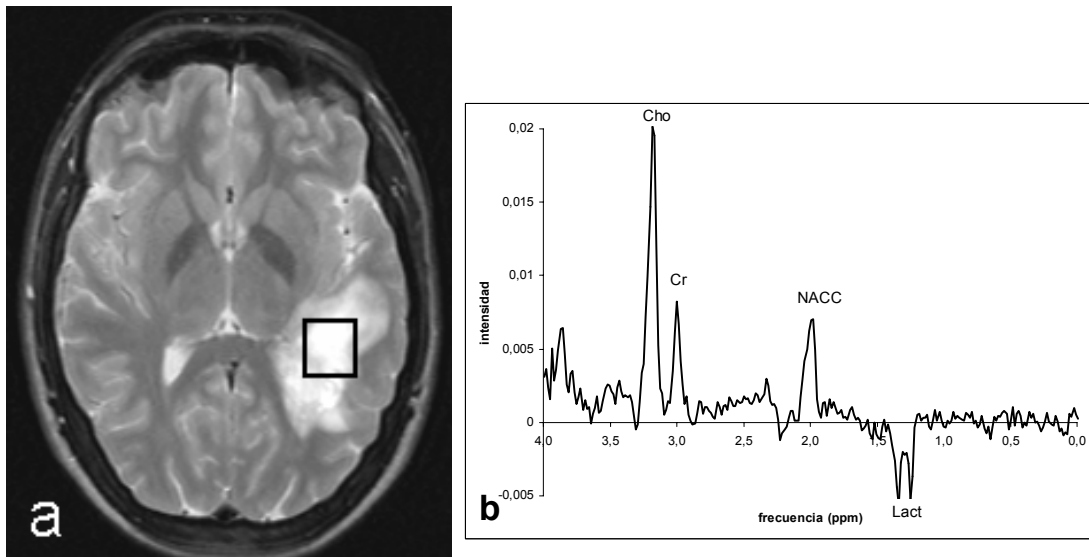


Figura 13. Falso positivo de la ERM  $^1\text{H}$  para tumor de bajo grado en un caso de Esclerosis Múltiple. La figura (a) muestra una lesión focal temporal izquierda de aspecto tumoral en la secuencia potenciada en T2. El espectro obtenido con TE de 136 ms muestra un significativo aumento de la ratio Cho/Cr y Cho/NACC (superior a 2) que sugiere una tumoración de bajo grado. El diagnóstico definitivo fue Esclerosis Múltiple.

### 1.2.5. Tumores gliales. Diferenciación del grado tumoral

Los hallazgos descritos como típicos de los astrocitomas incluyen una reducción del nivel de NACC, moderada reducción de niveles de Cr y elevación de Cho (figuras 14, 15 y 16) (3, 27, 44). Múltiples estudios han analizado la capacidad de la ERM para distinguir entre diferentes grados tumorales en astrocitomas y han propuesto diferentes marcadores:

#### 1.2.5.1. Incremento de los compuestos derivados de la colina con el grado tumoral

En múltiples trabajos se ha afirmado correlación directa entre el área de Cho y el grado tumoral en tumores astrocíticos (8, 12, 28, 32, 33, 45, 46, 47,

48, 49). No obstante, este incremento lineal con el grado no se ha constatado en todos los estudios. Es un hecho prevalente que los niveles de Cho en astrocitoma anaplásico son mayores que en astrocitoma de bajo grado, pero diversos estudios han encontrado niveles de Cho menores en glioblastoma que en astrocitoma anaplásico (8, 21, 31, 45, 46). Puede ser debido a predominio en el voxel de áreas necróticas sobre áreas celulares proliferativas. Esto explicaría también la variabilidad presente entre estudios, dependiendo de la estrategia utilizada para posicionar el voxel sobre el tumor, y cierta discordancia entre estudios practicados “in vitro” e “in vivo”, dado que los primeros sólo consideran áreas de tumor viable no necrótico.

#### **1.2.5.2. Papel del lactato en la gradación de tumores**

También se ha señalado la presencia de lactato como indicador de alto grado tumoral (3, 5, 27, 28, 29, 45, 47, 50, 51, 52, 53, 54). La justificación del aumento de lactato con el grado tumoral sería que el aumento de la actividad metabólica desplazaría el metabolismo celular hacia la vía anaerobia, provocando depósito de lactato. Otros estudios han demostrado gran variabilidad en la cantidad de lactato (3), que se justifica porque la presencia de este metabolito no depende únicamente de su producción por parte de las células, sino de la capacidad de lavado del mismo. De este modo se acumularía en áreas quísticas o con mala llegada del árbol vascular (45).

#### **1.2.5.3. Papel de los lípidos en la gradación de tumores**

Los lípidos se han relacionado con áreas de necrosis, y por tanto se encontrarían en tumores de alto grado tumoral (2, 32, 45). Serían pues indicadores de alto grado tumoral y se encontrarían presentes en glioblastomas. Se han descrito en diferentes proporciones en astrocitomas anaplásicos dependiendo de los estudios. Con respecto a los glioblastomas, algunos grupos han distinguido entre glioblastomas con lípidos y glioblastomas sin lípidos de cara a su clasificación (33, 55), y han intentado correlacionar estos dos patrones con el grado de actividad tumoral.

#### **1.2.5.4. Papel del Myo-Inositol y la glicina en la gradación de tumores**

Estos compuestos resuenan aproximadamente en la misma posición del espectro (3,55 – 3,56 ppm), de manera que no es posible diferenciarlos únicamente por su posición. Se ha descrito un descenso del Myo-inositol con el grado tumoral (8, 31, 56, 57). Por otro lado, estudios “in vitro” han detectado un aumento de la cantidad de glicina en glioblastoma (31, 58).

Con respecto a estos marcadores, cabe destacar que existe una significativa superposición entre grados tumorales, probablemente debido a las limitaciones descritas en el apartado 1.2.3.

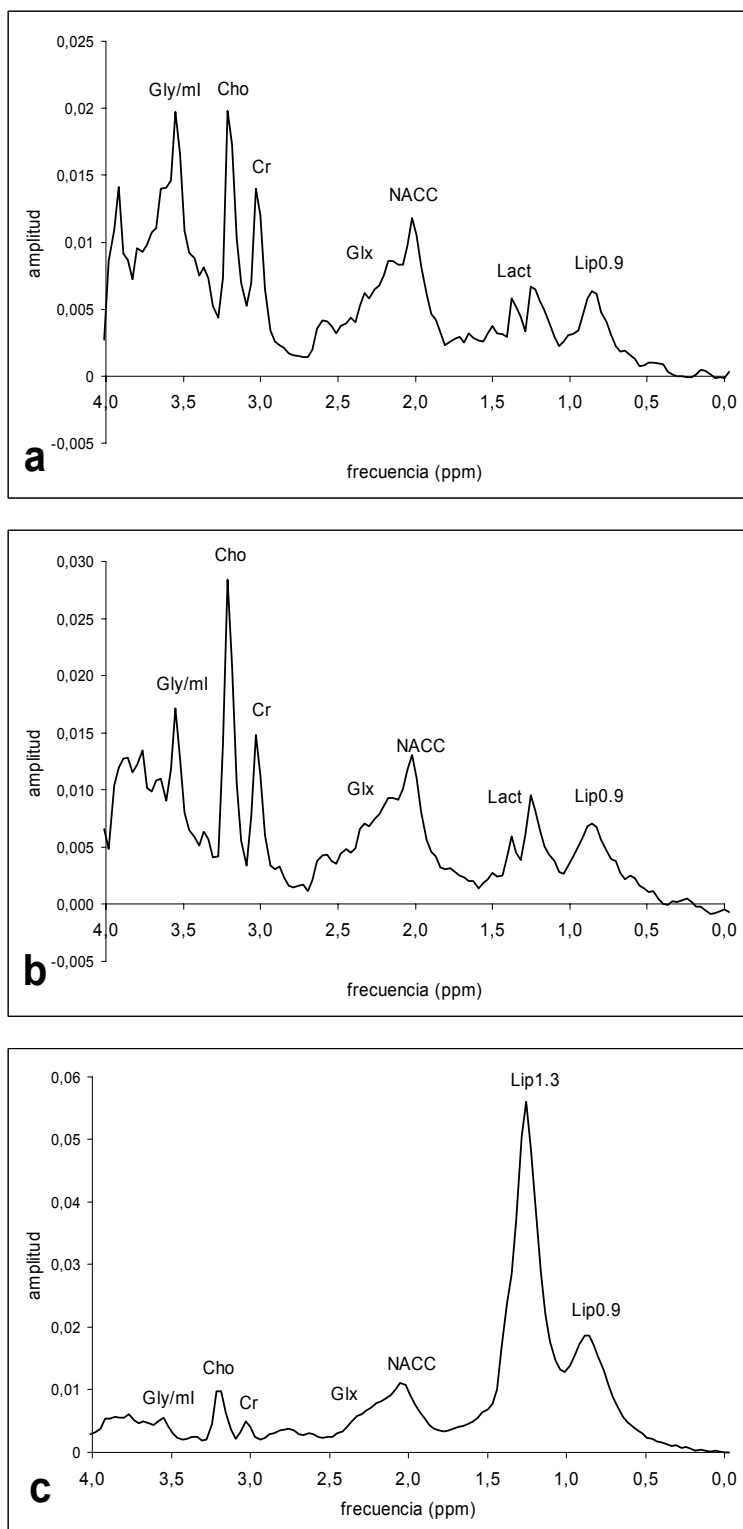


Figura 14. Registro promedio a TE corto a partir de 12 astrocitomas de bajo grado (a), 16 astrocitomas anaplásicos (b) y 54 glioblastomas (c).

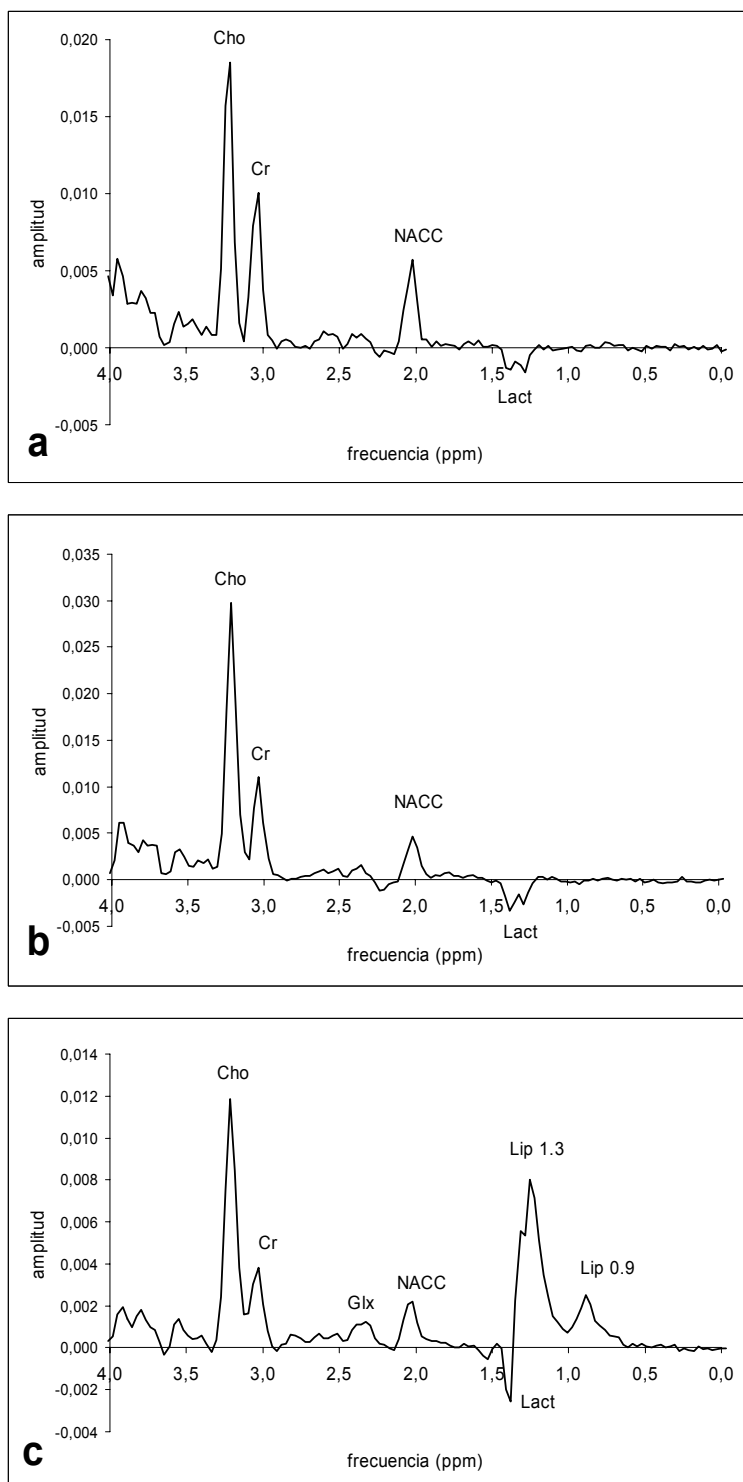


Figura 15. Registro promedio a TE largo a partir de 12 astrocitomas de bajo grado (a), 16 astrocitomas anaplásicos (b) y 54 glioblastomas (c).

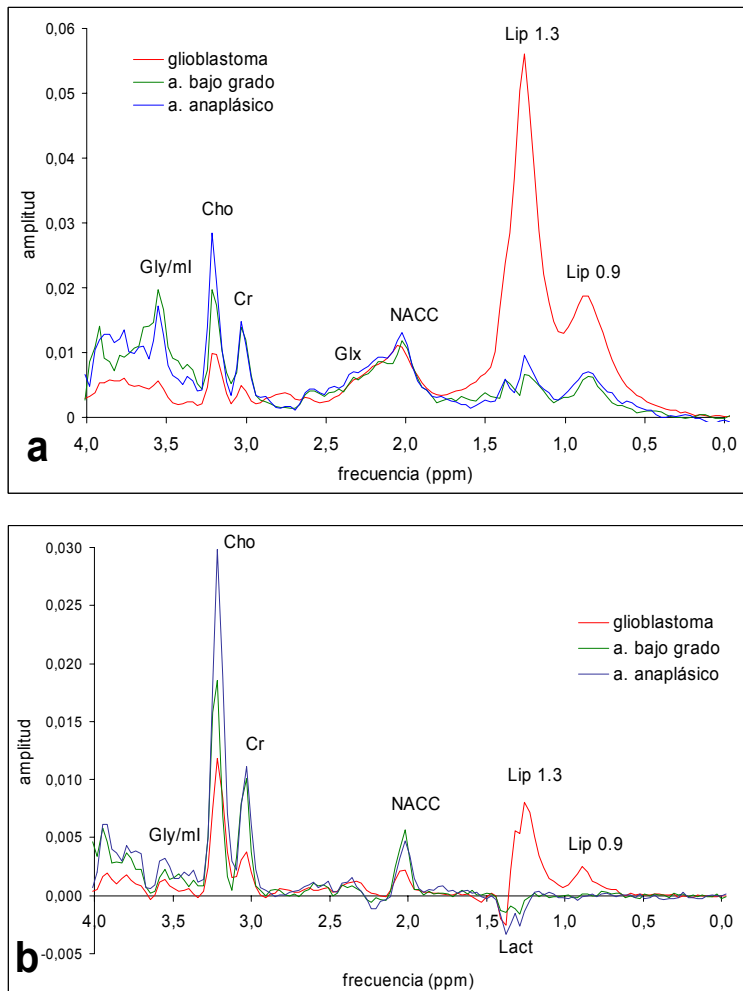


Figura 16. Superposición de los espectros promedio de tumores gliales para TE corto (a) y TE largo (b). La presencia de lípidos es característica de glioblastoma. Los valores de Cho son mayores en astrocitoma anaplásico que en bajo grado, y mayores en ambos que en glioblastoma. Nótese aumento de Gly/ml a TE corto en astrocitoma de bajo grado.

### 1.2.6. Meningiomas

Los meningiomas constituyen un grupo de tumores sobre los que se han descrito diferentes hallazgos característicos:

### **1.2.6.1. N-Acetyl Aspartato y otros compuestos N-acetilados en meningiomas**

Dado que los meningiomas se originan fuera del parénquima neuronal, en teoría no deberían contener NAA (27). Sin embargo, en la práctica clínica es frecuente observar resonancia en 2,02 ppm en el espectro, que en teoría debería corresponder a NAA (figura 17). Diferentes argumentos se han aportado para explicar este hecho. En primer lugar se atribuyó a contaminación de tejido no meningiomatoso, por mal posicionamiento del voxel o mala delimitación del mismo (3). Esta explicación en muchos casos no es factible. En la actualidad esta resonancia se atribuye a otros tipos de compuestos N-acetilados, diferentes de NAA (59). De todos modos, es prevalente una marcada reducción del pico centrado en 2,02 ppm (NACC) en meningiomas.

### **1.2.6.2. Compuestos derivados de la colina y creatina-fosfocreatina en meningiomas**

En meningiomas, la señal de Cho está marcadamente aumentada. Existe también una marcada reducción en la señal de Cr, hecho que se ha confirmado en estudios realizados “in vitro” (60).

### 1.2.6.3. Lactato y alanina en meningiomas

El Lact y la Ala también pueden estar elevadas en algunos meningiomas. De momento no hay explicación para este aumento de Ala, pero parece ser un hallazgo prevalente y característico (figura 17) (3, 27, 28, 34, 50, 61).

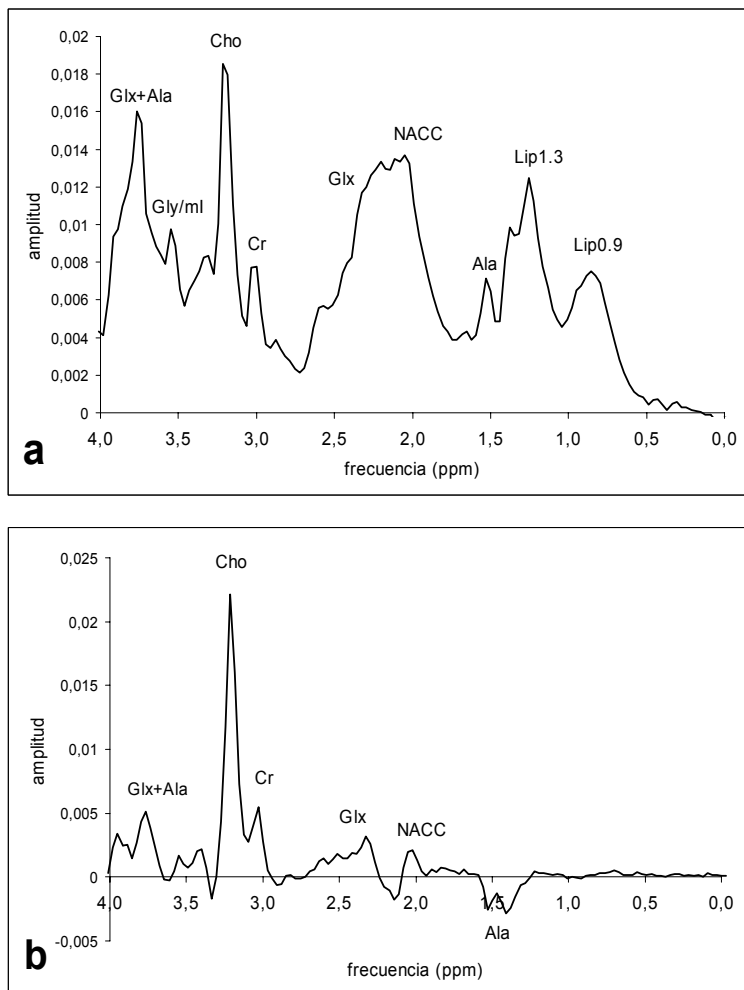


Figura 17. Espectro promedio de meningioma ( $n=37$ ) a TE corto (a) y TE largo (b). Destaca la presencia de resonancia de Ala con abundante cantidad de Glx, marcado aumento de la ratio Cho/Cr y una resonancia a 3,8 ppm que puede tener componente tanto de Glx como de Ala.

#### **1.2.6.4. Glutamina y glutamato en meningiomas**

Se ha detectado también un aumento de Glx en extractos de meningioma (46). Este dato se ha mostrado de utilidad para diferenciar "in vitro" entre meningioma y astrocitoma (31). Un hallazgo referido recientemente como característico de meningiomas ha sido una elevación de glutation en resonancias alrededor de 2,36; 2,9; 3,4 y 3,78 ppm (62).

A pesar de que estos hallazgos parecen ser muy prevalentes y reproducibles, su aplicación en el diagnóstico de meningiomas no ha sido analizada en profundidad en un estudio clínico.

#### **1.2.7. Metástasis**

En presencia de una lesión única es clínicamente importante distinguir entre tumor cerebral primario y secundario. Esta diferenciación es frecuentemente difícil (si no imposible) sin histología. La mayoría de las metástasis muestran de moderada a marcada reducción de NACC, reducción de Cr y elevados niveles de Cho (figuras 18 y 19). Estos hallazgos son idénticos a los de algunos astrocitomas. Frecuentemente las metástasis pueden contener lípidos y lactato, al igual que ocurre con tumores gliales de alto grado, atribuido a la presencia de áreas de necrosis intratumoral (3, 50, 63, 64, 65). El estudio de los patrones espectrales en base al origen del tumor

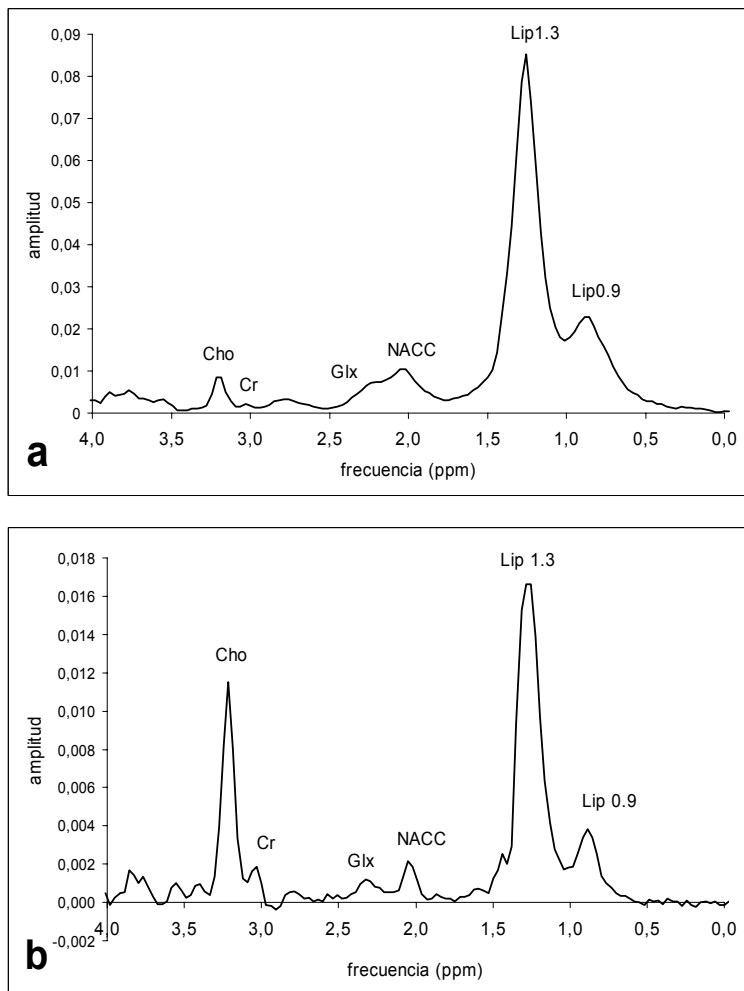


Figura 18. Espectro promedio obtenido a partir de 32 metástasis a TE corto (a) y TE largo (b). Destaca la presencia de abundante cantidad de lípidos en las posiciones de 0,9 y 1,3 ppm.

primario no ha detectado diferencias suficientemente significativas (66). Diferentes hallazgos se han propuesto para diferenciar entre metástasis y glioblastoma por diferentes grupos, sin que ninguno haya sido confirmado hasta la fecha: aumento de Glx en metástasis (67), aumento de la relación Lip 1.3/Lip 0.9 en metástasis (8) ausencia de Cr en metástasis (10). Se ha sugerido ausencia de NACC como característico de metástasis, dado que este tumor se origina fuera del cerebro. La mayoría de trabajos no han encontrado.

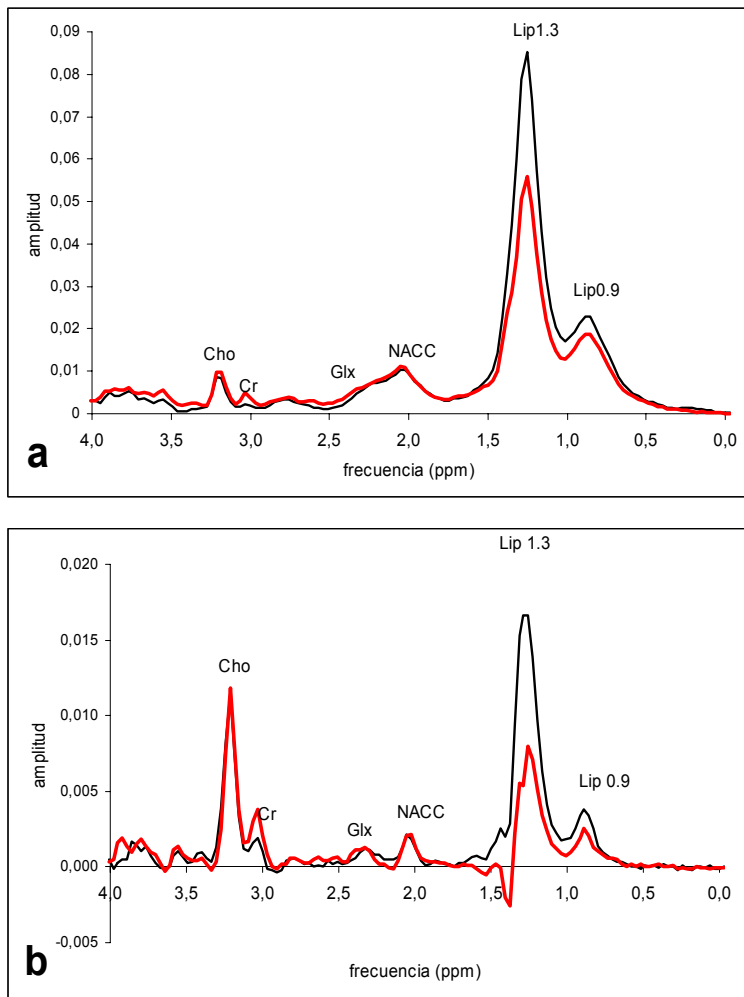


Figura 19. Gráfico comparativo de espectros promedio de metástasis (negro) y glioblastoma (rojo) a TE corto (a) y largo (b). Los registros son muy similares y únicamente difieren en mayor cantidad de lípidos en metástasis y de Cr en glioblastoma. No se objetivaron diferencias significativas en el estudio estadístico.

reproducibilidad de este hallazgo, de manera similar y con explicaciones también similares a como sucede en el caso de los meningiomas (apartado 1.2.6.1)

### 1.2.8. Tumor Neuroectodérmico Primitivo (TNEP)

Son tumores más frecuentes en niños. Estos tumores muestran incrementos de Cho superiores a los encontrados en astrocitomas y ependimomas (68). Se han detectado también patrones característicos de myoinositol, taurina, glutamina y glutamato, de interpretación incierta (figura 20) (31, 69).

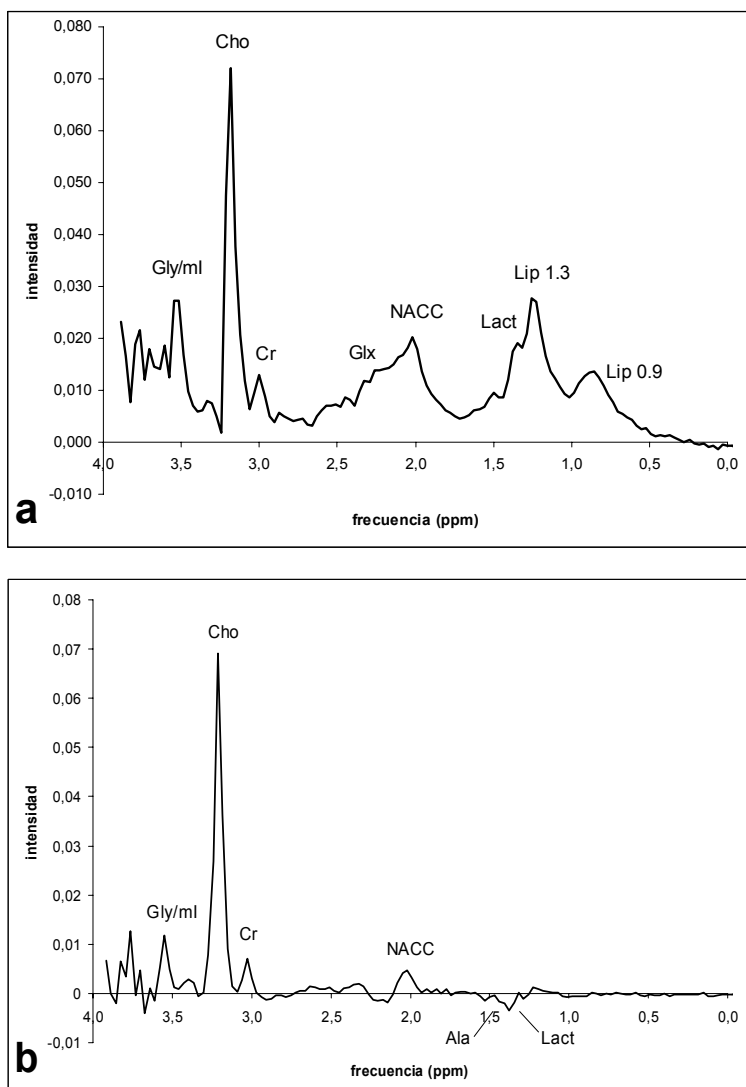


Figura 20. Espectro promedio obtenido a partir de 12 TNEP a TE corto (a) y TE largo (b). Destaca un aumento muy marcado de Cho, superior al del resto de tipos tumorales, presencia de Gly/ml y trazas de Ala.

## **2. HIPOTESIS DE TRABAJO. OBJETIVOS**



## 2.1. Hipótesis de trabajo. Interés de la tesis

La ERM  $^1\text{H}$ , como técnica que valora los cambios bioquímicos en los tejidos, debería proporcionar información útil para diferenciar los distintos grupos tumorales, a partir de sus características bioquímicas.

La información proporcionada por la ERM  $^1\text{H}$  debería poder ser aplicada en la práctica clínica para diferenciar entre tipos tumorales “in vivo”. Para ello es necesario:

1. Conocer el patrón espectral en ERM  $^1\text{H}$  de cada grupo tumoral.
2. Conocer que variables espectroscópicas diferencian mejor los diferentes grupos.
3. Disponer de un método que aplique estas características diferenciales en la clasificación de tumores cerebrales.
4. Conocer los resultados esperados, y si éstos justifican la utilización de la ERM  $^1\text{H}$  en tumores cerebrales.

La mayor parte de trabajos previos, tal como se ha visto en la introducción, se han centrado en el punto 1, con escaso desarrollo de los puntos 2, 3 y 4. Esta tesis enfoca el tema de la clasificación de tumores cerebrales en la práctica clínica incidiendo sobre los cuatro puntos.

Por otro lado existe significativa dispersión de resultados, e incluso resultados contradictorios, entre los diferentes trabajos. Esto se puede explicar por diferentes razones: gran variabilidad de parámetros para realizar el estudio ERM, diferentes estrategias de posicionamiento del voxel, diferentes matices en la valoración del “gold standard” (anatomía patológica), diferentes prevalencias de subtipos tumorales, variabilidad intrínseca de patrones espectrales en los diferentes grupos tumorales. Esto justificaría el interés de desarrollar completamente el punto 1 en esta tesis, dado que la experiencia previa no está suficientemente validada para su aplicación directa (de hecho en algunos casos es contradictoria). Justificaría también la necesidad de elaborar un método de clasificación dúctil que pueda ser adaptado a la variabilidad de resultados en diferentes grupos de estudio.

Dada la diferente prevalencia de los tumores cerebrales, se han planteado dos enfoques para la clasificación del total de tumores:

1. En primer lugar se ha considerado un núcleo de tumores constituido por los cinco grupos más frecuentes: meningioma, astrocitoma de bajo grado, astrocitoma anaplásico, glioblastoma y metástasis. En nuestra experiencia, este grupo de tumores constituye aproximadamente un 85 % del total. Para este grupo se ha considerado necesario un método que clasifique cada caso en uno de los cinco grupos en un único procedimiento, respondiendo a la pregunta “¿el tumor estudiado corresponde con mayor probabilidad a un

meningioma, astrocitoma de bajo grado, astrocitoma anaplásico, glioblastoma o metástasis a partir de sus hallazgos espectroscópicos?”

2. El diagnóstico del resto de tumores (por ejemplo los tumores neuroectodérmicos primitivos), con una prevalencia mucho menor, se ha planteado a partir del diagnóstico diferencial entre estos tumores y los del primer grupo, en procedimientos “de dos en dos”. Este método permite utilizar la información obtenida previamente en los estudios de imagen para acotar el diagnóstico diferencial y mejorar los resultados en un grupo de tumores de baja incidencia. Permitiría responder la pregunta “¿el tumor estudiado corresponde con mayor probabilidad al grupo tumoral A o al grupo tumoral B a partir de sus hallazgos espectroscópicos?”. El mismo método permitiría también ajustar el diagnóstico diferencial entre los tumores del primer grupo en el caso de que se utilice la información obtenida en los estudios de imagen para acotar el diagnóstico diferencial.

## **2.2. Objetivos generales**

1. Caracterizar el patrón espectral de ERM  $^1\text{H}$  de los diferentes grupos de tumores cerebrales.
2. Avanzar en la aplicación de la ERM  $^1\text{H}$  en el diagnóstico clínico de tumores cerebrales.

### **2.3. Objetivos específicos**

1. Caracterizar el patrón espectral de ERM  $^1\text{H}$  de los tumores cerebrales más frecuentes en el adulto (meningioma, astrocitoma de bajo grado, astrocitoma anaplásico, glioblastoma y metástasis) y las variables espectroscópicas que mejor diferencian estos tumores entre sí (trabajo 1).
2. Elaborar un método para aplicar las variables espectroscópicas definidas en el apartado anterior en el diagnóstico de los tumores cerebrales más frecuentes del adulto en la práctica clínica (trabajo 1).
3. Caracterizar el patrón espectral de ERM  $^1\text{H}$  de un tumor cerebral poco frecuente en el adulto, el tumor neuroectodérmico primitivo (TNEP), e identificar las variables espectroscópicas que mejor diferencian este grupo tumoral de los tumores cerebrales más frecuentes del adulto (trabajo 2).
4. Elaborar un método para aplicar las variables espectroscópicas definidas en el apartado anterior en el diagnóstico del TNEP en la práctica clínica (trabajo 2). Este método servirá de base para aplicar la ERM  $^1\text{H}$  en el diagnóstico de tumores de baja prevalencia.

5. Elaborar un método para mejorar el diagnóstico diferencial del meningioma con los otros tumores cerebrales más frecuentes (trabajo 3). Servirá de base para aplicar la ERM  $^1\text{H}$  en el diagnóstico de tumores cerebrales frecuentes con mejores resultados, cuando el diagnóstico por imagen es sugestivo pero no concluyente.
  
6. Comprobar la utilidad de la ERM  $^1\text{H}$  para diagnosticar meningiomas cerebrales de aspecto radiológico atípico (trabajo 3).



### **3. MATERIAL Y MÉTODOS**



En este apartado se resumen los aspectos comunes en cuanto a Material y Métodos de los tres artículos de esta tesis. En el apartado de Material y Métodos de cada artículo se podrán encontrar más detalles y algunas particularidades propias del enfoque de cada trabajo.

### **3.1. Pacientes**

Los trabajos que constituyen esta tesis valoraron retrospectivamente 144 espectroscopias de tumores cerebrales no tratados, que incluían: 37 meningiomas, 18 astrocitomas de bajo grado, 14 astrocitomas anaplásicos, 30 glioblastomas, 11 TNEP y 34 metástasis. Se incluyó 79 varones y 65 mujeres con edades comprendidas entre los 14 y los 81 años (media de edad de 54 años). Todos los diagnósticos se confirmaron mediante anatomía patológica, excepto 10 metástasis en que el diagnóstico se basó en la presencia de múltiples lesiones intracraneales en pacientes con un tumor primario conocido. Los estudios fueron aprobados por el Comité Ético de Investigación Clínica (CEIC) del Hospital Universitario de Bellvitge (HUB). En todos los pacientes se obtuvo Consentimiento Informado.

### 3.2. Espectroscopia por Resonancia Magnética de Protón

En todos los casos la ERM  $^1\text{H}$  se añadió al final del estudio de IRM. La ERM  $^1\text{H}$  se realizó en el centro del Institut de Diagnòstic per la Imatge (IDI) del Hospital Universitario de Bellvitge en una máquina Philips (ACS-NT, Philips Medical Systems, Best, Holanda) de 1,5 Teslas. Se utilizó una secuencia PRESS (Point-Resolved Spectroscopic Sequence) de voxel único con un volumen de interés de entre  $1,5 \times 1,5 \times 1,5 \text{ cm}^3$  (3,4 mL) y  $2 \times 2 \times 2 \text{ cm}^3$  (8 mL) dependiendo del tamaño del tumor. La estrategia para el posicionamiento del voxel fue la de estudiar el mayor volumen posible del área tumoral sólida, evitando áreas quísticas, y minimizando la contaminación por tejido periférico no tumoral. Para ello se analizaron todas las secuencias disponibles, incluyendo las obtenidas tras la administración de contraste endovenoso.

La homogeneidad del campo magnético en el volumen de interés se optimizó con un sistema automático de tres bobinas de los gradientes lineales (X, Y, Z). A continuación de optimizó la supresión de agua mediante la aplicación de un pulso de excitación selectiva a la frecuencia del agua.

Los principales parámetros utilizados para la realización del espectro fueron:

- Tiempo de repetición (TR): 2000 ms
- Tiempo de eco (TE): 136 ms

- Puntos definidos en el espectro: 512
- Amplitud de banda: 1000 HZ
- Excitaciones: 128 á 192 (dependiendo del tamaño del voxel)

El análisis del espectro fue realizado en una consola auxiliar con ayuda del programa MRUI (1), accesible a través de <http://www.carbon.uab.es/mrui>. Este programa calcula la intensidad de cada resonancia en el dominio del tiempo, que equivale al área en el dominio de la frecuencia. Previamente al ajuste del espectro se filtró el agua residual con el algoritmo de Henkel-Lanczos (1). Se analizó el espectro en el dominio del tiempo con el método VARPRO (variable projection method) (1) después de introducir como valores iniciales una estimación de la posición y anchura a media altura de cada una de las resonancias. Para evitar sesgos por el operador, la cuantificación de las resonancias se realizó definiendo siempre todas las resonancias de interés, incluso cuando éstas eran difíciles de diferenciar del ruido, con el criterio de que la posterior cuantificación y análisis debería detectar diferencias entre ruido y resonancia real sin influencia del operador.

Se definieron las siguientes resonancias de interés en el espectro:

- Lip 0.9 centrado en 0,90 ppm
- Lip 1.3 centrado en 1,30 ppm
- Lact como un doblete centrado en 1,35 ppm
- Ala como un doblete centrado en 1,47 ppm

- NACC centrado en 2,02 ppm
- Glx centrado entre 2,10 y 2,40 ppm
- Cr centrado en 3,03 ppm
- Cho centrado en 3,20 ppm
- Gly/ml centrado en 3,55 ppm

Cada una de estas resonancias se consideró por separado para cuantificación y análisis estadístico. La resonancia Cr (3,03 ppm) y/o el agua (4,75 ppm) fueron seleccionadas como resonancias de referencia para corrección de posibles desplazamientos en el dominio de la frecuencia.

Los datos obtenidos se normalizaron mediante la fórmula “ $x = 100 \cdot x_i / (NACC^2 + Cr^2 + Cho^2)^{1/2}$ ” (siendo  $x_i$  el valor del área original de la resonancia a normalizar). En el caso de los lípidos (Lip 0.9 y Lip 1.3) se utilizó la fórmula “ $x = 100 \cdot x_i / (NACC^2 + Cr^2 + Cho^2 + Lip 0.9^2 + Lip 1.3^2)^{1/2}$ ”.

### 3.3. Análisis estadístico

El análisis estadístico para identificar la presencia de diferencias significativas entre los diferentes grupos se realizó mediante tests no paramétricos. Se utilizó el test de Kruskal-Wallis el análisis de cada resonancia valorando todos los grupos de tumores a la vez. Posteriormente se buscaron

diferencias entre grupos mediante el test T3 de Dunnett. En el caso de comparaciones 2 a 2 se utilizó el test de la U de Mann Whitney.

Dado que se analizaron varios procedimientos para cada resonancia, los valores de la P fueron corregidos utilizando el método de Hochberg. La definición de diferencias significativas se realizó sobre los valores de P corregidos ( $P^*$ ). Diferencias de  $P^*$  menores de 0,05 fueron consideradas estadísticamente significativos.

Los análisis estadísticos se realizaron con el programa SPSS (SPSS, Chicago, Illinois, EUA).

### **3.4. Métodos para la clasificación de los tumores**

En este apartado existe cierta variabilidad entre los diferentes trabajos, dado que cada método se adaptó en función a la pregunta que se quería responder.

En todos los casos se utilizó un algoritmo diagnóstico que clasificaba los casos nuevos según el valor de las resonancias que mejor discriminaban entre grupos tumorales. Para establecer el punto de corte se utilizó un criterio no paramétrico, como es el límite del percentil del 90 % (o del 10% según los casos) de los tumores.

### **3.5. Comprobación de resultados**

En los trabajos 1 y 2 se reservó un grupo de tumores como grupo “test”. De esta manera se desarrollaron los clasificadores utilizando el grupo de entrenamiento y, una vez establecidos estos clasificadores, se comprobó su funcionamiento en el grupo de test.

En el trabajo 3 se utilizó el método de “dejar-uno-fuera”. Para utilizar este método se retira un caso de la base de datos, el cual se “deja fuera”. Se desarrollan los clasificadores sin tener en cuenta el caso, el cual se utilizará posteriormente como test. Se repite el procedimiento de elaboración de los clasificadores tantas veces como casos existen en la base de datos, reservando cada vez un caso diferente fuera. De esta manera se obtendrán tantas comprobaciones como casos existen en la base de datos.

**4. TRABAJOS PUBLICADOS**



**4.1. Trabajo 1:**

Proton Magnetic Resonance Spectroscopy ( $^1\text{H}$  MRS) of human brain tumours: assessment of differences between tumour types and its applicability in brain tumour categorization. Majós C, Alonso J, Aguilera C, Serrallonga M, Pérez-Martín J, Acebes JJ, Arús C, Gili J. Eur Radiol 2003; 13: 582-591.



Carles Majós  
Juli Alonso  
Carles Aguilera  
Marta Serrallonga  
Javier Pérez-Martín  
Juan J. Acebes  
Carles Arús  
Jaume Gili

## Proton magnetic resonance spectroscopy ( $^1\text{H}$ MRS) of human brain tumours: assessment of differences between tumour types and its applicability in brain tumour categorization

Received: 21 February 2002

Revised: 14 May 2002

Accepted: 27 May 2002

Published online: 2 August 2002

© Springer-Verlag 2002

C. Majós (✉) · J. Alonso · C. Aguilera  
M. Serrallonga · J. Gili  
Institut de Diagnòstic per la Imatge (IDI),  
Hospital Duran i Reynals, CSU de Bellvitge,  
Autovia de Casteldefels km 2.7,  
08907 L'Hospitalet de Llobregat,  
Barcelona, Spain  
e-mail: cmajos@csub.scs.es  
Tel.: +34-93-2630121  
Fax: +34-93-2630144

J. Pérez-Martín  
Clinical Research Unit,  
Institut Català d'Oncologia (ICO),  
Hospital Duran i Reynals, CSU de Bellvitge,  
Autovia de Casteldefels km 2.7,  
08907 L'Hospitalet de Llobregat,  
Barcelona, Spain

J.J. Acebes  
Department of Neurosurgery,  
Hospital Príncipes de España,  
CSU de Bellvitge, Feixa Llarga s/n,  
08907 L'Hospitalet de Llobregat,  
Barcelona, Spain

C. Arús  
Departament de Bioquímica  
i Biología Molecular, Unitat de Ciències,  
Universitat Autònoma de Barcelona,  
Edifici C, 08193 Cerdanyola del Vallès,  
Spain

**Abstract** Our objective was to evaluate the usefulness of proton magnetic resonance spectroscopy ( $^1\text{H}$  MRS) in categorizing brain tumours. In vivo single-voxel  $^1\text{H}$  MRS at an echo time of 136 ms was performed in 108 patients with brain neoplasms that included 29 meningiomas (MEN), 15 low-grade astrocytomas (LGA), 12 anaplastic astrocytomas (AA), 25 glioblastomas (GBM) and 27 metastases (MET). Time-domain fitted areas of nine resonances were evaluated in all spectra. Twenty-five additional tumours were prospectively included as independent test set. Differences in at least two resonances were found in all pairwise comparisons of tumour groups except in GBM vs MET. Large lipid resonance at 1.30 ppm was found to be characteristic of GBM and MET, and alanine was characteristic of MEN. Significant differences were found between LGA and AA in choline-containing compounds and total creatine resonances. When implemented in a stepwise algorithm, these findings correctly classified 84% (21 of 25) tumours in the independent test set.

Some additional utility was found in glycine/myo-inositol at 3.55 ppm for bilateral differentiation between GBM and MET (9 of 11, 82% correct classification in the test set).  $^1\text{H}$  MRS provides useful information to categorize the most common brain tumours that can be implemented in clinical practice with satisfactory results.

**Keywords** Magnetic resonance · Spectroscopy · Brain neoplasms · Diagnosis · MR

### Introduction

Diagnosis of brain tumours can become a difficult challenge to clinicians and radiologists in some cases. Non-invasive diagnosis relies mostly on clinical history and radiological exams. Using these data, a first diagnostic

orientation can be given, but histopathological examination of a biopsy sample is often required before starting aggressive treatments. This is so even in cases in which surgical procedures are not the first choice in the final treatment. In this context, additional information provided by other non-invasive radiological techniques can be

of high interest for taking clinical decisions about patient management and, hopefully in the future, for trying to avoid some surgical diagnostic procedures.

Proton MR spectroscopy ( $^1\text{H}$  MRS) is a non-invasive technique for measuring the biochemical content of living tissues that can be performed on most 1.5-T clinical MR equipment. This technique provides metabolic information complementary to the anatomical changes found in radiological exams which have proved useful in providing extra information from various brain diseases. Nevertheless, this information has not been fully integrated yet in most diagnostic protocols of brain tumours. From a radiological point of view, an important question is whether  $^1\text{H}$  MRS can be used as a diagnostic tool in this field. For this, it is necessary to:

1. Know which findings better differentiate between tumour groups in  $^1\text{H}$  MRS
2. Have available a user-friendly method to apply these findings in clinical brain tumour classification
3. Know the results forecasted for this diagnostic tool in every clinical situation

Our aim was to focus on the potential of this technique to distinguish among the major types of cerebral neoplasms. With this purpose, we studied in a quantitative approach nine major metabolite resonances in single-voxel MR spectra obtained from brain tumours at long echo time (136 ms), and compared their values among groups. We applied our results to the development of an empirical diagnostic approach path and we assessed its accuracy for objectively classifying those tumour groups.

## Materials and methods

### Patients

We retrospectively evaluated 108 consecutive proton MR spectroscopic studies in 108 patients (51 women and 57 men, age range 14–81 years, mean age 54 years) with a variety of intracranial tumours that included meningiomas (MEN;  $n=29$ ), low-grade astrocytomas (LGA;  $n=15$ ), anaplastic astrocytomas (AA;  $n=12$ ), glioblastomas (GBM;  $n=25$ ) and metastases (MET;  $n=27$ ). Twenty-five consecutive additional tumours (8 MEN, 3 LGA, 2 AA, 5 GBM and 7 MET) were included in a prospective test set with the aim of assessing the reproducibility of results in an independent group of tumours not included in the training set. All neoplasms were confirmed pathologically with the exception of 9 MET in which the diagnosis was based on the presence of multiple lesions in patients suffering from a known primary neoplasm. The maximum diameter of the tumours was measured in order to assess the possible influence of size in the differences found in  $^1\text{H}$  MRS. The study was approved by our institutional review board and informed consent was obtained from all patients.

### Spectroscopy

The  $^1\text{H}$  MRS was performed before any treatment on a 1.5-T MR unit (ACS-NT, Philips Medical Systems, Best, The Netherlands) using a point-resolved spectroscopic sequence (PRESS) with a

volume of interest (VOI) between  $1.5 \times 1.5 \times 1.5 \text{ cm}^3$  (3.4 ml) and  $2 \times 2 \times 2 \text{ cm}^3$  (8 ml), depending on tumour size. The standard receiver head coil was used in all cases, and the spectroscopic exam was incorporated into a routine MR imaging study. The aim was to position the largest possible voxel within the solid tumoral area, avoiding areas of cysts, and with minimum contamination from the surrounding non-tumoral tissue. Automatic shimming of the linear X, Y and Z channels was used to optimize the field homogeneity. The water resonance was set on resonance and the water suppression pulse was optimized. Proton spectra were recorded with a repetition time of 2000 ms and an echo time of 136 ms. A total of 512 data points were collected over a spectral width of 1000 Hz. Four dummy scans plus 128 or 192 excitations, depending on VOI size, were accumulated for each spectrum. Spectrum analysis was performed off-line by means of the MRUI software [1]. The time domain data were analyzed with the variable projection method (VARPRO). This is a non-linear least-squares fitting method that calculates the frequency of the resonances, the amplitude corresponding to the area in the frequency domain and the line width at half-height for each signal. Before applying the VARPRO method, the residual water signal was filtered with the Henkel-Lanczos singular value decomposition algorithm.

Assignment of the resonances of interest, including N-acetyl-aspartate and other N-acetyl containing compounds (NAc) at 2.02 ppm, creatine plus phosphocreatine (Cr) at 3.03 ppm, choline and other trimethyl-amine-containing compounds (Cho) at 3.20 ppm, lipids (Lip 0.9) at 0.90 ppm and (Lip 1.3) at 1.30 ppm, glutamate and glutamine (Glx) at 2.35 ppm and glycine and/or myo-inositol (Gly/mI) at 3.55 ppm was based on previous documented studies of brain tumours [2, 3, 4, 5, 6, 7, 8]. Two doublets inverted owing to phase modulation due to J coupling were defined, corresponding to lactate (Lact) at 1.35 ppm and to alanine (Ala) at 1.47 ppm. Water resonance frequency (4.75 ppm) and/or Cr (3.03 ppm) were chosen as reference resonances for correction of possible shifting in the frequency domain. Each one of these nine resonances (Lip 0.9, Lip 1.3, Lact, Ala, NAc, Glx, Cr, Cho and Gly/mI) was considered separately for quantification and statistical analysis.

For comparative purposes, fitted resonance areas by MRUI of Lact, Ala, NAc, Glx, Cr, Cho and Gly/mI were normalized dividing each value by the square root of the sum of the squares of the three main spectroscopic resonances ( $x = 100 * x_i / (\text{NAc}^2 + \text{Cr}^2 + \text{Cho}^2)^{1/2}$ , where  $x_i$  is the area of the resonance being normalized) in a modification of the method described by Tate et al. [2]. For normalization of resonance areas of lipids the square value of Lip 0.9 and Lip 1.3 was included in the sum of the denominator ( $x = 100 * x_i / (\text{NAc}^2 + \text{Cr}^2 + \text{Cho}^2 + \text{Lip } 0.9^2 + \text{Lip } 1.3^2)^{1/2}$ ) in order to avoid extremely high values in the comparison of metabolites that have been considered to pertain to different metabolic compartments [9]. Data obtained were compared between tumour types in order to assess which findings were characteristic of each type and the utility of each metabolite resonance signal in classifying the different tumours. Assessment of differences between normal brain parenchyma and tumoral tissue, a fact that has been well established in previous work [3, 10, 11, 12, 13, 14], was beyond the scope of this study.

### Statistics

Significance of differences between various groups for each metabolite was tested with the Kruskal-Wallis non-parametric analysis of variance. A post hoc analysis was performed between groups using the Dunnett's T3 test. The same statistic tests were used to test differences in tumour size between groups. Differences of  $p < 0.05$  were considered to be statistically significant. We then searched for the resonances that showed higher differences between every tumour type and the rest of types. All analyses were performed by using a software program (SPSS for Windows, SPSS, Chicago, Ill.).

## Empirical diagnostic approach path

The results of the above analysis were assembled in an algorithm that used the 90% percentiles of the most discriminative resonances to classify every particular case. We elaborated this path with two major aims:

1. To corroborate and quantify the utility of the spectroscopic trends found
2. To obtain a preliminary and easily reproducible tool for clinical brain tumour classification on the basis of  $^1\text{H}$  MRS

The performance of this empiric diagnostic approach was tested with the “leave-one-out” method [2, 15] in the 108 tumours retrospectively included in the study. The performance of this path in differentiating between pairs of groups was also evaluated. Finally, this algorithm was applied to an independent test set of 25 tumours not used for training the system.

## Results

Table 1 summarizes the mean and standard deviation obtained for the different resonance areas and tumour groups, whereas Table 2 shows the metabolite resonances that showed statistically significant differences in the comparison between tumour groups. Tumour sizes ranged between 17 and 96 mm of maximum diameter. Mean and standard deviation of sizes for every group are shown in Table 1. No significant differences were found in size between groups. Accordingly, this parameter was not taken into account for further discrimination attempts. Eight of the nine resonances evaluated in the study (Lip 0.9, Lip 1.3, Lact, Ala, NAc, Glx, Cr and Cho) showed significant differences in their normalized values between tumours. Representative spectra of the different tumour groups of the study are shown in Fig. 1.

### Meningiomas

Alanine was the most characteristic resonance of MEN. This resonance showed high levels of statistical significance for all bilateral comparisons (Table 2); in consequence, we considered it a marker of MEN. Only few non-meningeal tumours showed resonance doublets attributable to Ala in the spectrum. Other findings characteristic of MEN were:

1. Relative decrease of Cr with respect to astrocytic tumours
2. Increase of Cho with respect to LGA, GBM and MET
3. Increase of Glx in reference to LGA and AA
4. Absence of Lip 1.3 with respect to GBM and MET

### Astrocytic tumours

The GBM was well differentiated from the rest of astrocytic tumours and from MEN by the presence of a broad

**Table 1** Normalized area values of nine metabolite resonances in the 108 brain tumours analyzed by  $^1\text{H}$  MRS. *Lip* 0.9 lipid component centred at 0.9 ppm; *Lip* 1.3 lipid component centred at 1.3 ppm; *Lact* Lactate; *Ala* alanine; *NAc* N-acetyl aspartate and/or myo-inositol

	N	Size <sup>a</sup>	Lip 0.9	Lip 1.3	Lact	Ala	NAc	Glx	Cr	Cho	Gly/ml
Meningioma	29	50.48±15.89	1.61±6.52	0.52±2.80	3.87±7.90	28.07±18.29	13.32±5.66	30.18±21.85	18.75±10.76	96.55±2.65	4.72±1.68
Low-grade astrocytoma	15	57.33±18.48	0±0	0±0	19.22±15.64	0.68±2.63	26.42±16.40	7.06±9.34	42.32±7.89	84.41±9.06	3.63±4.30
Anaplastic astrocytoma	12	50.00±16.42	3.16±10.96	12.41±23.51	28.35±51.67	5.01±8.32	16.81±12.00	11.28±15.00	28.47±8.00	93.26±4.53	5.59±9.42
Glioblastoma	25	47.28±13.68	7.04±8.18	71.00±30.66	75.93±153.13	5.69±12.14	21.83±9.20	20.98±15.85	27.85±9.46	92.49±5.33	9.57±12.81
Metastasis	27	39.67±17.92	9.60±8.03	70.33±33.15	51.50±108.09	0.74±3.87	29.65±17.16	13.15±15.87	20.33±13.33	90.38±9.02	1.96±3.16

Values shown are mean±standard deviation

<sup>a</sup> Size measured as the maximal tumour diameter in millimetres. No significant differences were found between tumour groups

**Fig. 1a–e** Representative  $^1\text{H}$  MRS of brain tumours obtained at long echo time (TE 136 ms). **a** Meningioma. **b** Low-grade astrocytoma. **c** Anaplastic astrocytoma. **d** Glioblastoma. **e** Metastasis

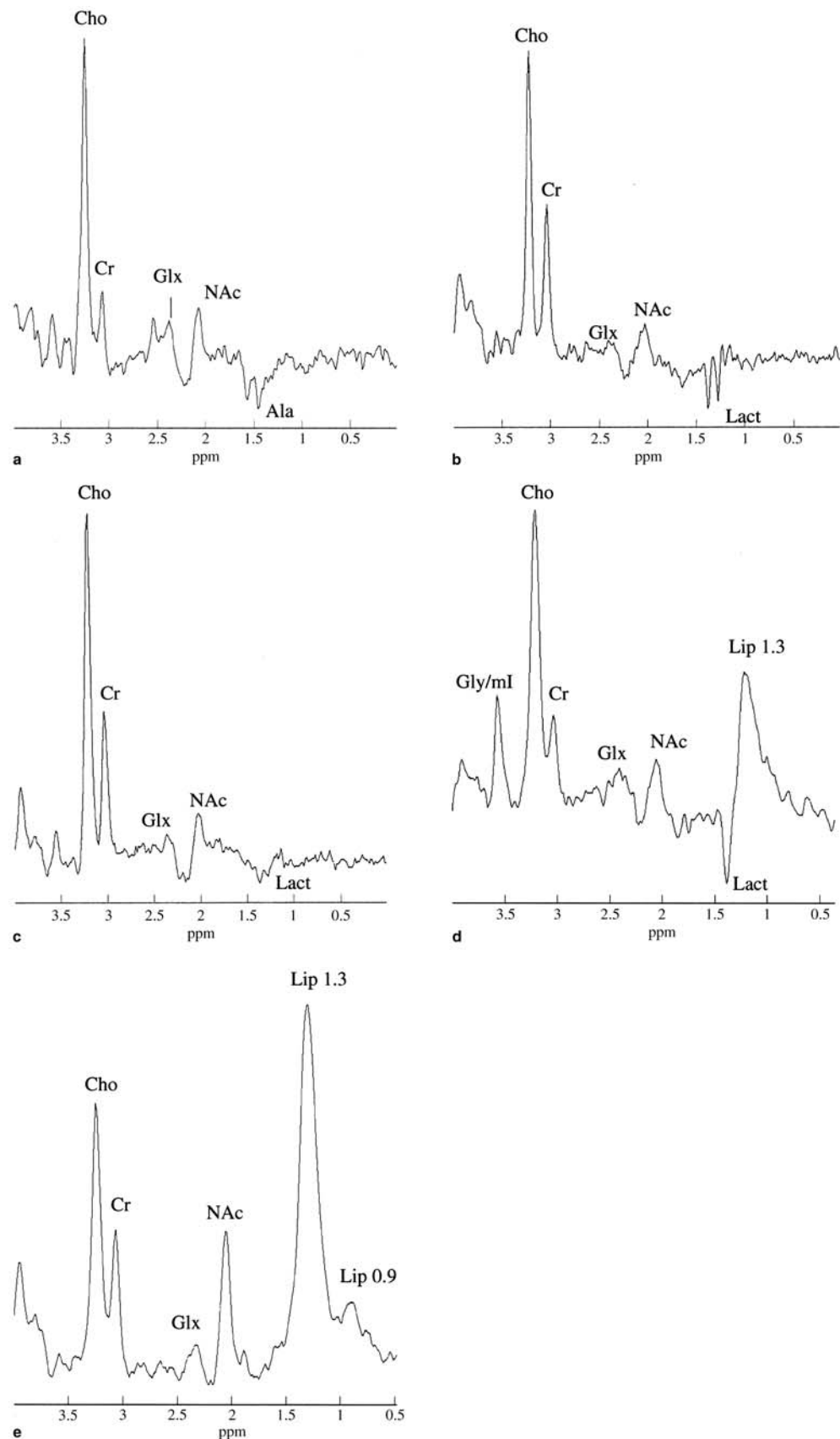


**Table 2** Metabolite resonances with statistically significant differences between tumour groups

	Meningioma	Low-grade astrocytoma	Anaplastic astrocytoma	Glioblastoma	Metastasis
Meningioma	–	Lact * Ala*** Glx*** Cr*** Cho**	Ala*** Glx* Cr*	Lip 1.3*** Ala*** NAc** Cr* Cho*	Lip 0.9** Lip 1.3*** Ala*** NAc*** Glx* Cho*
Low-grade astrocytoma	Lact * Ala*** Glx*** Cr*** Cho**	–	Cr** Cho*	Lip 0.9** Lip 1.3*** *	Lip 0.9*** Lip 1.3*** Cr***
Anaplastic astrocytoma	Ala*** Glx* Cr*	Cr** Cho*	–	Lip 1.3***	Lip 1.3***
Glioblastoma	Lip 1.3*** Ala*** NAc** Cr* Cho*	Lip 0.9** Lip 1.3*** Glx* Cr*** Cho*	Lip 1.3***	–	See footnote <sup>a</sup>
Metastasis	Lip 0.9** Lip 1.3*** Ala*** NAc*** Glx* Cho*	Lip 0.9*** Lip 1.3*** Cr***	Lip 1.3***	See footnote <sup>a</sup>	–

\* $p<0.05$ ; \*\* $p<0.01$ ; \*\*\* $p<0.001$

<sup>a</sup>No statistically significant differences were found between glioblastoma and metastasis using single resonances; nevertheless, some differentiation was achieved with Gly/mI

resonance centred at 1.3 ppm, attributable to lipids. Nevertheless, no statistically significant differences were found between GBM and MET in this study. Accordingly, both tumours were combined in a single group for classification purposes.

The Cr and Cho resonances showed significant differences between LGA and the other astrocytic tumours – AA and GBM – (Table 2). Cho was lower in LGA, whereas Cr was significantly higher. Although differences between AA and the rest of tumours were found for several resonances (Table 2), this tumour group was the one that showed higher overlap with the rest of tumours.

#### Glioblastoma-metastasis

The most characteristic finding of GBM and MET was the presence of a broad resonance of Lip 1.3. This resonance was increased with respect to all the remaining groups. The resonance that showed the highest tendency to differ between GBM and MET was Gly/mI, although no statistically significant values were found.

#### Empirical diagnostic approach path

The resonances that showed the strongest discriminative performance between tumours (Lip 1.3, Ala, Cho and Cr) were included in the discriminatory algorithm (Fig. 2). This algorithm suggested one of four possible outputs (GBM-MET, MEN, LGA and AA) for every particular case using the 90% percentiles of the areas of the involved resonances. The performance of the algorithm was assessed in the database by means of the leave-one-out method. The correct diagnosis was suggested in 83 of 108 cases (77%), whereas in 10 of 108

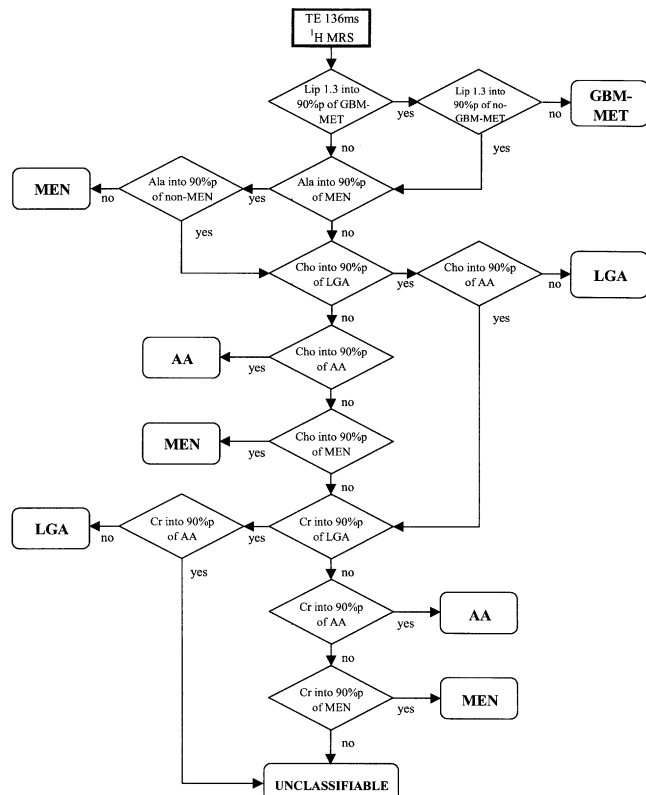


**Fig. 2** Algorithm showing the path followed for discrimination of the most common brain tumours. 90% p 90% percentile; GBM-MET glioblastoma or metastasis; MEN meningioma; LGA low-grade astrocytoma; AA anaplastic astrocytoma

cases (9%) a diagnosis could not be confidently suggested ("unclassifiable tumours"), and in only 15 of 108 cases (14%) did the diagnosis suggested not match with the definitive one. When the algorithm was prospectively applied to an independent test set of 25 tumours, 21

**Table 3** Performance of the empirical method in bilateral differentiation

	Glioblastoma+metastasis			Anaplastic astrocytoma			Low-grade astrocytoma		
	+	?	-	+	?	-	+	?	-
Meningioma	91% (74 of 81)	5% (4 of 81)	4% (3 of 81)	83% (34 of 41)	0	17% (7 of 41)	95% (42 of 44)	0	5% (2 of 44)
Low-grade astrocytoma	93% (62 of 67)	0	7% (5 of 67)	52% (14 of 27)	37% (10 of 27)	11% (3 of 27)			
Anaplastic astrocytoma	86% (55 of 64)	0	14% (9 of 64)						

+ Correct classifications; ? unclassifiable; - incorrect classifications

Totals: + 87% (281 of 324); ? 4% (14 of 324); - 9% (29 of 324)

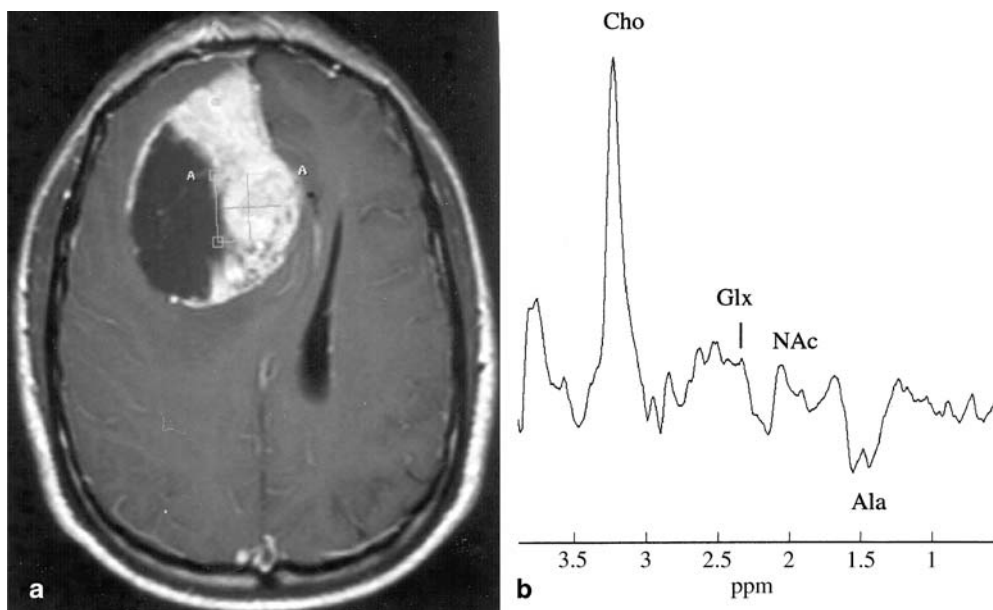


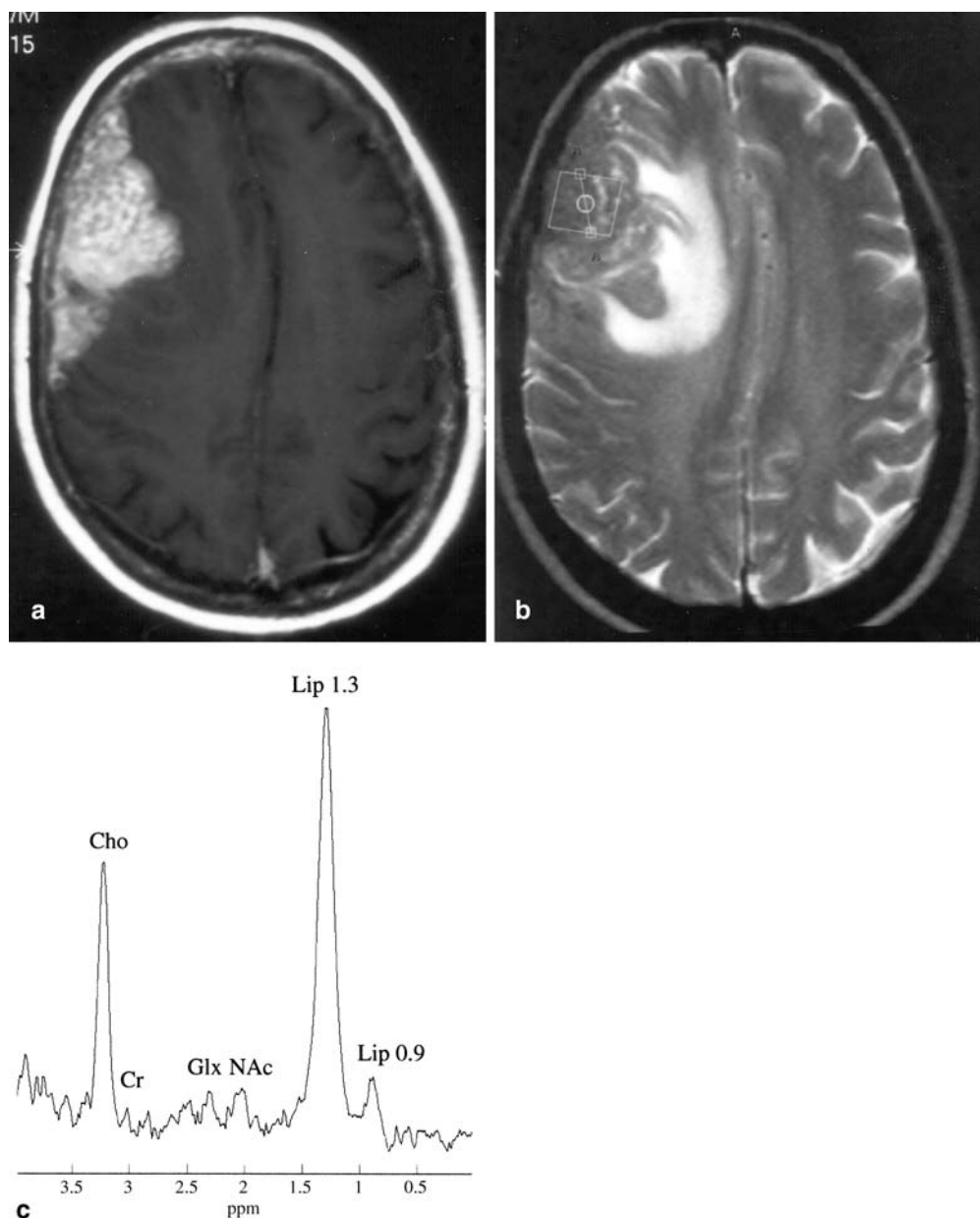
**Fig. 3a, b** Pathologically proven malignant meningioma in a 45-year-old man. **a** Axial T1-weighted contrast-enhanced MR image (TR 541 ms/TE 15 ms) shows a right frontal mixed tumour. There is a solid enhancing medial area and a lateral non-enhancing hypointense area suggesting cyst or necrosis. Peripheral enhancement is also seen. Extra-axial origin, as well as a diagnosis of meningioma, could not be confidently suggested from MRI alone. The  $^1\text{H}$  MRS was carried out in this case for obtaining additional information. The voxel position for  $^1\text{H}$  MRS is shown in the figure. A–A at the edges of the voxel are inerasable marks of the spectroscopic software used. **b** Localized  $^1\text{H}$  MRS (SE; TR/TE/no. of acquisitions: 2000 ms/136 ms/128) of the tumour voxel (line broadening=1 Hz) shows a prominent inverted doublet centred at 1.47 ppm, attributable to Ala. A highly prominent resonance from Cho, as well as some amount of Glx, is also seen in the spectrum. The tumour was classified as meningioma by the empirical algorithm. This diagnosis satisfactorily matched with the final histological one

cases (84%) reached the correct diagnosis, and 4 cases (16%) were incorrectly classified. The potential in discriminating between pairs of groups by this path was also assessed (Table 3), as an approach to the perfor-

mance that radiologist would forecast after excluding some groups of the differential diagnosis list. The GBM and MET were assembled in a single group because no significant differences were found between them in the statistical analysis. Gly/mI was the resonance that showed a higher tendency to differ between these tumour groups. An attempt for differentiation between them was carried out with the 90% range of this resonance. Tumours were empirically classified as MET when the value of Gly/mI was into the 90% range of MET, and as GBM when the value went beyond the 90% percentile of MET. In the training set, 75% (36 of 48) of tumours included in the GBM–MET group was correctly split into GBM or MET by this approach, whereas 25% (12 of 48) tumours were incorrectly classified. Four GBM–MET tumours were excluded for this evaluation because the region of the spectrum corresponding to Gly/mI was considered non-measurable due to superimposition of residual unsuppressed water. In the test set, 9 of 11 GBM–MET tumours (82%) were satisfactorily split into

**Fig. 4a–c** Dural metastasis in a 48-year-old woman suffering from breast cancer. **a** Axial T1-weighted contrast-enhanced MR image (TR 541 ms/TE 15 ms) shows an extra-axial mass in the right frontal lobe. The lesion shows intense and relatively heterogeneous contrast enhancement. **b** Axial T2-weighted MR image (TR 2175 ms/TE 85 ms) shows heterogeneous signal of the tumour. There is oedema in the white matter and mass effect to the surrounding structures. Dural metastasis is the most feasible diagnosis. Nevertheless, no other lesion was found in any other location and, accordingly, meningioma was also considered in the differential diagnosis. Voxel location for  $^1\text{H}$  MRS is shown in the figure. A–A' at the edges of the voxel are inerasable marks of the spectroscopic software used.

**c** Localized  $^1\text{H}$  MRS (SE; TR 2000 ms/TE 136 ms/no. of acquisitions 128) of the tumour (line broadening=1 Hz) shows prominent resonance of lipids at 1.3 ppm with an increase in Cho and a decrease in Cr and NAc. The tumour was classified as glioblastoma–metastasis by means of the empirical path algorithm, giving additional support to the diagnosis of metastasis. Further differentiation between glioblastoma and metastasis by means of Gly/mI included the tumour into the metastasis group



GBM and MET by this approach, whereas 2 of 11 (18%) were incorrectly classified. A MET of the test set was excluded of this procedure, as in the case of the training set, because of poor evaluation of Gly/mI area.

As an example, two cases from our data set in which  $^1\text{H}$  MRS would be of utility for clinical diagnosis are shown in Figs. 3 and 4. Figure 3 shows a heterogeneous para-sagittal tumour in which presence of Ala in  $^1\text{H}$  MRS gave support to a difficult diagnosis of MEN. Figure 4 shows a solitary extra-axial tumour in a 49-year-old woman suffering from a breast carcinoma in which  $^1\text{H}$  MRS provided additional support to the diagnosis of metastasis.

## Discussion

Proton MR spectroscopy ( $^1\text{H}$  MRS) has been recognized as a safe diagnostic technique that can improve the non-invasive categorization of brain disorders and that is starting to have a role in everyday clinical medicine [9, 10, 11, 16, 17, 18, 19, 20]. Presently,  $^1\text{H}$  MRS can be performed with low time requirements on most 1.5-T MR units. This brings to the radiologist the chance of correlating  $^1\text{H}$  MRS information with anatomical MRI findings in the course of a single MR exam. Assembling all this information can be of special interest in the diagnosis of brain tumours. It is well known that MRI find-

ings may be nonspecific in a non-negligible number of patients having focal brain masses, and that a concise diagnosis cannot be suggested occasionally. The  $^1\text{H}$  MRS gives additional biochemical information that may be useful in complementing the MRI findings (Figs. 3, 4) [9, 16, 21]. Nevertheless,  $^1\text{H}$  MRS has not yet been fully introduced in most clinical protocols of brain tumour examination. Knowing the characteristics that better identify every tumour group, as well as having user-friendly methods to apply these characteristics in brain tumour classification, could give an additional support for its introduction in everyday clinical practice. In our study we analyzed the spectroscopic findings of the five more common brain tumour types and evaluated the metabolite resonances that better differed among them. We normalized the values obtained for each resonance area with a method that evaluates not only the relation between two resonances, but also the relationship of every single resonance with the three main ones in normal brain parenchyma (NAc, Cr and Cho). This is a modification of the method described by Tate et al. [2], of easy introduction in daily practice. Our aim was to apply a user-friendly normalization method that provides a global evaluation of the spectrum, avoiding the need for external references, time-consuming measurements of additional parameters or the need of assuming as certain some premises that could bring us uncertain values. The ideal echo time for tumour classification by  $^1\text{H}$  MRS is a point under discussion. In this study we used an echo time of 136 ms because of:

1. Good differentiation between Lact, Ala and lipids due to J-modulation
2. Possible different significance of the observation of lipids in long echo time with respect to short echo time
3. Lower baseline distortion
4. Easy quantification and more reproducible results

Another point under discussion is the selection of single-voxel (SV) or multi-voxel (CSI) MRS techniques. We consider that SV has some major advantages presently in clinical brain tumour discrimination when spatial resolution is not requested (i.e. low time requirements, quicker post-processing of data for obtaining quantitative assessment, and better magnetic field homogeneity in the VOI). Accordingly, we used a SV technique, under the consideration that knowledge obtained could be also applied in future CSI studies. Eight resonances (Lip 0.9, Lip1.3, Lact, Ala, NAc, Glx, Cr and Cho), including some that received little consideration before for brain tumour studies, showed significant differences between tumour groups. It is well known that contribution from  $^1\text{H}$  of different biochemical compounds can appear in the same area of the spectrum, producing a single resonance. Correspondence between a resonance and a particular metabolite would need further ex vivo and in vitro ex-

ams [4, 5, 22] that were beyond the scope of this work. In consequence, we focused on the correlation between spectroscopic patterns and clinical diagnosis, avoiding deductions in the biochemical field that could be uncertain.

We found that MEN, LGA, AA and the highest-grade brain tumours – GBM and MET – can be well differentiated by  $^1\text{H}$  MRS at 136 ms. The MEN is characterized by long echo time  $^1\text{H}$  MRS by the presence of Ala, low Cr and NAc, high Cho and Glx, and absence or low quantities of lipids at 0.90 and 1.30 ppm. Increase in Ala, defined as an inverted doublet centred at 1.47 ppm, has been found to be a consistent and relatively specific finding for MEN [12, 17, 21, 23, 24, 25, 26]. Our results agree with this, as Ala values were higher in MEN than in the rest of tumours included in the study. Three main groups can be considered within astrocytic tumours: LGA; AA; and GBM. In correlation with previous reports in this respect [6, 27], GBM can be identified in this group by high values of Lip 0.9 and Lip 1.3. These two broad resonances have been ascribed to necrotic regions in the in vivo spectra and indicate a high grade of malignancy [6, 27, 28, 29]. Increase in Cho and decrease in Cr in high-grade tumours supported differentiation between AA and LGA. An increase on the metabolites that contribute to the Cho resonance has been considered to correlate with malignancy in astrocytic tumours [6, 23], and with the diagnosis of MEN [3, 12]. In our study, Cho was higher in MEN than in glial tumours. In astrocytomas, Cho was higher in AA and GBM than in LGA; nevertheless, Cho was slightly smaller in GBM than in AA. This could be caused by a preponderance of necrotic areas over viable proliferative cellular areas in the sampled voxel for GBM, a fact that may vary between studies depending on voxel positioning strategy and size [23]. The AA was the tumour that showed worse results in terms of tumour classification (Table 3). These results must be evaluated taking into account that some inconsistencies between biopsy samples and  $^1\text{H}$  MRS may be due to the histological heterogeneity of astrocytic tumours and to some overlap between grades. Besides, reproducibility in tumour grading by histology has also been reported to be difficult [30].

Metastases are high-grade brain lesions in which presence of necrosis, represented by long echo time spectrum by broad resonances centred at 0.90 and 1.30 ppm, may be expected. Our study confirms a significant increase of these lipid resonances in MET, in contrast with lower-grade tumours. We did not find any statistically significant difference between GBM and MET in the resonances defined in our study; accordingly, we considered them as a single group for classification purposes. Unfortunately, to date, single-voxel  $^1\text{H}$  MRS has not shown robust enough results in their differentiation [13, 18, 29]. In vitro studies with biopsy samples have suggested an increase in glycine being discriminative be-

tween GBM and MET [23]. Gly/mI showed a tendency to be higher in GBM than in MET in our study. We obtained promising results in differentiation between GBM and MET by means of Gly/mI values, with successful separation of 36 of 48 cases (75%) in the training set and 9 of 11 cases (82%) in the test set.

On the basis of the differences found, we developed an empirical method that classified every case into one of four groups (GBM–MET, MEN, LGA or AA). This method produced a success percentage of 77%, with only 14% incorrect classifications, suggesting that the findings obtained in our study could be of utility in classifying tumours. We also had satisfactory results in bilateral discrimination between pairs of groups, illustrating the possible improvement of results forecasted when some groups could be confidently excluded from the differential diagnosis by previous non-MRS information. These results are in the range of previous work in brain tumours [2, 9, 31, 32], especially taking into account that we have discriminated between four groups, and that we included differentiation between LGA, AA and GBM–MET in the algorithm. Introduction of an independent test set of tumours, not used for training the system, with 84% (21 of 25) correct classifications, provides strong validation for our results [2, 33, 34]. Previous work has assessed the utility of  $^1\text{H}$  MRS in brain tumour classification. In this respect, Preul et al. achieved a 99% rate success with CSI, evaluating six major biochemical resonances in 105 spectra, and applying linear

discriminant analysis (LDA) [15]. Using a similar spectroscopic approach, Burtscher et al. [10] did not confirm this high diagnostic accuracy. Usenius et al. [9] assessed PRESS  $^1\text{H}$  MRS as a diagnostic method for differentiating between benign glial tumours, malignant glial tumours and “others” in a series of 33 tumours, with an 82% rate of success. Tate et al. [2] used LDA for differentiating between spectra from meningioma, oligodendrogloma, metastasis and two groups of astrocytic tumours (with high and low intensity of lipid signal). They obtained good results in the pairwise comparison between all tumours. We report here a simple method of brain tumour discrimination that uses an empirical path based on the 90% percentiles of some “discriminative” resonance areas. Until a definitive robust classification method appears, preliminary methods, such as the one reported by us, provide a way to exploit the quantitative potential of  $^1\text{H}$  MRS, as well as to prospectively test the usefulness and reproducibility of some spectroscopic findings in brain tumour discrimination. The major advantages of our method are that it allows an easy identification of the resonances on which the suggestion of a particular diagnosis rests, and that it is of easy implementation in a clinical setting.

**Acknowledgment** This work was supported in part by grants CIRIT XT-2000-43, SGR-2001-194, CICYT SAF-1999-101 and EU IST-1999-10310.

## References

- Van den Boogaart A (1997) Quantitative data analysis of in vivo MRS data sets. *Magn Reson Chem* 35:S146–S152
- Tate AR, Griffiths JR, Martínez-Pérez I et al. (1998) Towards a method for automated classification of  $^1\text{H}$  MRS spectra from brain tumours. *NMR Biomed* 11:177–191
- Kugel H, Heindel W, Ernestus RI, Bunke J, du Mesnil R, Friedmann G (1992) Human brain tumors: spectral patterns detected with localized H-1 MR spectroscopy. *Radiology* 183:701–709
- Martínez-Pérez I, Moreno A, Alonso J et al. (1997) Diagnosis of brain abscess by magnetic resonance spectroscopy. Report of two cases. *J Neurosurg* 86:708–713
- Barba I, Moreno A, Martínez-Pérez I et al. (2001) Magnetic resonance spectroscopy of brain hemangiopericytomas: high myoinositol concentrations and discrimination from meningiomas. *J Neurosurg* 94:55–60
- Negendank WG, Sauter R, Brown TR et al. (1996) Proton magnetic resonance spectroscopy in patients with glial tumors: a multicenter study. *J Neurosurg* 84:449–458
- Ernst T, Hennig J (1991) Coupling effects in volume selective  $^1\text{H}$  spectroscopy of major brain metabolites. *Magn Reson Med* 21:82–96
- De Edelenyi FS, Rubin C, Estève F et al. (2000) A new approach for analyzing proton magnetic resonance spectroscopic images of brain tumors: nosologic images. *Nat Med* 6:1287–1289
- Usenius JR, Kauppinen RA, Vainio PA et al. (1994) Quantitative metabolite patterns of human brain tumors: detection by  $^1\text{H}$  NMR spectroscopy in vivo and in vitro. *J Comput Assist Tomogr* 18:705–713
- Burtscher IM, Skagerberg G, Geijer B, Englund E, Ståhlberg F, Holtås S (2000) Proton MR spectroscopy and preoperative diagnostic accuracy: an evaluation of intracranial mass lesions characterized by stereotactic biopsy findings. *Am J Neuroradiol* 21:84–93
- Adamson AJ, Rand SD, Prost RW, Kim TA, Schultz C, Haughton VM (1998) Focal brain lesions: effect of single-voxel proton MR spectroscopic findings on treatment decisions. *Radiology* 209:73–78
- Shimizu H, Kumabe T, Tominaga T et al. (1996) Noninvasive evaluation of malignancy of brain tumors with proton MR spectroscopy. *Am J Neuroradiol* 17:737–747
- Poptani H, Gupta RK, Roy R, Pandey R, Jain VK, Chhabra DK (1995) Characterization of intracranial mass lesions with in vivo proton MR spectroscopy. *Am J Neuroradiol* 16:1593–1603
- Rand SD, Prost D, Haughton V et al. (1997) Accuracy of single-voxel proton MR spectroscopy in distinguishing neoplastic from nonneoplastic brain lesions. *Am J Neuroradiol* 18:1695–1704

15. Preul MC, Caramanos Z, Collins DL et al. (1996) Accurate, noninvasive diagnosis of human brain tumors by using proton magnetic resonance spectroscopy. *Nat Med* 2:323–325
16. Dowling C, Bollen AW, Noworolski SM et al. (2001) Preoperative proton MR spectroscopy imaging of brain tumors: correlation with histopathologic analysis of resection specimens. *Am J Neuroradiol* 22:604–612
17. Ross B, Michaelis T (1994) Clinical applications of magnetic resonance spectroscopy. *Magn Reson Q* 10:191–247
18. Ott D, Henning J, Ernst T (1993) Human brain tumors: assessment with in vivo proton MR spectroscopy. *Radiology* 186:745–752
19. Castillo M, Kwock L, Mukherji SK (1996) Clinical applications of proton MR spectroscopy. *Am J Neuroradiol* 17:1–15
20. Ishimaru H, Morikawa M, Iwanaga S, Kaminogo M, Ochi M, Hayashi K (2001) Differentiation between high-grade glioma and metastatic brain tumor using single-voxel proton MR spectroscopy. *Eur Radiol* 11:1784–1791
21. Majós C, Cucurella G, Aguilera C, Coll S, Pons LC (1999) Intraventricular meningiomas: MR imaging and MR spectroscopic findings in two cases. *Am J Neuroradiol* 20:882–885
22. Grand S, Passaro G, Ziegler A et al. (1999) Necrotic tumors versus brain abscess: importance of amino acids detected at  $^1\text{H}$  MR spectroscopy. Initial results. *Radiology* 213:785–793
23. Kinoshita Y, Yokota A (1997) Absolute concentrations of metabolites in human brain tumors using *in vitro* proton magnetic resonance spectroscopy. *NMR Biomed* 10:2–12
24. Kinoshita Y, Kajiwara H, Yokota A, Koga Y (1994) Proton magnetic resonance spectroscopy of brain tumors: an *in vitro* study. *Neurosurgery* 35:606–614
25. Lehnhardt FG, Röhn G, Ernestus RI, Grüne M, Hoehn M (2001)  $^1\text{H}$ - and  $^{31}\text{P}$ -MR spectroscopy of primary and recurrent human brain tumors *in vitro*: malignancy-characteristic profiles of water soluble and lipophilic spectral components. *NMR Biomed* 14:307–317
26. Castillo M, Kwock L, Scatliff J, Mukherji SK (1998) Proton MR spectroscopy in neoplastic and non-neoplastic brain disorders. *MRI Clin North Am* 6:1–20
27. Tien RD, Lai PH, Smith JS, Lazeyras F (1996) Single-voxel proton brain spectroscopy exam (PROBE/SV) in patients with primary brain tumors. *Am J Roentgenol* 167:201–209
28. Sijens PE, Knopp MV, Brunetti A et al. (1995)  $^1\text{H}$  MR spectroscopy in patients with metastatic brain tumors: a multi-center study. *Magn Reson Med* 33:818–826
29. Gotsis ED, Fountas K, Kapsalaki E, Toulas P, Peristeris G, Papadakis N (1996) In vivo proton MR spectroscopy: the diagnostic possibilities of lipid resonances in brain tumors. *Anticancer Res* 16:1565–1568
30. Mittler MA, Walters BC, Stopa EG (1996) Observer reliability in histological grading of astrocytoma stereotactic biopsies. *J Neurosurg* 85:1091–1094
31. Wang Z, Sutton LN, Cnaan A et al. (1995) Proton MR spectroscopy of pediatric cerebellar tumors. *Am J Neuroradiol* 16:1821–1833
32. Arle JE, Morris C, Wang ZJ, Zimmerman RA, Phillips PG, Sutton LN (1997) Prediction of posterior fossa tumor type in children by means of magnetic resonance image properties, spectroscopy, and neural networks. *J Neurosurg* 86:755–761
33. Roser W, Harberg G, Mader I et al. (1997) Assignment of glial brain tumors in humans by *in vivo*  $^1\text{H}$  magnetic resonance spectroscopy and multidimensional metabolic classification. *Magma* 5:179–183
34. Miller AJ (ed) (1990) Subset selection in regression. Chapman and Hall, London



**4.2. Trabajo 2:**

Adult primitive neuroectodermal tumor: Proton MR Spectroscopic findings with possible application for differential diagnosis. Majós C, Alonso J, Aguilera C, Serrallonga M, Acebes JJ, Arús C, Gili J. Radiology 2002; 225: 556-566.



Carles Majós, MD  
 Juli Alonso, PhD  
 Carles Aguilera, MD  
 Marta Serrallonga, MD  
 Juan J. Acebes, MD, PhD  
 Carles Arús, PhD  
 Jaume Gili, MD, PhD

**Index terms:**

Brain neoplasms, diagnosis, 10.36  
 Brain neoplasms, MR, 10.121411,  
 10.121413, 10.12143  
 Magnetic resonance (MR) spectroscopy,  
 10.12145  
 Primitive neuroectodermal tumor,  
 10.3637, 10.364

Published online before print  
 10.1148/radiol.2252011592  
*Radiology* 2002; 225:556–566

**Abbreviations:**

Ala = alanine  
 CHO = choline and other trimethyl-amine-containing compounds  
 CR = creatine plus phosphocreatine  
 GLX = glutamate and glutamine  
 Gly/MI = glycine and/or myoinositol  
 LACT = lactate  
 LIP = lipid  
 LIP 0.90 = LIP at 0.90 ppm  
 LIP 1.30 = LIP at 1.30 ppm  
 NACC = *N*-acetyl-containing compounds  
 $P^*$  = corrected *P* value  
 PNET = primitive neuroectodermal tumor

<sup>1</sup> From the Institut de Diagnostic per la Imatge (IDI), Department of Diagnostic Imaging, Hospital Duran i Reynals, CSU de Bellvitge, Autovía de Castelldefels km 2,7, 08907 L'Hospitalet de Llobregat, Barcelona, Spain (C.M., J.A., C. Aguilera, M.S., J.G.); Department of Neurosurgery, Hospital Príncipes de España, CSU de Bellvitge, L'Hospitalet de Llobregat, Barcelona, Spain (J.J.A.); and Department of Biochemistry and Molecular Biology, Universitat Autònoma de Barcelona, Cerdanyola del Vallès, Spain (C. Arús). Received October 1, 2001; revision requested December 10; revision received January 28, 2002; accepted March 14. Supported in part by the Generalitat de Catalunya (grants CIRIT XT2000 43 and SGR1999-328), the Interministerial Commission on Science and Technology (CICYT SAF1999-101), and the European Union (IST1999-10310). Address correspondence to C.M. (e-mail: cmajos@csub.scs.es).

**Author contributions:**

Guarantors of integrity of entire study, C.M., J.A.; study concepts, C.M., J.A., C. Aguilera, J.G.; study design, C.M., C. Aguilera, M.S., J.J.A., C. Arús; literature research, C.M., J.A., M.S., C. Arús; clinical studies, J.J.A.; data acquisition, C.M., M.S., C. Aguilera; data analysis/interpretation, C.M., J.A., C. Aguilera, J.G.; statistical analysis, C.M., C. Aguilera; manuscript preparation, C.M., J.A., C. Aguilera; manuscript definition of intellectual content, C.M., J.A., C. Arús, J.G.; manuscript editing and revision/review, C.M., C. Aguilera; manuscript final version approval, all authors.

© RSNA, 2002

# Adult Primitive Neuroectodermal Tumor: Proton MR Spectroscopic Findings with Possible Application for Differential Diagnosis<sup>1</sup>

**PURPOSE:** To assess the utility of proton magnetic resonance (MR) spectroscopy in the clinical categorization of primitive neuroectodermal tumors (PNETs) in adults.

**MATERIALS AND METHODS:** In vivo proton MR spectroscopy was performed with an echo time of 136 msec in nine adults with PNET, and findings were retrospectively compared with spectroscopic findings of 22 meningiomas, 12 low-grade astrocytomas, eight anaplastic astrocytomas, 23 glioblastomas, and 21 metastases. Nine resonances were semiquantitatively evaluated. Statistical analysis was performed by using Kruskal-Wallis and Mann-Whitney *U* tests. The Hochberg correction was applied for multiple comparisons. Results were prospectively validated in 24 tumors of the six types included in the study.

**RESULTS:** The resonances of choice for identifying PNET were alanine ( $P < .001$ ) and glutamate and glutamine ( $P = .004$ ), both decreased with respect to meningioma; choline increased with respect to low-grade ( $P < .001$ ) and anaplastic astrocytoma ( $P = .055$ ); and lipids at 1.30 ppm decreased and choline and other trimethyl-amine-containing compounds increased with respect to glioblastoma ( $P < .001$  and  $P = .004$ , respectively) and metastasis ( $P < .001$  and  $P = .021$ , respectively). We developed an algorithm for bilateral differential diagnosis between PNET and other tumor types. The leave-one-out method was used to test the five possible differential situations in the retrospective data set, with the following results: PNET versus meningioma, 31/23/5/3 (number of total/correct/unclassifiable/incorrect procedures); PNET versus low-grade astrocytoma, 21/19/2/0; PNET versus anaplastic astrocytoma, 17/6/9/2; PNET versus glioblastoma, 32/28/2/2; and PNET versus metastasis, 30/27/1/2. In total, 131 consecutive procedures produced 103 (79%) correct classifications and nine (7%) misclassifications. Twenty-five (78%) of 32 possible procedures in the prospective independent test set produced correct classifications and four (13%) produced incorrect classifications.

**CONCLUSION:** In vivo proton MR spectroscopy provides useful information in clinical differentiation between PNETs and common brain tumors in adults.

© RSNA, 2002

Primitive neuroectodermal tumors (PNETs) include a heterogeneous group of tumors thought to originate from primitive or undifferentiated neuroepithelial cells that typically occur in pediatric patients. The prototype of these tumors is cerebellar medulloblastoma, which constitutes 13%–25% of all pediatric brain tumors (1–3). Only 20%–30% of PNETs occur in adults, constituting up to 1% of all brain tumors in this age group (1,2,4,5). The typical cerebellar PNET is a midline tumor of well-defined margins that homogeneously enhances after contrast material administration at both computed tomographic (CT) and magnetic resonance (MR) imaging (1–3,6,7). As opposed to pediatric tumors, medulloblas-

tomas in adults tend to result in a higher frequency of atypical findings (4,8), to the point that some authors have suggested always considering medulloblastoma in the differential diagnosis of a posterior fossa mass in an adult (4). On the other hand, supratentorial PNETs are uncommon highly heterogeneous tumors that can mimic other high-grade tumors on MR images (9). The high frequency of atypical findings and the low incidence of PNET in adults can make PNET diagnosis difficult in some cases. In this context, additional information from new diagnostic techniques such as proton MR spectroscopy would be welcomed to reinforce the differential diagnosis with other tumors.

Proton MR spectroscopy is a noninvasive imaging technique for measuring the biochemical content of living tissue that can now be performed with most 1.5-T clinical MR imaging instruments. This biochemical information may produce additional data about tumor metabolism that may be useful in tumor diagnosis. Several studies (10–28) have evaluated proton MR spectroscopy in the most common brain tumors both *in vivo* and *in vitro*, but little interest has been shown in PNET, especially in adults. The aim of the present study was to assess the utility of proton MR spectroscopy as a noninvasive tool for clinical categorization of PNET in adults.

## MATERIALS AND METHODS

### Patients

We retrospectively evaluated nine consecutive proton MR spectroscopic examinations in nine patients (eight men and one woman; 18–67 years of age; mean age, 30.8 years) with intracranial PNET (two supratentorial and seven infratentorial). Tumors were untreated in six patients and recurrent in the other three. All neoplasms were confirmed histopathologically. We compared the results obtained in PNETs with a data set of 86 proton MR spectra of the most frequent brain tumors in 86 adults (45 women and 41 men; 14–81 years of age; mean age, 54.7 years). This comparative data set included meningiomas ( $n = 22$ ), low-grade astrocytomas ( $n = 12$ ), anaplastic astrocytomas ( $n = 8$ ), glioblastomas ( $n = 23$ ), and metastases ( $n = 21$ ). Proton MR spectroscopic findings obtained under identical conditions in the white matter of six healthy volunteers were also considered references. Nevertheless, assessment of differences be-

tween normal brain parenchyma and tumoral tissue, well established in previous work (10–14), was considered to be out of the scope of this study.

To test the reproducibility of differences found between tumors and their application in diagnosis, 51 consecutive proton MR spectroscopic examinations were prospectively performed in 51 patients with brain lesions that suggested tumor. Cases in which a definitive diagnosis was available on the basis of the same criteria as the retrospective training set and in which the diagnosis was one of the six tumor types included in the study were included in the definitive test set. Twenty-seven patients (no definitive diagnosis,  $n = 13$ ; diagnosis other than tumor,  $n = 7$ ; diagnosis of tumor other than one of the six types included in the study,  $n = 7$ ) did not match these criteria and were excluded from the test set. The definitive test set included 24 proton MR spectra corresponding to PNET ( $n = 2$ ; one supratentorial and one infratentorial), meningioma ( $n = 7$ ), low-grade astrocytoma ( $n = 3$ ), anaplastic astrocytoma ( $n = 4$ ), glioblastoma ( $n = 2$ ), and metastasis ( $n = 6$ ). The study was approved by our institutional review board and informed consent obtained from all patients and volunteers.

### MR Imaging

In all patients, MR imaging was performed with a 1.5-T unit (ACS-NT; Philips Medical Systems, Best, the Netherlands) in the three orthogonal planes, including at least T1- (536–541/15) (repetition time [TR] msec/echo time [TE] msec), intermediate- (2,175/20) and T2- (2,175/85) weighted images. T1-weighted images were obtained in at least two planes after intravenous administration of 0.1 mmol per kilogram of body weight of gadolinium-based contrast material (Magnevist; Schering, Berlin, Germany, or Omniscan; Nycomed, Oslo, Norway). Fast fluid-attenuated inversion recovery, or FLAIR (6,706/120/2,000 [TR msec/TE msec/inversion time msec]; turbo factor, 15 msec) images were available for six PNETs.

### Proton MR Spectroscopy

In all 125 cases (nine retrospective PNETs, 86 retrospective comparative data set tumors, six healthy volunteers, and 24 prospective test set tumors), proton MR spectroscopy was performed with the same MR unit by using a point-resolved spectroscopic sequence. A volume of in-

terest between  $1.5 \times 1.5 \times 1.5 \text{ cm}^3$  (3.4 mL) and  $2 \times 2 \times 2 \text{ cm}^3$  (8.0 mL) was placed by one of three authors (C.M., C. Aguilera, or M.S.) following the meeting of consensus criteria. The volume of interest size and position were determined by examining the MR images in all three dimensions (sagittal, coronal, and transverse planes), with the aim of positioning the largest possible voxel within the solid tumoral area, as judged at MR image inspection, with avoidance of areas of cysts or necrosis and with minimum contamination from the surrounding nontumoral tissue. A standard receiver head coil was used in all cases, and spectroscopy was incorporated into the course of a conventional MR imaging examination. Automatic shimming of the linear X, Y, and Z channels was used to optimize field homogeneity. The water resonance was set on resonance, and the water suppression pulse was optimized. Proton MR spectroscopic examinations were performed by using a spin-echo pulse sequence with parameters of 2,000/136. A total of 512 data points were collected over a spectral width of 1,000 Hz. Four dummy scans and 128 or 192 signals acquired, depending on voxel size, were obtained for each spectrum. Spectral analysis was performed off-line with the use of MRUI software (available through the MRUI Project, [www.carbon.uab.es/mrui](http://www.carbon.uab.es/mrui)) (29). Time domain data were analyzed with the variable projection method (29) after filtering the residual water signal by using the Henkel-Lanczos singular-value decomposition algorithm.

Assignment of the resonances of interest, including N-acetylaspartate and other N-acetyl-containing compounds (NACCs) at 2.02 ppm, creatine plus phosphocreatine (CR) at 3.03 ppm, choline and other trimethyl-amine-containing compounds (CHO) at 3.20 ppm, lipids (LIPs) at 0.90 ppm (LIP 0.90) and 1.30 ppm (LIP 1.30), glutamate and glutamine (GLX) at 2.35 ppm, and glycine and/or myoinositol (Gly/MI) at 3.55 ppm was based on previous studies of brain tumors (10,11,15–21,30–33) and phantoms (15,30). Two inverted doublets due to phase modulation from J coupling were defined that corresponded to lactate (LACT) centered at 1.35 ppm and to alanine (Ala) at 1.47 ppm. Each of these nine resonances (LIP 0.90, LIP 1.30, LACT, Ala, NACC, GLX, CR, CHO, and Gly/MI) was considered separately for statistical analysis. Resonances in the region of taurine above the noise level were not detectable in most cases and, accordingly, taurine resonance

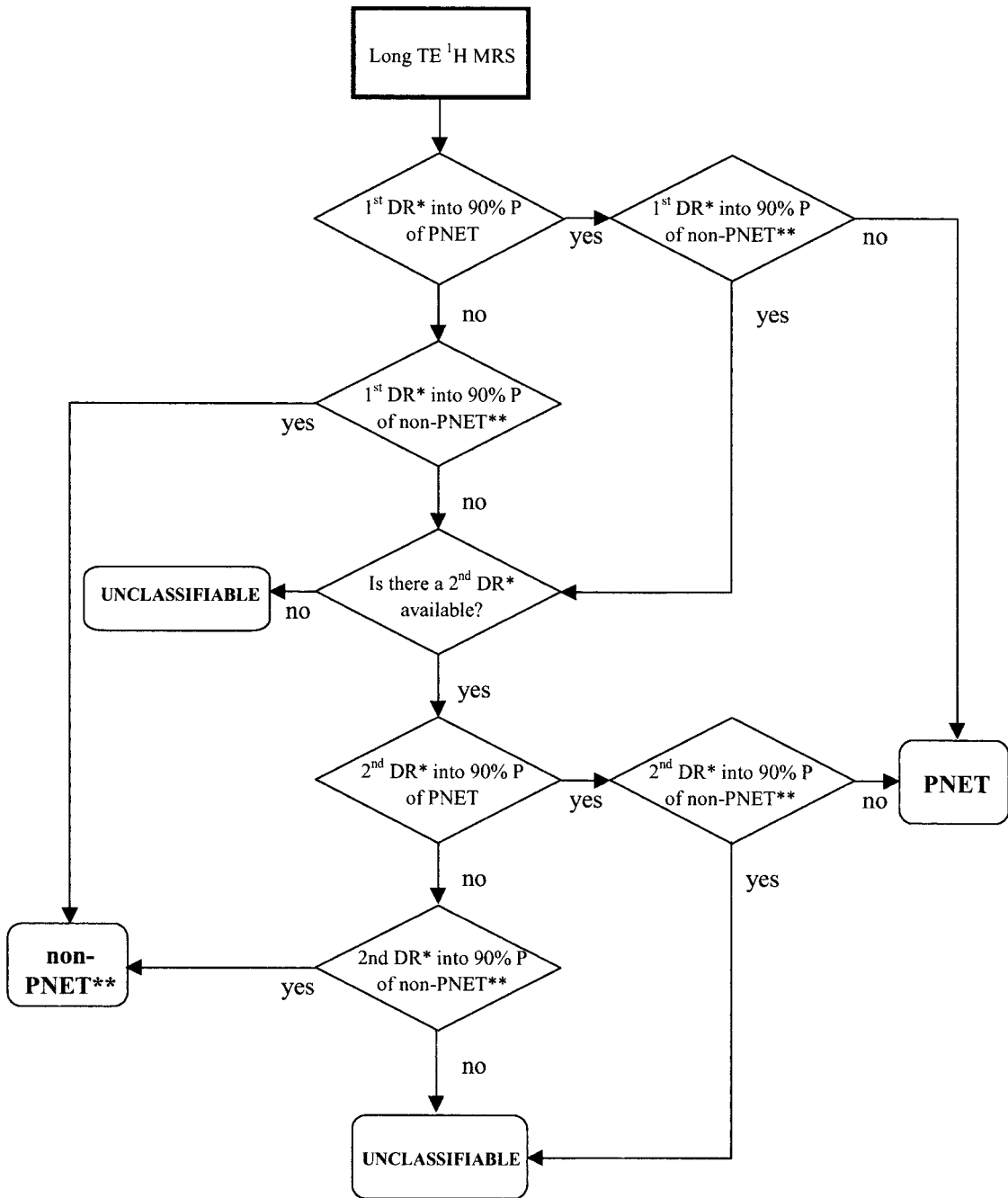


**Figure 1.** Flow chart shows the empiric path used for bilateral differential diagnosis of PNET. DR = discriminative resonance, <sup>1</sup>H MRS = proton MR spectroscopy, 90% P = 90th percentile. \* = First and second discriminative resonances may vary depending on the tumor type to be differentiated from PNET. \*\* = Non-PNET tumors were meningioma, low-grade astrocytoma, anaplastic astrocytoma, glioblastoma, and metastasis. TE = echo time.

was not quantified. Water (4.75 ppm) and/or CR (3.03 ppm) were chosen as chemical shift reference resonances to correct possible shifting in the frequency domain. To avoid operator bias, resonance peaks were defined in the frequency domain even when there were doubts about their differentiation from noise. Our criterion was that further

quantification and analysis result in differences between noise and metabolite signal without operator influence. An area of "0" was assigned only to resonances in which the software program used did not satisfactorily fit a peak in the area of interest.

For comparative purposes, the program-fitted resonance areas for LACT, Ala,

NACC, GLX, CR, CHO, and Gly/MI resonances were normalized by dividing each value by the square root of the sum of the squares of the three main spectroscopic resonances ( $x = 100 \times \frac{x_i}{(NACC^2 + CR^2 + CHO^2)^{1/2}}$ , where  $x_i$  is the original area of the resonance being normalized), in a modification of the method used by Tate et al (16). For normalization of the

**TABLE 1**  
MR Imaging Findings in PNETs in Nine Adults

Patient No./Age (y)	PNET Location	Maximum Diameter (mm)	MR Imaging						Margin Definition	Lesion Heterogeneity	Blood into the Tumor	Necrosis and/or Cysts
			T1-weighted	Intermediate-weighted	T2-weighted	FLAIR	Contrast Enhancement					
1/67	Frontal lobe	75	Hypo	Hyper	Hyper	NA	Intense	Good	Highly heterogeneous	Yes	Yes	
2/28	Cerebellar hemisphere	56	Hypo	Iso	Hyper	NA	Moderate	Poor	Heterogeneous	No	No	
3/40	Cerebellar hemisphere	44	Hypo	Hyper	Hyper	Hyper	Intense	Poor	Heterogeneous	No	Yes	
4/24	Frontal lobe and corpus callosum	70	Iso	Iso	Iso	Iso	Moderate	Poor	Highly heterogeneous	Yes	Yes	
5/18	Cerebellar vermis	34	Hypo	Iso	Hyper	NA	Moderate	Good	Homogeneous	No	No	
6/21	Cerebellar hemisphere	52	Hypo	Hyper	Hypo	Hyper	Intense	Poor	Heterogeneous	No	Yes	
7/29	Cerebellar vermis	58	Hypo	Iso	Hyper	Iso	Moderate	Good	Heterogeneous	No	Yes	
8/27	Cerebellar hemisphere	46	Hypo	Iso	Iso	Iso	Moderate	Poor	Heterogeneous	No	Yes	
9/23	Cerebellar hemisphere	44	Hypo	Hyper	Hyper	Hyper	Intense	Good	Heterogeneous	No	Yes	

Hyper = hyperintense with respect to gray matter, Hypo = hypointense with respect to gray matter, Iso = isointense with respect to gray matter, NA = not available.

resonance areas of LIPs, the square value of LIP 0.90 and 1.30 was included in the sum of the denominator [ $x = 100 \times xi / [(NACC^2 + CR^2 + CHO^2 + LIP 0.90^2 + LIP 1.30^2)^{1/2}]$ ]. Data obtained were used to compare PNETs with the other tumor types to assess which findings were characteristic of this tumor at *in vivo* spectroscopy. We should emphasize, as have authors of previous studies (22,31), that we assigned these characteristic resonances not to a particular metabolite but to a resonance in the spectrum, taking into account that a particular resonance origin should not be directly extrapolated to a particular metabolite without further *ex vivo* and *in vitro* examination (15,32,34).

## Statistics

The goal of the current study was to determine whether there were significant differences between PNETs and each of the other common brain tumors in adults (meningiomas, low-grade astrocytomas, anaplastic astrocytomas, glioblastomas, and metastases) and to design a procedure to distinguish PNETs from the rest of the tumors. To this end, we considered the nine metabolite resonances and determined which tumor type produced significant differences with respect to PNETs.

We performed Kruskal-Wallis nonparametric analysis of variance for each metabolite resonance to test for significant differences among the six tumor types.

Then, to compare the group of interest (PNETs) with the other tumor types, Mann-Whitney *U* tests were performed. Because we considered five statistical tests for every metabolite resonance, we corrected the obtained *P* values by using the Hochberg method (35). Then the significant differences were defined by using the corrected *P* values (*P*\* instead of the original *P* value. Differences of *P*\* less than .05 were considered statistically significant. Statistics were computed with SPSS software (SPSS, Chicago, Ill).

## Empirical Method for Bilateral Differential Diagnosis of PNET

With the aim of testing the usefulness of differences between PNETs and the rest of the tumors in PNET identification, we elaborated an empiric path for discrimination between PNETs and the rest of the tumors in pairwise comparisons. This path used the 90th percentiles of the resonances that showed the strongest discriminative performance (one or two for every bilateral comparison) in the tumors under consideration. A scheme of this path is shown in Figure 1. In the first step, the case was included in one of the two tumor groups being compared if the value for the first discriminative resonance was in the 90th percentile of one of the tumor types. Values in the overlapping area of the 90th percentile or between the boundaries of these percentiles were considered transitorily unclassifiable. A second step was performed, when

possible, in the transitorily unclassifiable group by using a second discriminative resonance. This path was developed by using the retrospective data set. Its performance was tested in the retrospective training set by using the leave-one-out method and in a prospective independent test set.

## RESULTS

### MR Imaging

The imaging findings in the nine PNETs are summarized in Table 1. Only one (14%) of the seven posterior fossa PNETs showed the typical aspect of medulloblastomas reported in childhood as a homogeneous lesion of the inferior vermis with well-defined margins and homogeneous enhancement with contrast material administration (3,6–8,36). The rest were heterogeneous tumors. Five (71%) of seven infratentorial PNETs were located in the cerebellar hemisphere, while only two (29%) were in their typical location in the vermis. The signal intensity of the tumors was diverse with the sequences performed. In the current study, PNETs were most commonly found to be heterogeneous lesions with poorly defined margins located in the cerebellar hemisphere (four [44%] of nine tumors). Three (43%) of seven posterior fossa PNETs were heterogeneous poorly defined tumors located in the cerebellar hemispheres with areas of cysts and/or necrosis.

## Proton MR Spectroscopy

The means and SDs of resonances in the nine PNETs, the 86 other tumors in the retrospective data set, and the six healthy volunteers are shown in Table 2. The metabolite resonances found to differ significantly between PNETs and other tumor groups are indicated, and relevant  $P^*$  values are shown.

PNETs were characterized by high CHO resonances and low Ala, NACC, CR, and LIP resonances (Table 2). Scatter diagrams of the resonances that showed greater differences between tumors are shown in Figure 2. CHO and NACC were the strongest discriminative resonances in the pairwise comparison between PNETs and the rest of the tumors and showed significant differences at comparison with low-grade astrocytoma ( $P^* < .001$  and  $P^* = .013$  for CHO and NACC, respectively), glioblastoma ( $P^* = .004$  and  $P^* = .013$ ), and metastasis ( $P^* = .021$  and  $P^* = .010$ ) (Fig 2, Table 2). CR also showed significant differences at comparison with low-grade astrocytoma ( $P^* < .001$ ) and glioblastoma ( $P^* = .012$ ). Ala and GLX were significantly decreased with respect to meningiomas ( $P^* < .001$  and  $P^* = .004$ , respectively) (Table 2). Ala resonance was detectable in four PNETs in amounts lower than those in meningiomas. Broad resonances at 1.30 ppm that were attributable to LIPs were found in only one PNET, with a lower signal than those in glioblastomas and metastases (Fig 2c). In the rest of the cases, no LIP signals were detectable ( $P^* < .001$  for LIP 1.30 between PNET and glioblastoma;  $P^* < .001$  for LIP 1.30 between PNET and metastasis). In this context, CHO, NACC, and CR were the resonances of choice for discriminating PNET from low-grade astrocytomas; LIP 1.30, for distinguishing PNET from glioblastoma and metastasis; and Ala, for discriminating between PNET and meningioma. Anaplastic astrocytomas showed the greatest similarity to PNET, with overlapping of most resonance values (Fig 2; Table 2) and a lack of significant differences. In this context, the resonances that showed the greatest tendency to differ between this tumor group and PNETs were CHO ( $P^* = .055$ ) and CR ( $P^* = .062$ ).

Comparison of supra- and infratentorial PNETs, as well as of treated and untreated tumors, showed no major differences at visual evaluation and after quantification. Statistical analysis was still considered inappropriate because of the small number of cases in some un-

common subgroups (ie, supratentorial PNET).

## Empirical Method for Bilateral Differential Diagnosis of PNET

The resonances that showed the strongest discriminative performance and thus were considered "first discriminative resonances" with PNET were Ala for meningioma, CHO for low-grade and anaplastic astrocytoma, and LIP 1.30 for glioblastoma and metastasis. Additional discriminative utility was found in GLX for meningioma and in CHO for metastasis and glioblastoma; accordingly, these resonances were chosen as second discriminative resonances for these tumors. This second step was considered inappropriate for low-grade and anaplastic astrocytomas, since the values of the alternative resonances (NACC and CR) had a possible correlation with the elective one (CHO) because of the normalization method used. Table 3 shows the resonances of choice for pairwise comparison in this study, the boundaries used for application of the path shown in Figure 1, and the results obtained at categorization of the retrospective data set, as assessed by using the leave-one-out method (16,22). A total of 131 differential procedures were used to test the system in the retrospective training set by using the leave-one-out method: (a) five testing procedures were performed with every PNET ( $n = 9$ ) to test the algorithm versus every one of the other five tumor types (total, 45 procedures); (b) only one testing procedure was performed in every non-PNET tumor ( $n = 86$ ) to test the procedure that differentiated this tumor type from PNET (total, 86 procedures). One hundred three (79%) of 131 total bilateral procedures produced a correct classification, while 19 (14%) were unclassifiable, and nine (7%) were incorrectly classified. We point out that these global rates are not a direct absolute estimate of the global probability of correct classification but an orientational evaluation of the performance of the method. Table 3 shows the range of results in the five bilateral comparison algorithms considered.

Examples of the potential use of proton MR spectroscopy in the differential diagnosis of PNET are shown in Figures 3–7. Figures 3–5 include examples of midline posterior fossa tumors with similar homogeneous MR imaging signal patterns, in which a definitive diagnosis could not be established with MR imaging alone. These figures include PNET (Fig 3), metastasis (Fig 4), and meningi-

**TABLE 2**  
Normalized Area Values of Nine Metabolite Resonances from Database of 95 Brain Tumors Analyzed with *In Vivo* Proton MR Spectroscopy

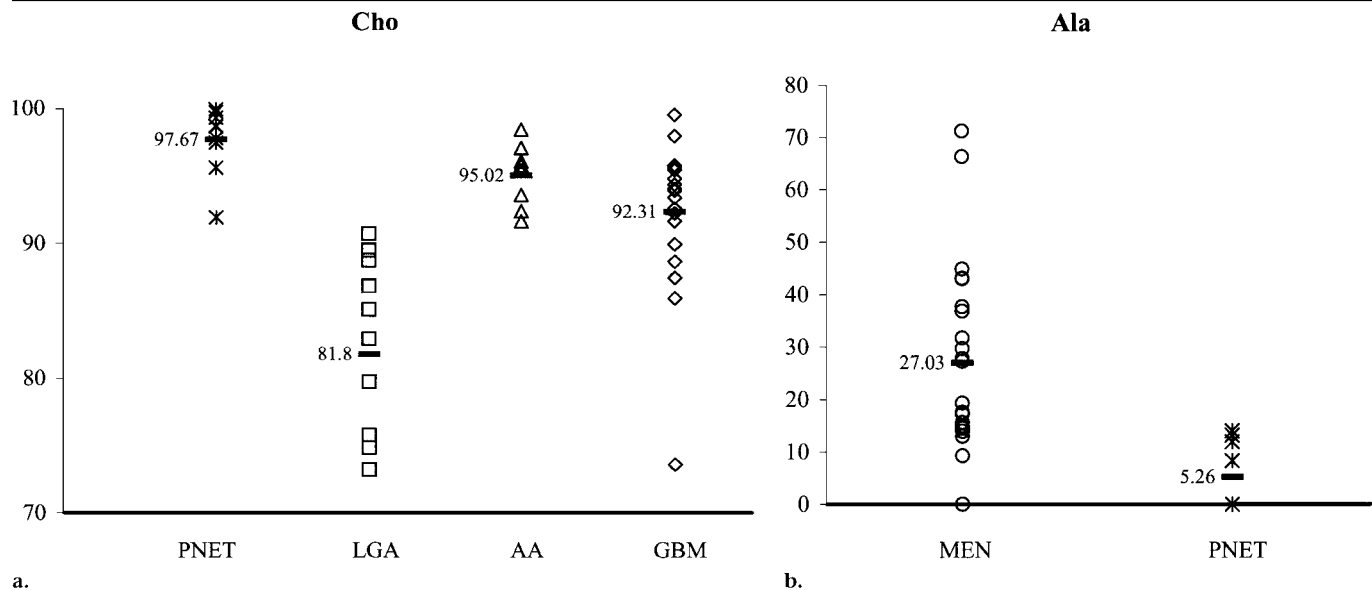
Tumor type	<i>n</i>	Metabolite Resonance*								
		LIP 0.90	LIP 1.30	LACT	Ala	NACC	GLX	CR	CHO	Glyc/Ml
PNET	9	0.31 ± 0.94	4.69 ± 14.07	7.94 ± 8.75	5.26 ± 6.43	11.78 ± 6.52	9.11 ± 6.82	13.67 ± 10.13	97.67 ± 2.54	9.68 ± 10.11
MEN	22	0.63 ± 2.94	0.69 ± 3.22	2.67 ± 5.11	27.03 ± 18.76 ( $P < .001$ ) <sup>y</sup>	14.33 ± 5.84	24.27 ± 14.24 ( $P = .004$ ) <sup>y</sup>	17.52 ± 9.56	96.77 ± 2.10	2.12 ± 3.67
LGA	12	0 ± 0	0 ± 0	20.80 ± 16.92	30.31 ± 16.10 ( $P = .013$ ) <sup>y</sup>	5.09 ± 3.74	45.59 ± 3.66 ( $P < .001$ ) <sup>y</sup>	81.80 ± 8.16 ( $P < .001$ ) <sup>y</sup>	2.23 ± 3.31	.001 <sup>y</sup>
AA	8	0 ± 0	3.69 ± 10.46	27.70 ± 51.83	2.56 ± 5.04	12.90 ± 8.37	7.30 ± 6.24	26.60 ± 5.96 ( $P = .062$ ) <sup>y</sup>	55.02 ± 2.34 ( $P = .055$ ) <sup>y</sup>	2.71 ± 3.33
CBM	23	7.13 ± 8.35	70.67 ± 31.16 ( $P < .001$ ) <sup>y</sup>	81.38 ± 158.68	5.58 ± 12.50	21.96 ± 9.41 ( $P = .013$ ) <sup>y</sup>	21.03 ± 16.24	92.31 ± 5.39 ( $P = .004$ ) <sup>y</sup>	9.13 ± 12.95	.012 <sup>y</sup>
MET	21	9.19 ± 8.37 ( $P = .029$ ) <sup>y</sup>	69.71 ± 31.42 ( $P < .001$ ) <sup>y</sup>	22.38 ± 36.00	0.96 ± 4.39	28.47 ± 15.91 ( $P = .010$ ) <sup>y</sup>	12.41 ± 14.64	22.42 ± 13.38	90.52 ± 8.81 ( $P = .021$ ) <sup>y</sup>	1.82 ± 2.45
Normal parenchyma†	6	0 ± 0	0 ± 0	0.52 ± 1.26	0 ± 0	83.46 ± 3.33	11.02 ± 2.63	36.61 ± 1.64	40.67 ± 5.84	2.42 ± 1.53

Note.—Data are means ± SDs. AA = Anaplastic astrocytoma, CBM = glioblastoma, LGA = low-grade astrocytoma, MEN = meningioma, MET = metastasis.

\* None of the resonances showed a significant difference between PNET and anaplastic astrocytoma. CHO and CR showed a higher tendency to differ.

† Resonances were found to be significantly different with respect to PNET.  $P$  values were corrected by using the Hochberg method for multiple comparisons.

‡ Values shown as reference values for comparison purposes only.



a.

**Figure 2.** Scatterplots show the distribution of normalized area values (ordinates, arbitrary units) of the resonances that allowed better differentiation of PNET (\*) and other tumor types. The mean value for every tumor group is also labeled (—) and its numeric value given. (a) Scatterplot shows the distribution of the resonance that corresponds to CHO in PNET, low-grade astrocytoma (LGA) (□), anaplastic astrocytoma (AA) (△), and glioblastoma (GBM) (◇). Note the higher values for PNET (\*). The tumor group showing the most overlap with PNET is anaplastic astrocytoma. Glioblastoma also shows overlap that is of low diagnostic effect, as the main differences between PNET and glioblastoma are found in LIP 1.30 (Figs 2c and 7). (b) Scatterplot shows the distribution of Ala in meningioma (MEN) (○) and PNET. The mean value is significantly higher in meningioma. (c) Scatterplot shows the distribution of LIP 1.30 in glioblastoma (GBM) (◇), metastasis (MET) (×), and PNET. The mean value is significantly higher in glioblastoma and metastasis than in PNET.

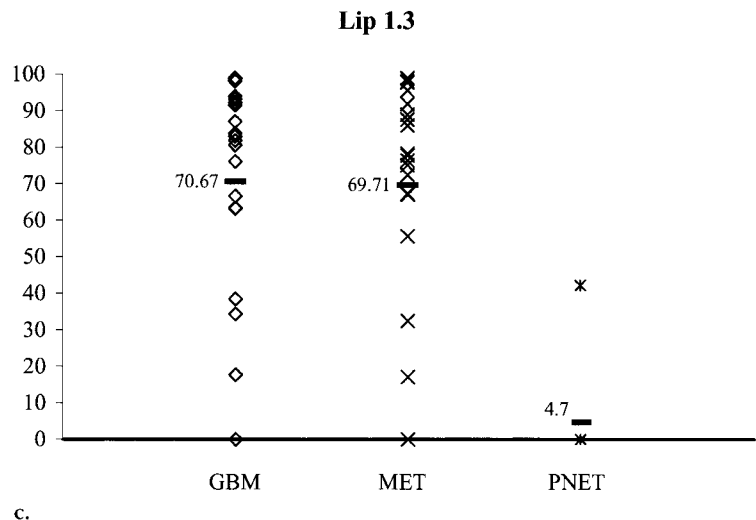
oma (Fig 5). Prominent resonances from LIP at 1.30 ppm in Figure 4 and Ala at 1.47 ppm in Figure 5 give additional support to a presumptive diagnosis of metastasis (or glioblastoma) and meningioma. Figures 6 and 7 illustrate the differential diagnosis between PNET and glioblastoma in heterogeneous hemispheric tumors. LIP resonance in Figure 7 oriented the case as glioblastoma (or metastasis). All diagnoses were histopathologically proved.

This empiric classification approach was tested in a prospective test set of 24 tumors, two of which were PNETs. Because both PNETs were used to test the algorithms for differentiation from all five of the other groups (10 testing procedures for two PNETs), a total of 32 procedures were performed to prospectively test the algorithms for bilateral differential diagnosis between PNETs and other tumors, as described previously. Of the 32 total procedures, 25 (78%) yielded correct classifications, three (9%) yielded

unclassifiable tumors, and four (13%) yielded misclassifications (Table 4).

## DISCUSSION

PNETs are undifferentiated round cell tumors that typically occur in childhood. Only 20%–30% of these tumors occur in adulthood, at which time, as opposed to the pediatric tumors, they tend to show a higher frequency of atypical features (4,8). This is the reason that some authors have suggested that medulloblastoma always be considered in the differential diagnosis of a mass in the posterior fossa of an adult (4). Our results agree with this atypical aspect of medulloblastoma in adulthood. In the current study participants, the most common pattern for posterior fossa PNET in 43% of medullo-



c.

blastomas was a heterogeneous poorly defined tumor located in the cerebellar hemisphere with areas of cystic or necrotic degeneration into the tumor. On the other hand, supratentorial PNETs, similar to other supratentorial tumors, tend to show a highly heterogeneous pattern with areas of necrosis (9). Thus, additional information for diagnosis of these tumors would be of interest, especially when considering that diagnosis of PNET prior to surgery has important repercussions in therapeutic decisions and prognosis (ie, suspicion of PNET could indicate spinal staging MR imaging to discard drop metastases throughout the cerebrospinal fluid before surgery [1,2]; insertion of a ventriculoperitoneal shunt should be considered only if strictly necessary because it may be a channel for neoplastic spread to extraneural sites [37], and the

**TABLE 3**  
Criteria for Bilateral Tumor Discrimination of PNET and Assessment of Results in 95 Retrospective Cases

**A: Bilateral Tumor Discrimination Criteria**

Tumors Compared	Discriminative Resonance*	Discriminative Criteria	
		PNET	Comparison Tumor
PNET, MEN	1st, Ala; 2nd, GLX	<2.78 <5.04	>14.00 >30.14
PNET, LGA	1st, CHO	>91.90	<90.34
PNET, AA	1st, CHO	>98.42	<91.90
PNET, GBM	1st, LIP 1.30; 2nd, CHO	<7.08 >97.50	>42.40 <91.90
PNET, MET	1st, LIP 1.30; 2nd, CHO	<3.41 >98.81	>42.40 <91.90

\* The second discriminative resonance was used only when discrimination was not possible with the first.

**B: Bilateral Differential Diagnosis Results**

Tumors Compared	Bilateral Differential Diagnosis Results*		
	Correct	Unclassifiable	Incorrect
PNET vs MEN			
PNET	6/9	2/9	1/9
MEN	17/22	3/22	2/22
Total	23/31 (74)	5/31 (16)	3/31 (10)
PNET vs LGA			
PNET	8/9	1/9	0/9
LGA	11/12	1/12	0/12
Total	19/21 (90)	2/21 (10)	0/21 (0)
PNET vs AA			
PNET	5/9	3/9	1/9
AA	1/8	6/8	1/8
Total	6/17 (35)	9/17 (53)	2/17 (12)
PNET vs GBM			
PNET	9/9	0/9	0/9
GBM	19/23	2/23	2/23
Total	28/32 (88)	2/32 (6)	2/32 (6)
PNET vs MET			
PNET	9/9	0/9	0/9
MET	18/21	1/21	2/21
Total	27/30 (90)	1/30 (3)	2/30 (7)
Overall†	103/131 (79)	19/131 (14)	9/131 (7)

Note.—Data are numbers of correct, unclassifiable, and incorrect results obtained for the 131 procedures evaluated in the retrospective training set. Numbers in parentheses are percentages. AA = anaplastic astrocytoma, GBM = glioblastoma, LGA = low-grade astrocytoma, MEN = meningioma, MET = metastasis.

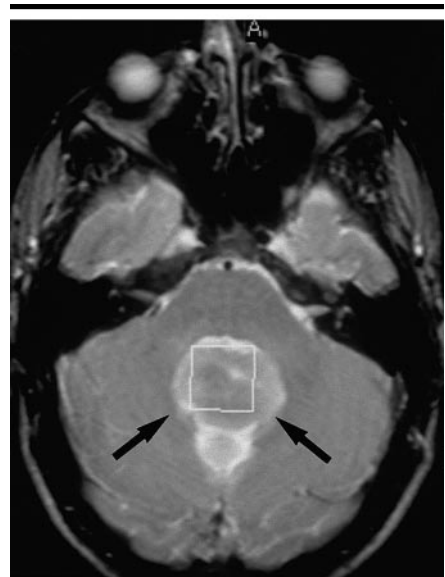
\* Assessed by using the leave-one-out method. Discriminative criteria were calculated for every case.

† PNETs were bilaterally compared with all five groups; thus, 95 spectra yielded 131 classifications.

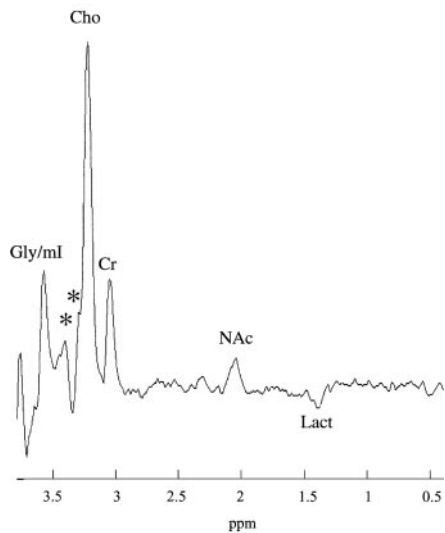
high sensitivity of these tumors to chemotherapy and radiation therapy could have a major effect on patient care [37].

The biochemical information sampled with proton MR spectroscopy brings additional data about the metabolism and pathophysiologic status of brain tumors, provides diagnostic orientation on the basis of the use of molecular or metabolic profiles, and complements the information gathered at anatomic imaging. Nevertheless, before applying proton MR spectroscopy for tumor classification in daily clinical practice, it is necessary to

know the characteristics of every tumor group and the most useful findings in differentiating between tumor types. Authors of many studies (10–20,22–25) have evaluated proton MR spectroscopy in the most common brain tumors both *in vivo* and *in vitro*, and their spectral characteristics are being progressively established, with promising results in differentiating between them. Evaluation of less common tumors constitutes an additional step in the introduction of proton MR spectroscopy in clinical practice, which is essential for completing the



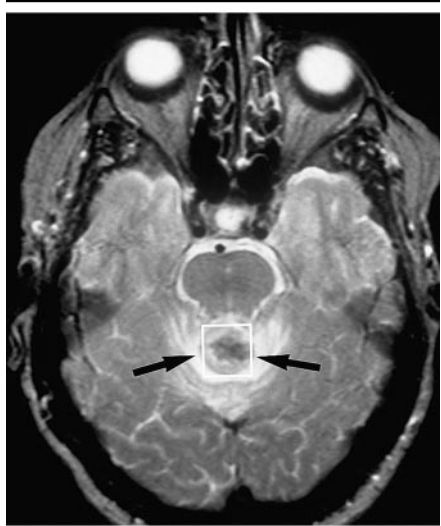
a.



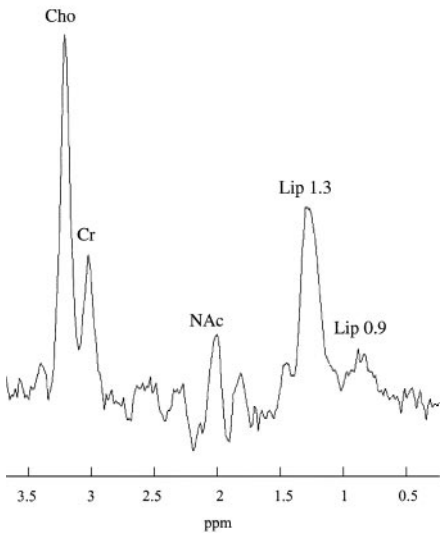
b.

**Figure 3.** PNET. (a) Transverse T2-weighted MR image (2,175/85) shows a relatively homogeneous tumor (arrows) in the posterior fossa, adjacent to the posterior wall of the fourth ventricle. The voxel position for proton MR spectroscopy (box) is also shown. (b) Localized spin-echo proton MR spectrum (2,000/136, 128 acquisitions) of the tumor shows prominent resonances from Cho and low CR and NACC resonance. There is a small amount of LACT (Lact) and a resonance at 3.55 ppm that is attributable to Gly/MI. Some peaks (\*) around 3.30 and 3.40 ppm suggest the presence of taurine in this particular case. The histologic diagnosis was PNET. The empiric algorithm satisfactorily classified this tumor as PNET at bilateral comparisons with the main tumors included in the differential diagnosis (metastasis and meningioma).

study of the clinical application of proton MR spectroscopy to diagnose brain tumors. In this respect, little interest

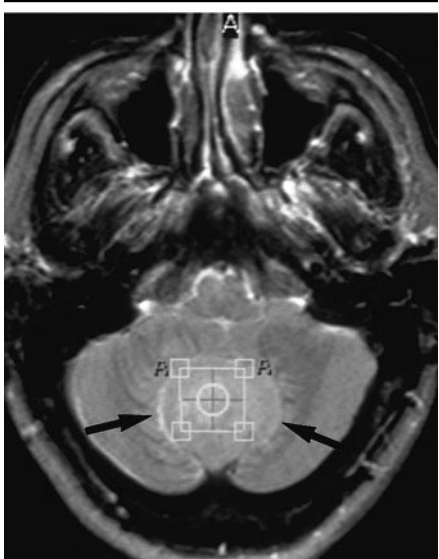


a.

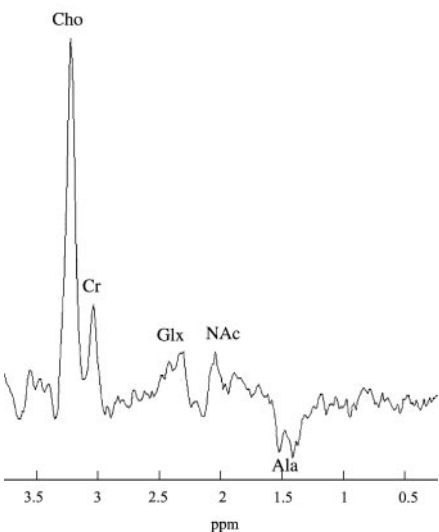


b.

**Figure 4.** Metastasis. (a) Transverse T2-weighted MR image (2,175/85) shows a well-defined midline tumor (arrows) adjacent to the aqueduct and fourth ventricle. There is some heterogeneity with central low signal intensity and peritumoral edema. The voxel position for proton MR spectroscopy (box) is shown. (b) Localized spin-echo proton MR spectrum (2,000/136, 128 signals acquired) of the tumor shows LIP resonance at 1.30 ppm and a small amount at 0.90 ppm. This finding is highly suggestive of metastasis or glioblastoma. The diagnosis after tumor removal was metastasis. Bilateral comparison with PNET satisfactorily suggested metastasis.

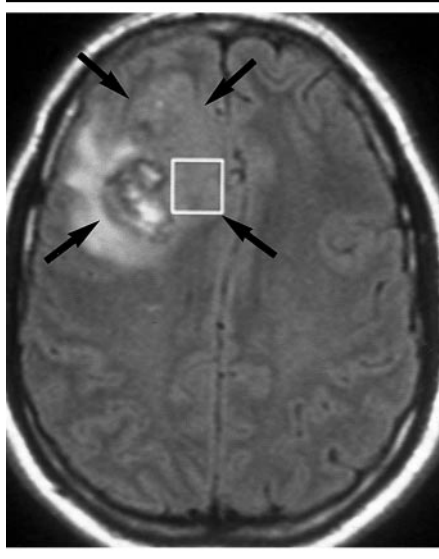


a.

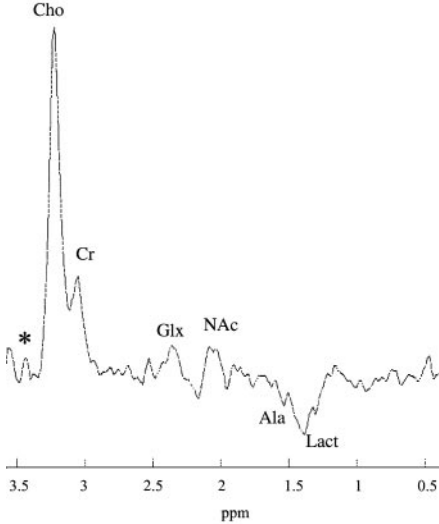


b.

**Figure 5.** Meningioma. (a) Transverse T2-weighted MR image (2,175/85) shows a well-defined midline tumor (arrows). The voxel position for proton MR spectroscopy (box) is depicted. "A" marks correspond to unremovable marks made by the spectroscopic software package used. (b) Localized spin-echo proton MR spectrum (2,000/136, 128 signals acquired) of the tumor shows prominent resonance from CHO and low CR and NACC resonances. A certain amount of LACT is probably overlapping with Ala. Note also a clear resonance of GLX. The histologic diagnosis was meningioma. Bilateral comparison satisfactorily resulted in differentiation of this tumor from PNET.



a.



b.

**Figure 6.** PNET. (a) Transverse fast FLAIR MR image (6,706/120/2,000; turbo factor, 15) shows a heterogeneous tumor (arrows) with a cystic and/or necrotic area. The voxel position for proton MR spectroscopy (box) is shown. (b) Localized spin-echo proton MR spectrum (2,000/136, 192 signals acquired) of the tumor shows prominent resonance from CHO and low CR and NACC resonances. A certain amount of LACT is probably overlapping with Ala. Note also a small peak (\*) at 3.4 ppm that is difficult to differentiate from noise and could suggest resonance from taurine. The definitive diagnosis after partial tumor removal was PNET. Bilateral differentiation from glioblastoma satisfactorily suggested PNET.

has been shown in proton MR spectroscopy of PNETs, especially in adults. Most PNETs described in the spectroscopic literature correspond to a few cases included in large series of brain tumors.

In vivo proton MR spectroscopy in children has focused on differentiation

between the three most common posterior fossa tumors in this age group: PNET, ependymoma, and astrocytoma, with good results in most series (21,26). Authors of previous studies (21,26) found low ratios of NACC/CHO, CR/CHO, and

LACT/CHO to be characteristic of medulloblastoma in children and resulted in improvement in discriminating among PNETs, low-grade astrocytomas, and ependymomas in children when proton MR spectroscopic findings were considered

**TABLE 4**  
**Results of 32 Differential Diagnostic Procedures in a Prospective Test Set of 24 Tumors to Test the Empirical Method for Bilateral Differential Diagnosis of PNET**

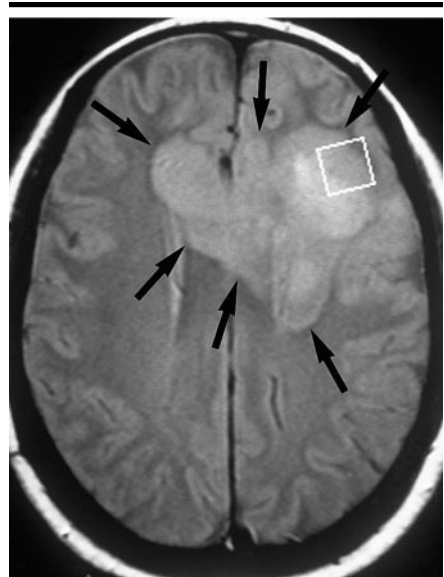
Case No./Definitive Diagnosis	Procedure No.	Bilateral Differential Diagnostic Procedure	Final Classification	Result
1/LGA	1	PNET vs LGA	PNET	Incorrect
2/MEN	2	PNET vs MEN	MEN	Correct
3/LGA	3	PNET vs LGA	PNET	Incorrect
4/AA	4	PNET vs AA	AA	Correct
5/GBM	5	PNET vs GBM	GBM	Correct
6/MEN	6	PNET vs MEN	MEN	Correct
7/MET	7	PNET vs MET	MET	Correct
8/MEN	8	PNET vs MEN	MEN	Correct
9/AA	9	PNET vs AA	Unclassifiable	Unclassifiable
10/LGA	10	PNET vs LGA	PNET	Incorrect
11/PNET	11	PNET vs MEN	PNET	Correct
	12	PNET vs LGA	PNET	Correct
	13	PNET vs AA	PNET	Correct
	14	PNET vs GBM	PNET	Correct
	15	PNET vs MET	PNET	Correct
12/AA	16	PNET vs AA	AA	Correct
13/PNET	17	PNET vs MEN	Unclassifiable	Unclassifiable
	18	PNET vs LGA	PNET	Correct
	19	PNET vs AA	Unclassifiable	Unclassifiable
	20	PNET vs GBM	PNET	Correct
	21	PNET vs MET	PNET	Correct
14/MET	22	PNET vs MET	MET	Correct
15/MET	23	PNET vs MET	MET	Correct
16/MEN	24	PNET vs MEN	PNET	Incorrect
17/MEN	25	PNET vs MEN	MEN	Correct
18/MEN	26	PNET vs MEN	MEN	Correct
19/AA	27	PNET vs AA	AA	Correct
20/MEN	28	PNET vs MEN	MEN	Correct
21/MET	29	PNET vs MET	MET	Correct
22/MET	30	PNET vs MET	MET	Correct
23/MET	31	PNET vs MET	MET	Correct
24/GBM	32	PNET vs GBM	GBM	Correct

Note.—Of the results of 32 procedures, 25 (78%) were correct, three (9%) were unclassifiable, and four (13%) were wrong. AA = anaplastic astrocytoma, GBM = glioblastoma, LGA = low-grade astrocytoma, MEN = meningioma, MET = metastasis, PNET = primitive neuroectodermal tumor.

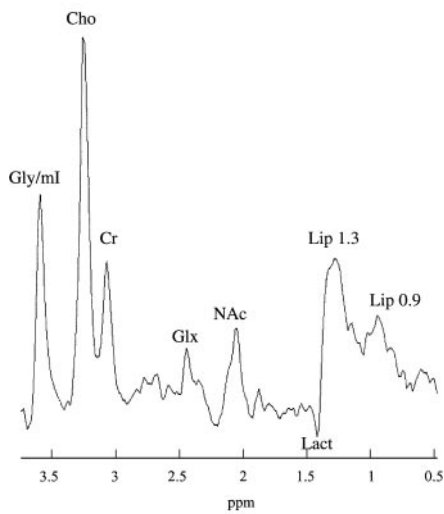
(26). Furthermore, most in vitro studies (23,24,27,28) have reported an increase in total CHO, taurine, Gly, and inositol levels in PNET. The differential diagnosis in adults is significantly different from that in children and should include the most common tumors in adults: meningioma, metastasis, and astrocytic tumor (low-grade astrocytoma, anaplastic astrocytoma, and glioblastoma). The first two may simulate medulloblastoma in homogeneous posterior fossa midline tumors or in tumors located peripherally in the hemispheres. Metastasis and astrocytic tumors can be confused with PNETs in cases of heterogeneous tumors located outside the vermis or in the cerebral hemispheres (Figs 6, 7). On the other hand, an identical spectroscopic pattern of medulloblastoma in children and adults cannot be taken for granted. PNET has shown different radiologic behavior in adults (4,8); for example, a desmoplastic histologic variant has been described to be more frequent in this age group

(4,5,8), and some authors have suggested a different origin of PNETs in adults with respect to children (38). Accordingly, our study focuses on the characteristics of PNET in adults and its differential diagnosis in this age group.

Our results were similar to those previously reported in pediatric PNETs. As in previous work in children (27,28), we found high relative CHO values in PNET with respect to the rest of the tumors, showing significant differences with all tumors except meningioma and anaplastic astrocytoma. These high CHO values would correlate with the high cellularity of PNET observed at histologic examination, with densely packed cells and scant cytoplasm (36). Another characteristic of PNET found in the current study was the absence of or low amounts of LIP signal, in contrast with that in other high-grade tumors (glioblastoma and metastases). LIP signals have been correlated with necrosis in tumors (39–42). The low intensity of LIPs in PNET, considered grade 4



a.



b.

**Figure 7.** Glioblastoma. (a) Transverse intermediate-weighted MR image (2,175/20) shows a heterogeneous tumor (arrows) with a necrotic cystlike area in the left frontal lobe. The voxel position for proton MR spectroscopy (box) is also shown. (b) Localized spin-echo proton MR spectrum (2,000/136, 192 signals acquired) of the tumor shows LIP resonance at 1.30 ppm that is highly suggestive of metastasis or glioblastoma. The histologic diagnosis after partial tumor removal was glioblastoma. Bilateral discrimination with PNET satisfactorily suggested glioblastoma.

malignancy by the World Health Organization (43), may be a result of their high cellularity and a low amount of necrosis. There were also differences in Ala and GLX between PNET and meningioma. Ala was significantly increased in meningiomas, a well-known finding with respect to other tumors (10,13,17,23,24)

that was also found with respect to PNET in the current study. We also evaluated GLX resonance, although it should be taken into account that it could have contributions from LIP resonances when prominent LIP signals are present at 0.90 and 1.30 ppm (39,40,44). Previous phantom studies (30,33) have shown that GLX is detectable with a echo time of 136 msec. We found this resonance to be increased in meningioma at comparison with that in PNET.

The ideal echo time for tumor classification with proton MR spectroscopy is under discussion. In the current study, we preferred to use a relatively long echo time (136 msec) sequence, since it allows good differentiation between LACT and Ala and LIPs because of J modulation, produces less baseline distortion, and is easier to quantify; we thus believed that it would give more reproducible results. Another point under discussion is the choice between single- or multivoxel techniques (45). Multivoxel techniques more completely represent the tumor heterogeneity. Nevertheless, single-voxel techniques may have major advantages for brain tumor discrimination in clinical practice: It takes less time to perform the examination, it is easier and quicker to process data to obtain quantitative results, and it is possible to obtain better magnetic field homogeneity in the volume of interest. Nevertheless, although we used a single-voxel technique, we hope that the spectroscopic pattern knowledge gained will be of interest in interpreting multivoxel data in the future.

The most accurate method of clinical proton MR spectroscopic interpretation also remains an open question. While a robust classification method is unanimously accepted, some preliminary methods could be useful to exploit the quantitative potential of proton MR spectroscopy. An additional use for such preliminary methods would be prospective testing of the usefulness and reproducibility of spectroscopic findings in differentiating between tumors. In this respect, we obtained satisfactory results in pairwise differentiation between PNET and the five more common brain tumors in adults in a retrospective training set, with correct classification of 79% (103 of 131) of cases, in the range seen in previous research on brain tumors (12,16,21,26). Of high interest for clinical application is that in 7% (nine of 131) of cases, an incorrect diagnosis was suggested as a result of our method. Differentiation of PNET in our study was carried out by using the 90th percentiles of

some specific discriminative resonances that included Ala and GLX for meningioma, CHO for low-grade and anaplastic astrocytomas, and LIP 1.30 and CHO for glioblastoma and metastasis. We confirmed the consistency and reproducibility of our findings by means of a prospective test set of 24 tumors (correctly classified, 78% [25 of 32 procedures]; unclassifiable, 9% [three of 32 procedures]; and misclassified, 13% [four of 32 procedures]). Only a few studies of brain tumor classification with proton MR spectroscopy (16,46) have included prospective test sets to validate the performance produced by their discrimination strategies. In the present study, we preferred to use such an independent test set because it avoids the possible bias of using the same cases for training and testing (16,47). In this way, we expected to gain better insight into the utility of our results for bilateral tumor discrimination in real new cases.

Our aim in elaborating a bilateral discriminative path was not to definitively establish a method for tumor classification but to test the findings reported in the study, its reproducibility, and its usefulness when applied in tumor discrimination. This method could be used as a guide for applying proton MR spectroscopic findings in tumor categorization. Nevertheless, boundaries (the 90th percentile in our case) should be recalculated and tested for every clinical setting because of differences in the acquisition protocols and MR imaging systems used. Nonetheless, our findings confirm that *in vivo* proton MR spectroscopy provides additional information for identifying PNETs in adults on the basis of the tumors' biochemical characteristics, which are reflected in their spectral pattern.

**Acknowledgment:** We thank the Statistic Support Facility of Universitat Autònoma de Barcelona for technical advice on statistical data processing.

#### References

- Zimmerman RA, Bilaniuk LT. Brain tumors. In: Zimmerman RA, Gibby WA, Carmody RF, eds. *Neuroimaging: clinical and physical principles*. New York, NY: Springer-Verlag; 1997: 1004–1009.
- Osborn AG. Meningiomas and other non-glial neoplasms. In: Osborn AG, ed. *Diagnostic neuroradiology*. St Louis, Mo: Mosby; 1994: 613–620.
- Meyers SP, Kemp SS, Tarr RW. MR imaging features of medulloblastomas. *AJR Am J Roentgenol* 1992; 158:859–865.
- Bourguin PM, Tampieri D, Grahovac SZ, Léger C, Del Carpio R, Melançon D. CT and MR imaging findings in adults with cerebellar medulloblastoma: comparison with findings in children. *AJR Am J Roentgenol* 1992; 159:609–612.
- Koci TM, Chiang F, Mehringer CM, et al. Adult cerebellar medulloblastoma: imaging features with emphasis on MR findings. *AJNR Am J Neuroradiol* 1993; 14: 929–939.
- Nelson M, Diebler C, Forbes WS. Paediatric medulloblastoma: atypical CT features at presentation in the SIOP II trial. *Neuroradiology* 1991; 33:140–142.
- Tortori-Donati P, Fondelli MP, Rossi A, et al. Medulloblastoma in children: CT and MRI findings. *Neuroradiology* 1996; 38: 352–359.
- Maleci A, Cervoni L, Delfini R. Medulloblastoma in children and in adults: a comparative study. *Acta Neurochir (Wien)* 1992; 119:62–67.
- Davis PC, Wichman RD, Takei Y, Hoffman JC Jr. Primary cerebral neuroblastoma: CT and MR findings in 12 cases. *AJNR Am J Neuroradiol* 1990; 11:115–120.
- Kugel H, Heindel W, Ernestus RI, Bunke J, du Mesnil R, Friedmann G. Human brain tumors: spectral patterns detected with localized H-1 MR spectroscopy. *Radiology* 1992; 183:701–709.
- Poptani H, Gupta RK, Roy R, Pandey R, Jain VK, Chhabra DK. Characterization of intracranial mass lesions with *in vivo* proton MR spectroscopy. *AJNR Am J Neuroradiol* 1995; 16:1593–1603.
- Usenius JP, Tuohimetsa S, Vainio P, Alakorpela M, Hiltunen Y, Kauppinen RA. Automated classification of human brain tumours by neural network analysis using *in vivo* 1H magnetic resonance spectroscopic metabolite phenotypes. *Neuroreport* 1996; 7:1597–1600.
- Shimizu H, Kumabe T, Tominaga T, et al. Noninvasive evaluation of malignancy of brain tumors with proton MR spectroscopy. *AJNR Am J Neuroradiol* 1996; 17: 737–747.
- Adamson AJ, Rand SD, Prost RW, Kim TA, Schultz C, Haughton VM. Focal brain lesions: effect of single-voxel proton MR spectroscopic findings on treatment decisions. *Radiology* 1998; 209:73–78.
- Barba I, Moreno A, Martínez-Pérez I, et al. Magnetic resonance spectroscopy of brain hemangiopericytomas: high myoinositol concentrations and discrimination from meningiomas. *J Neurosurg* 2001; 94:55–60.
- Tate AR, Griffiths JR, Martínez-Pérez I, et al. Towards a method for automated classification of 1H MRS spectra from brain tumours. *NMR Biomed* 1998; 11:177–191.
- Majós C, Cucurella G, Aguilera C, Coll S, Pons LC. Intraventricular meningiomas: MR imaging and MR spectroscopic findings in two cases. *AJNR Am J Neuroradiol* 1999; 20:882–885.
- Meyerand ME, Pipas JM, Mamourian A, Tosteson TD, Dunn JF. Classification of biopsy-confirmed brain tumors using single-voxel MR spectroscopy. *AJNR Am J Neuroradiol* 1999; 20:117–123.
- Negendank WG, Sauter R, Brown TR, et al. Proton magnetic resonance spectroscopy in patients with glial tumors: a multicenter study. *J Neurosurg* 1996; 84:449–458.
- Burtscher IM, Skagerberg G, Geijer B, Englund E, Stahlberg F, Holtas S. Proton MR spectroscopy and preoperative diagnostic accuracy: an evaluation of intracranial

- mass lesions characterized by stereotactic biopsy findings. *AJNR Am J Neuroradiol* 2000; 21:84–93.
21. Wang Z, Sutton LN, Cnaan A, et al. Proton MR spectroscopy of pediatric cerebellar tumors. *AJNR Am J Neuroradiol* 1995; 16:1821–1833.
  22. Preul MC, Caramanos Z, Collins DL, et al. Accurate, noninvasive diagnosis of human brain tumors by using proton magnetic resonance spectroscopy. *Nat Med* 1996; 2:323–325.
  23. Kinoshita Y, Kajiwara H, Yokota A, Koga Y. Proton magnetic resonance spectroscopy of brain tumors: an in vitro study. *Neurosurgery* 1994; 35:606–614.
  24. Kinoshita Y, Yokota A. Absolute concentrations of metabolites in human brain tumors using in vitro proton magnetic resonance spectroscopy. *NMR Biomed* 1997; 10:2–12.
  25. Tien RD, Lai PH, Smith JS, Lazeyras F. Single-voxel proton brain spectroscopy exam (PROBE/SV) in patients with primary brain tumors. *AJR Am J Roentgenol* 1996; 167:201–209.
  26. Arle JE, Morri C, Wang ZJ, Zimmerman RA, Phillips PG, Sutton LN. Prediction of posterior fossa tumor type in children by means of magnetic resonance image properties, spectroscopy, and neural networks. *J Neurosurg* 1997; 86:755–761.
  27. Carapella CM, Carpinelli G, Knijn A, Raus L, Caroli F, Podo F. Potential role of in vitro 1H magnetic resonance spectroscopy in the definition of malignancy grading of human neuroepithelial brain tumours. *Acta Neurochirur Suppl* 1997; 68:127–132.
  28. Sutton LN, Wehrli SL, Gennarelli L, et al. High-resolution 1H-magnetic resonance spectroscopy of pediatric posterior fossa tumors in vitro. *J Neurosurg* 1994; 81: 443–448.
  29. van den Boogaart A. Quantitative data analysis of in vivo MRS data sets. *Magn Reson Chem* 1997; 35:S146–S152.
  30. Ernst T, Hennig J. Coupling effects in volume selective 1H spectroscopy of major brain metabolites. *Magn Reson Med* 1991; 21:82–96.
  31. De Edelenyi FS, Rubin C, Estève F, et al. A new approach for analyzing proton magnetic resonance spectroscopic images of brain tumors: nosologic images. *Nat Med* 2000; 6:1287–1289.
  32. Martínez-Pérez I, Moreno A, Alonso J, et al. Diagnosis of brain abscess by magnetic resonance spectroscopy: report of two cases. *J Neurosurg* 1997; 86:708–713.
  33. Connelly A, Cross JH, Gadian DG, Hunter JV, Kirkham FJ, Leonard JV. Magnetic resonance spectroscopy shows increased brain glutamine in ornithine carbamoyl transferase deficiency. *Pediatr Res* 1993; 33:77–81.
  34. Grand S, Passaro G, Ziegler A, et al. Necrotic tumor versus brain abscess: importance of amino acids detected at 1H MR spectroscopy—initial results. *Radiology* 1999; 213:785–793.
  35. Hochberg Y, Tamhane AC, eds. *Multiple comparison procedures*. New York, NY: Wiley, 1987.
  36. Becker LE. Pathology of pediatric brain tumors. *Neuroimaging Clin North Am* 1999; 9:671–690.
  37. Brandes AA, Palmisano V, Monfardini S. Medulloblastoma in adults: clinical characteristics and treatment. *Cancer Treat Rev* 1999; 25:3–12.
  38. Rubinstein LJ. Embryonal central neuroepithelial tumors and their differentiating potential: a cytogenetic view of a complex neuro-oncological problem. *J Neurosurg* 1985; 62:795–805.
  39. Rémy C, Arés C, Ziegler A, et al. In vivo, ex vivo, and in vitro one- and two-dimensional nuclear magnetic resonance spectroscopy of an intracerebral glioma in rat brain: assignment of resonances. *J Neurochem* 1994; 62:166–179.
  40. Kuesel AC, Sutherland GR, Halliday W, Smith ICP. 1H MRS of high grade astrocytomas: mobile lipid accumulation in necrotic tissue. *NMR Biomed* 1994; 7:149–155.
  41. Sijens PE, Knopp MV, Brunetti A, et al. 1H MR spectroscopy in patients with metastatic brain tumors: a multicenter study. *Magn Reson Med* 1995; 33:818–826.
  42. Gotsis ED, Fountas K, Kapsalaki E, Toulas P, Peristeris G, Papadakis N. In vivo proton MR spectroscopy: the diagnostic possibilities of lipid resonances in brain tumors. *Anticancer Res* 1996; 16:1565–1568.
  43. Kleihues P, Burger PC, Scheithauer BW. The new WHO classification of brain tumors. *Brain Pathol* 1993; 3:255–268.
  44. Bell JD, Brown JCC, Nicholson JK, Sadler PJ. Assignment of resonances for “acute-phase” glycoproteins in high resolution proton NMR spectra of human blood plasma. *FEBS Lett* 1987; 215:311–315.
  45. Lenkinski RE. MR spectroscopy: clinical tool or research probe? (revisited). *Acad Radiol* 2001; 8:567–570.
  46. Roser W, Hagberg G, Mader I, et al. Assignment of glial brain tumors in humans by in vivo 1H-magnetic resonance spectroscopy and multidimensional metabolic classification. *MAGMA* 1997; 5:179–183.
  47. Miller AJ, ed. *Subset selection in regression*. London, England: Chapman & Hall, 1990.



**4.3. Trabajo 3:**

Utility of proton MR spectroscopy in the diagnosis of radiologically atypical intracranial meningiomas. Majós C, Alonso J, Aguilera C, Serrallonga M, Coll S, Acebes JJ, Arús C, Gili J. Neuroradiology 2003; 45: 129-136.



C. Majós  
J. Alonso  
C. Aguilera  
M. Serrallonga  
S. Coll  
J.J. Acebes  
C. Arús  
J. Gili

## Utility of proton MR spectroscopy in the diagnosis of radiologically atypical intracranial meningiomas

Received: 30 September 2002

Accepted: 5 December 2002

Published online: 19 February 2003

© Springer-Verlag 2003

C. Majós (✉) · J. Alonso · C. Aguilera  
M. Serrallonga · S. Coll · J. Gili  
Institut de Diagnòstic per la Imatge,  
Hospital Duran i Reynals,  
CSU de Bellvitge,  
Autovia de Castelldefels km 2.7, 08907  
L'Hospitalet de Llobregat,  
Barcelona, Spain  
E-mail: cmajos@csub.scs.es  
Tel.: +34-932-630121  
Fax: +34-932-630144

J. J. Acebes  
Department of Neurosurgery, Hospital  
Príncipes de España, CSU de Bellvitge,  
Feixa larga s/n, 08907 L'Hospitalet de  
Llobregat, Barcelona, Spain

C. Arús  
Departament de Bioquímica i Biología  
Molecular, Unitat de Ciències, Universitat  
Autònoma de Barcelona, Edifici C, 08193  
Cerdanyola del Vallès, Barcelona, Spain

**Abstract** Our aim was to evaluate the usefulness of proton MR spectroscopy ( $^1\text{H}$  MRS) in the diagnosis of radiologically atypical brain meningiomas. We studied 37 patients with intracranial meningiomas with MRI and  $^1\text{H}$  MRS (TE 136 ms). Their spectra were quantitatively assessed and compared with those of 93 other intracranial brain neoplasms: 15 low-grade and 14 anaplastic astrocytomas, 30 glioblastomas and 34 metastases. The most characteristic features of meningiomas were the presence of alanine, high relative concentrations of choline and glutamine/glutamate and low concentrations of creatine-containing compounds, N-acetyl-containing compounds and lipids. These resonances were assembled in algorithms for two-way differentiation between meningioma and the other tumours. The performance of

the algorithms was tested in the 130 patients using the leave-one-out method, with 94% success in differentiating between meningioma and other tumour. Of the 37 meningiomas, five (14%) were thought atypical on MRI, and in only one of these, found to be malignant on histology, was a diagnosis other than meningioma suggested by the algorithm. The other four were correctly classified. We suggest that  $^1\text{H}$  MRS provides information on intracranial meningiomas which may be useful in diagnosis of radiologically atypical cases.

**Keywords** Meningioma · Magnetic resonance imaging · Magnetic resonance spectroscopy

### Introduction

Intracranial meningiomas usually have typical radiological appearances and diagnosis by conventional imaging is relatively certain in most cases. A small percentage are atypical and diagnosis may not be confidently suggested by imaging alone [1, 2, 3]. Additional information from other noninvasive techniques such as proton MR spectroscopy ( $^1\text{H}$  MRS) could be relevant prior to surgery or radiotherapy. Accurate presurgical diagnosis in such cases could have important implica-

tions, suggesting preoperative endovascular embolisation in centres where that is thought to be useful, or simply follow-up imaging of patients for whom surgery is not indicated.

Our aim was to assess whether  $^1\text{H}$  MRS could be useful in diagnosis of intracranial meningiomas as a whole, and of radiologically atypical tumours in particular. We used a quantitative method recently reported for identification of intracranial tumours, subjecting the spectra of the lesion to two-way comparisons [4].

## Materials and methods

We reviewed 37 MRS studies of 13 men and 24 women, 18–80 years old, mean 56 years, with intracranial meningiomas (MEN). A data-set of 93 MRS studies of the most frequent intracranial tumours, obtained from 93 patients (37 women, 56 men, 14–81 years old, mean 56 years) were used for comparison: 15 low-grade (LGA) and 14 anaplastic astrocytomas (AA), 30 glioblastomas (GBM) and 34 metastases (MET). All were confirmed histologically with the exception of ten MET, in which the diagnosis was based on the presence of multiple intracranial lesions in patients with known primary tumour. MRS studies obtained under identical conditions from the white matter of six healthy volunteers were also used for reference. The study was approved by our Ethics Committee and informed consent was obtained from all patients and volunteers.

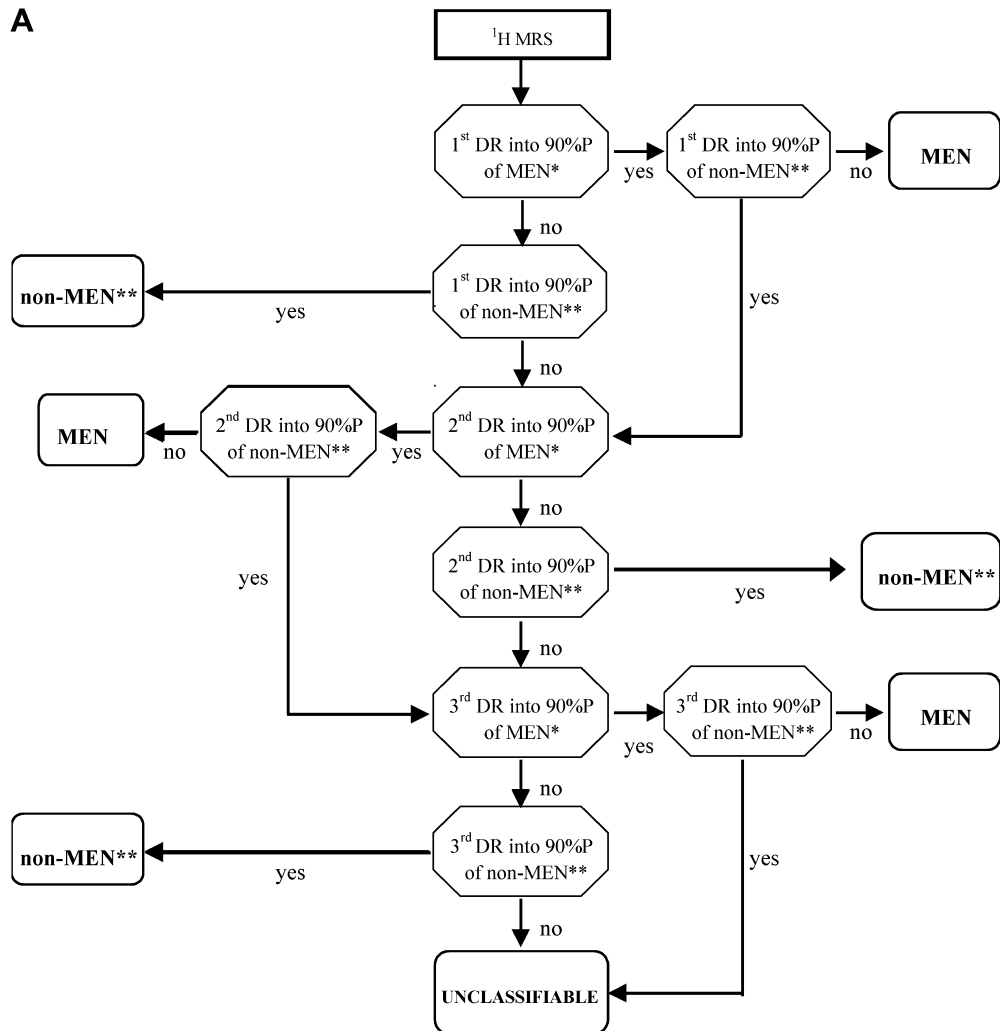
In the patients MRI was performed at 1.5 tesla, in three orthogonal planes, including T1- (TR 536 TE 15 ms), proton density- (2175, 20 ms), and T2- (2175, 85 ms) weighted images. Contrast-enhanced T1-weighted images were obtained in at least two planes. Three experienced neuroradiologists (C.Ag., M.S. and S.C.), blinded to the final diagnosis analysed the images of the 130 tumours and suggested the most likely diagnosis, or diagnoses,

for each. The meningiomas in which the diagnosis included possibilities other than MEN were listed as “meningiomas with uncertain imaging diagnosis”.

Single-voxel  $^1\text{H}$  MRS was incorporated in the standard imaging study. The volume of interest (VOI) was between  $1.5 \times 1.5 \times 1.5 \text{ cm}^3$  (3.4 cc) and  $2 \times 2 \times 2 \text{ cm}^3$  (8 cc). It was placed so as to position the largest possible voxel within the solid tumour seen on MRI, avoiding cysts or areas of necrosis, and with minimum contamination from the surrounding non-neoplastic tissue. The homogeneity of the magnetic field in the VOI was optimised automatically. The spectra were obtained with a water-suppressed, single-voxel, point-resolved spectroscopic sequence (PRESS) with TR 2000 TE 136, 128–192 excitations, 512 points acquired and 1000 Hz acquisition bandwidth. The standard receiver head coil was used in all cases. Spectral analysis was with the MRUI software [5]. The time domain-data were analysed with the variable projection method (VARPRO) [5] after filtering the residual water signal with the Henkel-Lanczos singular value decomposition algorithm.

The resonances of interest were the methylene groups of fatty acids in MRS-visible lipids (Lip 1.3) at 1.30 ppm, lactate (Lac) as an inverted doublet centered at 1.35 ppm, alanine (Ala) as an inverted doublet at 1.47 ppm, N-acetyl-aspartate and other N-acetyl containing compounds (NAc) at 2.02 ppm, glutamate and gluta-

**Fig. 1A, B** Algorithms for two-way differential diagnosis. **A** Model algorithm for two-way differential diagnosis. \*1st, 2nd and 3rd discriminative resonances (*DR*) may vary depending on the tumour type to be differentiated from MEN (meningioma) (Table 2). 90%*P* 90th centile. \*\*non-MEN may be LGA (low-grade astrocytoma), AA (anaplastic astrocytoma), GBM (glioblastoma multiforme) or MET (metastasis). **B** Algorithm for two-way differentiation between MEN and LGA, as an example. This particular algorithm is obtained introducing alanine (Ala), creatine-containing compounds (Cr) and glutamate and glutamine (Glx) as 1st, 2nd and 3rd DR. The same procedure should be done for obtaining the algorithms for MEN vs AA, MEN vs GBM, and MEN vs MET

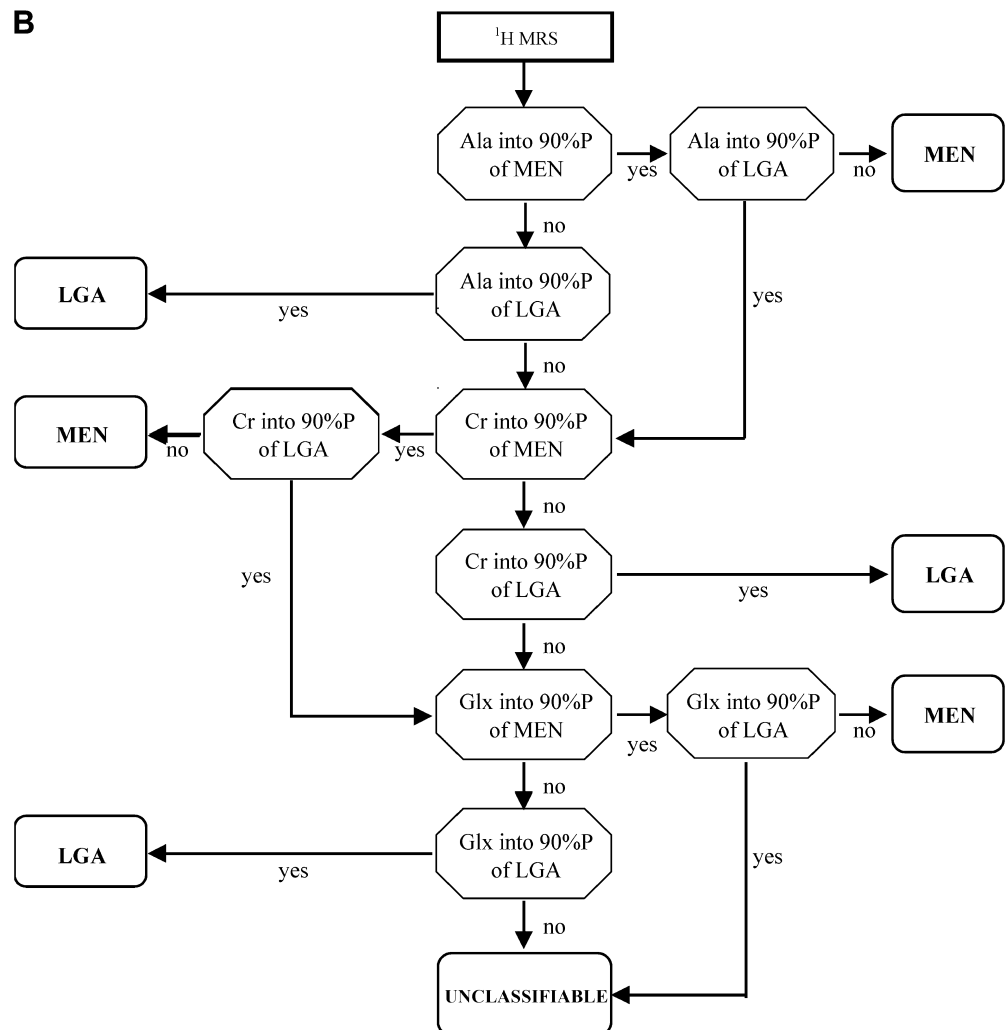


mine (Glx) at 2.35 ppm, creatine plus phosphocreatine (Cr) at 3.03 ppm, and choline and other trimethyl-amine-containing compounds (Cho) at 3.20 ppm. Assignment of these resonances was based on previous data on intracranial tumours [4, 6, 7, 8, 9, 10, 11, 12, 13, 14, 15, 16, 17, 18, 19] and phantom studies [6, 7]. Cr and/or water (4.7 ppm) were chosen as chemical-shift reference resonances to correct possible shifting in the frequency domain. Special attention was paid to differentiation between Lac and Ala on the basis of the position of the doublets, using the MRUI software. We defined the peaks in the frequency domain, even when there could be doubts about their differentiation from noise, using the criterion that further quantification and analysis should find differences between noise and metabolite signal without operator influence. Our aim was to avoid operator bias due to application of prior knowledge. An area of "0" was assigned only to resonances to which the program was unable to fit a peak in the area of interest.

Each the seven resonances of interest was considered separately in the analysis. Fitted resonance areas for Lac, Ala, NAc, Glx, Cr and Cho were normalised using a ratio between the resonance in question and the three main spectroscopic resonances ( $x = 100 \times x_i / (NAc^2 + Cr^2 + Cho^2)^{1/2}$ ), where  $x_i$  is the original area of the resonance being normalised) [4, 8, 9]. For normalisation of the resonance areas of lipids the square of the value Lip 1.3 was included in the denominator ( $x = 100 \times x_i / (NAc^2 + Cr^2 + Cho^2 + Lip 1.3^2)^{1/2}$ ).

**Fig. 1A, B (Contd.)**

**B**



Data obtained for MEN were compared to the other tumours to identify the characteristics of this tumour in *in vivo*  $^1\text{H}$  MRS. We did not assign the characteristic resonances to a particular metabolite, but simply to a resonance in the spectrum. Extrapolation of the origin of a particular resonance to a particular metabolite would require further *ex vivo* and *in vitro* studies beyond the scope of this clinical study [6, 10, 20].

Statistical significance of differences between various groups for each metabolite was tested with the Kruskal-Wallis nonparametric analysis of variance. A post-hoc pair-wise analysis was performed between MEN and the other groups using Dunnett's T3 test. Differences of  $P < 0.05$  were taken as statistically significant. We calculated 90th centiles for nonparametric variables in every resonance and tumour group. All statistical tests were performed using SPSS software. The resonances showing the largest differences between MEN and the other groups were incorporated into a three-step algorithm [4] (Fig. 1), the performance of which was tested by the leave-one-out method [4, 8, 21].

## Results

Means and standard deviations of the 37 MEN, 93 other tumours and six healthy volunteers are shown

**Table 1** Normalized area values (means  $\pm$  sd) of seven metabolite resonances of 130 brain tumours and six healthy volunteers analysed by in vivo proton MR spectroscopy ( $^1\text{H}$  MRS)

Tumour	Cases	Lipid 1.3 (Lip 1.3)	Lactate (Lac)	Alanine (Ala)	N-acetyl compounds (NAc)	Glutamate and glutamatate (Glx)	Creatine and phosphocreatine (Cr)	Choline (Cho)
Meningioma (MEN)	37	2.26 $\pm$ 11.47	4.93 $\pm$ 10.04	27.58 $\pm$ 17.22	12.43 $\pm$ 5.59	27.99 $\pm$ 20.04	17.40 $\pm$ 10.73	96.92 $\pm$ 2.58
Low-grade astrocytoma (LGA)	15	0 $\pm$ 0	19.22 $\pm$ 15.64	0.68 $\pm$ 2.63	26.42 $\pm$ 16.4	7.06 $\pm$ 9.34	42.32 $\pm$ 7.89	84.41 $\pm$ 9.06
P			<0.05	<10 $^{-9}$	<0.05	<10 $^{-4}$	<10 $^{-9}$	<0.001
Anaplastic astrocytoma (AA)	14	10.64 $\pm$ 22.09	27.91 $\pm$ 48.56	4.29 $\pm$ 7.87	18.08 $\pm$ 12.60	10.51 $\pm$ 13.95	30.60 $\pm$ 9.15	92.12 $\pm$ 5.28
P				<10 $^{-6}$		<0.05	<0.01	<0.05
Glioblastoma (GBM)	30	68.97 $\pm$ 29.42	71.60 $\pm$ 143.48	4.74 $\pm$ 11.25	20.64 $\pm$ 9.57	18.82 $\pm$ 15.18	26.72 $\pm$ 10.50	92.94 $\pm$ 5.41
P		P < 10 $^{-12}$		<10 $^{-6}$	<0.01		<0.01	<0.05
Metastases (MET)	34	73.75 $\pm$ 31.06	61.67 $\pm$ 120.61	0.73 $\pm$ 3.52	29.94 $\pm$ 18.43	15.98 $\pm$ 16.81	18.82 $\pm$ 13.32	90.30 $\pm$ 9.54
P		<10 $^{-9}$		<10 $^{-9}$	<0.001		<0.01	<0.01
Normal white matter <sup>a</sup>	6	0 $\pm$ 0	0.52 $\pm$ 1.26	0 $\pm$ 0	83.46 $\pm$ 3.33	11.02 $\pm$ 2.63	36.61 $\pm$ 1.64	40.67 $\pm$ 5.84

<sup>a</sup>no statistical comparison was attempted

P values are shown at the bottom for resonances found to be significantly different with respect to MEN

in Table 1. Ala was the most characteristic resonance of meningiomas. Increased Ala in MEN showed high levels of statistical significance in comparison with all other groups. Another characteristic finding of MEN, different from all other tumours, was high Cho. Nevertheless, low normalised Cr was of greater significance than Cho in LGA, AA and GBM comparisons, and was accordingly chosen as the discriminant resonance in these comparisons. Absence or low values of Lip 1.3 showed highly significant differences with GBM. Additional differences were found in Glx, NAc and Lac. Although metastases constitute a heterogeneous histological group, consistent differences were found between them and MEN in Lip 1.3, Ala, NAc and Cho.

We incorporated five resonances (Lip 1.3, Ala, Glx, Cr and Cho) (Table 2) in a model algorithm to produce four specific algorithms, one for every two-way differential considered: MEN vs LGA, vs AA, vs GBM and vs MET (Fig. 1). Only one of the three resonances included in the denominator of the normalisation method (Cr, Cho, NAc) was included in every algorithm, as their values correlated strongly, due to the method of normalisation. The whole data-set was used to test the system by the leave-one-out method. With this aim, all the possible procedures for every individual case were tested after recalculating the diagnostic criteria. Then, for every MEN, four two-way diagnostic procedures were tested (MEN vs LGA, vs AA, vs GBM and vs MET) to assess the performance of the method in a real clinical situation in which these differential diagnoses would be envisioned. For every non-meningioma case only the differential between this tumour group and MEN was tested (Table 2). Overall, 241 two-way classification procedures (148 for 37 meningiomas and 93 for the other tumours) produced 226 correct classifications (94%).

In five meningiomas (14%) the most likely diagnosis included one or more tumours other than MEN (Table 3). These were two large intraventricular meningiomas in young people, in which the most likely diagnosis would be a low-grade glial neoplasm [11, 22, 23, 24] (Fig. 2) and three tumours with large, nonenhancing cystic and/or necrotic areas in which an extra-axial origin could not be confidently suggested (Figs. 3, 4). Alternative diagnoses included GBM in two cases, solitary MET (in two), AA (five), LGA (three) and other tumours not included in this analysis such as oligodendrogloma and primitive neuroectodermal tumour (three). This produced 12 differential diagnostic procedures, of which ten (83%) suggested the correct diagnosis, while the diagnosis suggested in two was not MEN. Both concerned a single meningioma with a Lip 1.3 resonance (Fig. 4), found to be malignant on histology.

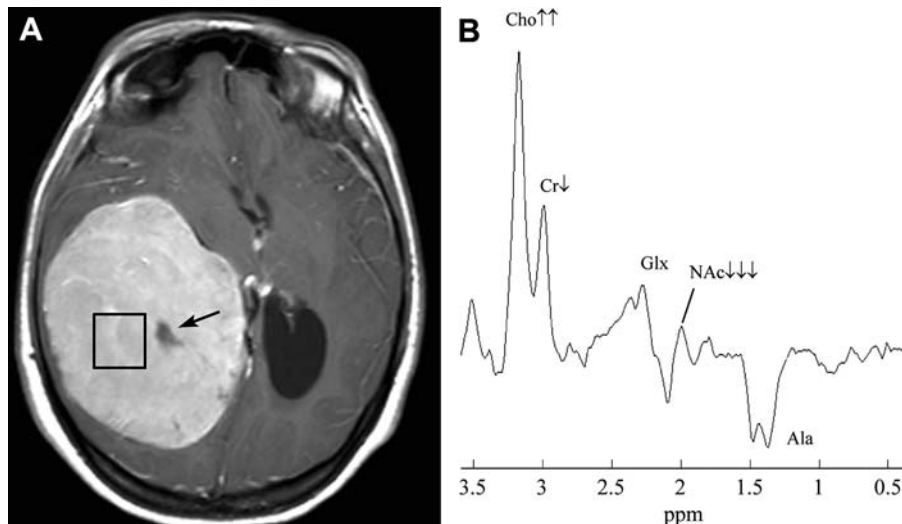
**Table 2** Results obtained applying the leave-one-out method to resonances selected for two-way tumor differentiation

Two-way classification	Discriminant resonances			Classification (%)		
	1st	2nd	3rd	Correct	Unclassifiable	Wrong
MEN vs LGA	Ala	Cr	Glx	51/52 (98)	0/52 (0)	1/52 (2)
MEN vs AA	Ala	Cr	Glx	45/51 (88)	4/51 (8)	2/51 (4)
MEN vs GBM	Lip 1.3	Ala	Cr	64/67 (96)	0/67 (0)	3/67 (4)
MEN vs MET	Lip 1.3	Ala	Cho	66/71 (93)	0/71 (0)	5/71 (7)
Overall				226/241 (94)	4/241 (2)	11/241 (4)

**Table 3** Performance of the diagnostic algorithm in five meningiomas with uncertain imaging diagnosis

Patient/age (years)	Site	Alternative diagnoses	Two-way comparisons	Spectroscopic diagnosis
1/18	Left frontal	LGA, AA, others	MEN vs LGA MEN vs AA	MEN
4/22	Right trigone	LGA, AA, others	MEN vs LGA MEN vs AA	MEN
25/20	Right trigone	LGA, AA, others	MEN vs LGA MEN vs AA	MEN
35/76	Left frontal	AA, GBM, MET	MEN vs AA MEN vs GBM MEN vs MET	MEN GBM MET
37/45	Right frontal	AA, GBM, MET	MEN vs AA MEN vs GBM MEN vs MET	MEN MEN MEN
Overall correct diagnoses				10/12 (83%)

**Fig. 2A, B** Intraventricular meningioma in a 20-year-old woman. **A** Axial contrast-enhanced T1-weighted image shows a large tumour in the right trigone. The tumour is slightly heterogeneous, with moderate contrast enhancement and a nonenhancing central area (arrow). At this age, the most common intraventricular tumours are low-grade gliomas. Meningioma and anaplastic astrocytoma were included in the differential diagnosis. The voxel for spectroscopy ( $^1\text{H}$  MRS) is shown. **B** The spectrum obtained shows a typical Ala doublet centered at 1.47 ppm, increased choline (Cho) and Glx and decreased Cr and N-acetyl-containing compounds (NAc). The tumour was classified as meningioma in all two-way comparisons



## Discussion

$^1\text{H}$  MRS is a noninvasive technique way of showing the biochemical content of living tissue, which yields additional data about the metabolism of tumours which can be useful in diagnosis [4, 9, 12, 25, 26, 27, 28, 29, 30]. In order to use MRS in clinical practice, we need a system which gives a limited range of diagnoses. It is of interest to know if  $^1\text{H}$  MRS can improve diagnostic accuracy in daily practice. Single (SV) or multivoxel (MV) strategies may be

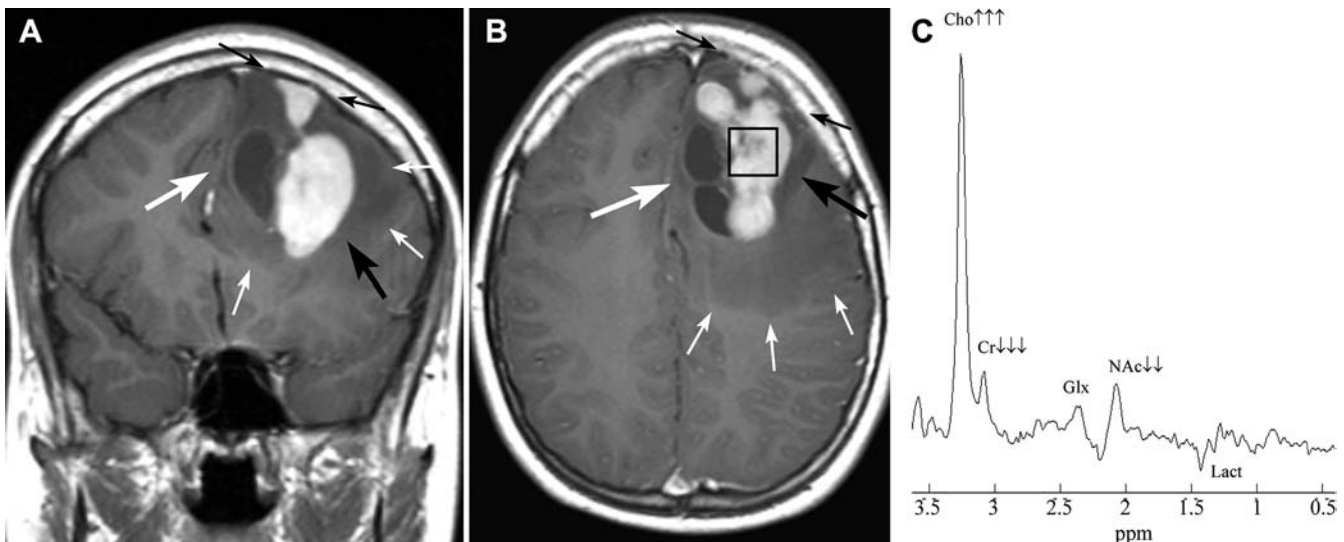
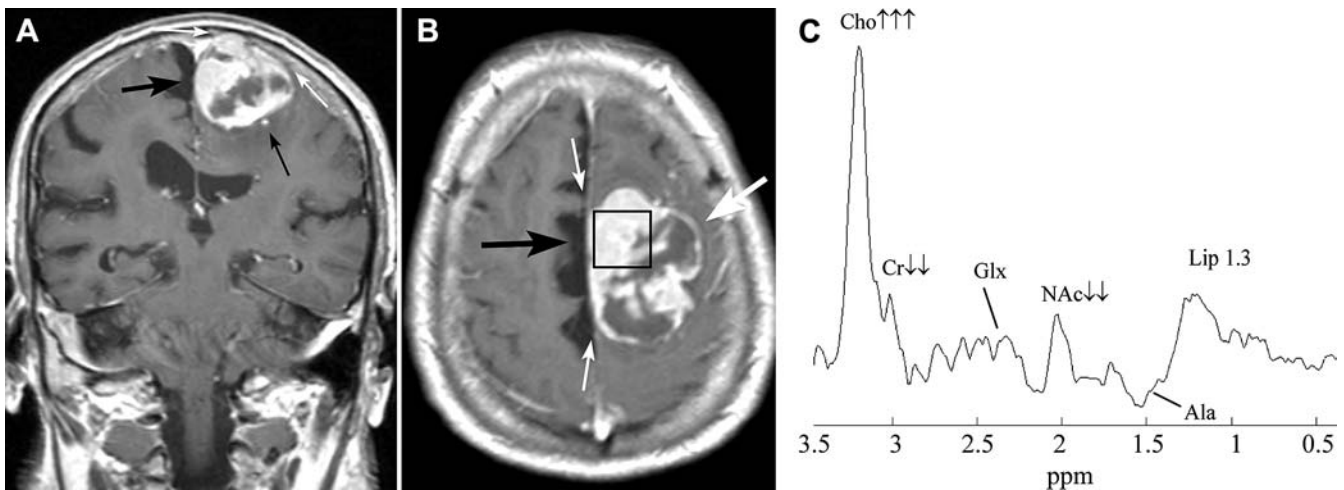


**Fig. 3A–C** Frontal meningioma in an 18-year-old man. **A** Coronal **B** axial contrast-enhanced T1-weighted images show a heterogeneous left frontal tumour with solid enhancing (large black arrows) and probably cystic nonenhancing areas (large white arrows). It contacts the meninges (small black arrows), but a meningeal origin cannot be suggested confidently. There is oedema in the white matter (small white arrows). Differential diagnosis included LGA, AA, meningioma and other tumours, including oligodendrogloma and primitive neuroectodermal tumour. The voxel for <sup>1</sup>H MRS is shown in **B**. **C** The spectrum does not show Ala. Nevertheless, the very high Cho and low Cr and NAc suggested meningioma in two-way comparisons

chosen. We chose the former because it is a less time-consuming, both for data acquisition and processing and therefore easier to accommodate in clinical practice; it allows better optimisation of magnetic field homogeneity, which facilitates accurate evaluation of certain resonance peaks; and it provides better voxel delineation, minimising contamination of the spectrum by tissue outside the volume selected. MV techniques allow assessment of tumour heterogeneity, and should be used in follow-up of

tumours after treatment, in differentiation between radi-oncrosis and tumour recurrence and in guiding stereotactic biopsy. SV techniques may play a prominent role in initial diagnosis for the reasons given above; knowledge gained from SV studies such as this may be of use for properly interpreting spectra acquired with MV studies.

**Fig. 4A–C** Left frontal meningioma in a 76-year-old man. **A** Coronal **B** and axial contrast-enhanced T1-weighted images show a heterogeneous tumour with solid areas (large black arrows), and nonenhancing cystic and/or necrotic areas (large white arrow). There is contact with the meninges (small white arrows). An extra-axial origin could not be confidently suggested, and differential diagnosis included AA, GBM and intra-axial MET. Meningioma or extra-axial metastasis were included because of the large vessel between the tumour and brain parenchyma (small black arrow). The voxel for <sup>1</sup>H MRS is shown in **B**, including most of the solid, enhancing tumour. **C** The lipid peak in the TE 136 ms spectrum suggested GBM or MET in two-way comparison with MEN. Large Cho and low Cr and NAc peaks correctly suggested MEN in the comparison with AA. The pathological on the resected tumour was malignant meningioma



Different echo times may also be chosen for  $^1\text{H}$  MRS. Although short echo times have some advantages, such as better assessment of Glx and myo-inositol, we chose a TE 136 ms because we think it provides better differentiation between Lac-Ala and lipids; low baseline distortion; and easy quantification of spectra. We normalised the values for each resonance with a previously reported method [4, 9], which evaluates not only the relation between two resonances, but the relationship of every single resonance with the three main ones in normal brain parenchyma (NAc, Cr and Cho). We believe this method can easily be introduced in daily practice and provides overall assessment of the spectrum avoiding the need for external references, measurement of additional parameters, or assuming some premisses which could yield uncertain values.

We assessed the potential impact of MRS in diagnosis of meningiomas. The majority may be confidently differentiated from other intracranial tumours on the basis of their spectroscopic pattern, especially the presence of large amounts of alanine, known from in vitro studies [31, 32]. This biochemical characteristic is shown in vivo by  $^1\text{H}$  MRS as a doublet centered at 1.47 ppm, inverted at the echo time we used due to J-coupling-induced modulation. Other characteristic trends are high Cho/Cr and Cho/NAc ratios, which may play a prominent diagnostic role when Ala is not detectable. We confirmed the prominent role of Ala in identifying meningiomas, as well as the usefulness of the relationship between Cho, Cr and NAc, and some usefulness of Glx. We found that normalised Cr was the parameter best implementing this characteristic relationship between Cho, Cr and NAc in clinical identification of meningiomas. Previous work has shown the detectability of Glx at an echo time of 136 ms [7, 13]. Nevertheless, little interest has been paid to this resonance in intracranial tumours. Characteristic markers of other tumours may also be useful for discrimination between them and meningiomas. This is true of glioblastomas and metastasis, in which Lip 1.3 is characteristic [14, 22]. When used in an algorithm, as reported previously [4], these findings produced 94% correct classification of meningiomas, 2% unclassifiable tumours, and only 4% incorrect classifications.

Meningiomas have been traditionally thought easy to diagnose by imaging alone. Many are, but in a small group the diagnosis is not unequivocal. Additional

noninvasive techniques such as diffusion, perfusion and  $^1\text{H}$  MRS may play a role in these cases. We have identified two such situations. First, intraventricular tumours in young patients suggest a differential diagnosis in which low-grade gliomas are the first option [11, 22, 23, 24]. Nevertheless, large homogeneous tumours may suggest meningioma or AA.  $^1\text{H}$  MRS may be of utility by reinforcing the suspicion of meningioma. The possibility of embolisation prior to surgery should be evaluated, to avoid massive bleeding [33]. Second, some meningiomas may resemble malignant intra-axial neoplasms, such as AA, GBM or MET, especially tumours with nonenhancing cystic or necrotic areas in which signs of their extra-axial origin are not evident, especially if they are surrounded by extensive oedema. Techniques which limit differential diagnosis could have prognostic implications and may be of interest for planning surgery. A third situation in which  $^1\text{H}$  MRS may be useful is the differentiation between solitary extra-axial metastasis and meningioma in patients with a known primary tumour, without evidence of other metastases [34]. A suggestion of meningioma may indicate surgery as the first option, while metastasis may open the field to palliative, more conservative treatment (although biopsy will generally be still required prior to treatment).

Our MRI diagnosis was uncertain in five meningiomas (14%); this rate is unexpectedly high. The reason may be we studied only meningiomas in which it was feasible to perform  $^1\text{H}$  MRS of good quality, thereby excluding some subtypes such as "en plaque" tumours, small sphenoid ridge lesions and other very characteristic meningiomas which could have increased the rate of confident diagnosis. The two incorrect results of our MRS analysis concerned a tumour in which the Lip 1.3 peak suggested GBM or MET. Lipid resonance in malignant meningiomas has been reported [35] and may be a cause for false-negative diagnosis of meningioma in the method reported, for further optimisation of our proposed diagnostic algorithm. The 94% certain diagnosis rate confirms  $^1\text{H}$  MRS as a valuable addition to the diagnosis of radiologically atypical meningiomas.

**Acknowledgements** This work was supported by la Generalitat de Catalunya (grants CIRIT XT2000-43 and SGR2001-194) and the European Union (EU IST1999-10310 INTERPRET project <http://carbon.uab.es/INTERPRET>).

## References

1. Osborn AG (1994) Diagnostic neuro-radiology. Mosby, St Louis, pp 584–601
2. Ginsberg LE (1996) Radiology of meningiomas. *J Neuro-oncol* 29: 229–238
3. Russell EJ, George AE, Kricheff II, Budzilovich G (1980) Atypical computed tomographic features of intracranial meningioma. *Radiology* 135: 673–682
4. Majós C, Alonso J, Aguilera C, et al (2002) Adult primitive neuroectodermal tumor (PNET): proton MR spectroscopy findings with possible application for differential diagnosis. *Radiology* 225: 556–566

5. van den Boogaart A (1997) Quantitative data analysis of in vivo MRS data sets. *Magn Reson Chem* 35: S146–S152
6. Barba I, Moreno A, Martínez-Pérez I, et al (2001) Magnetic resonance spectroscopy of brain hemangiopericytomas: high myoinositol concentrations and discrimination from meningiomas. *J Neurosurg* 94: 55–60
7. Ernst TH, Hennig J (1991) Coupling effects in volume selective  $^1\text{H}$  spectroscopy of major brain metabolites. *Magn Reson Med* 21: 82–96
8. Tate AR, Griffiths JR, Martínez-Pérez I, et al (1998) Towards a method for automated classification of  $^1\text{H}$  MRS spectra from brain tumours. *NMR Biomed* 11: 177–191
9. Majós C, Alonso C, Aguilera C, et al (2002) Proton magnetic resonance spectroscopy ( $^1\text{H}$  MRS) of human brain tumours: assessment of differences between tumour types and its applicability in brain tumour categorization. *Eur Radiol* 10: 1007
10. Martínez-Pérez I, Moreno A, Alonso J, et al (1997) Diagnosis of brain abscess by magnetic resonance spectroscopy. Report of two cases. *J Neurosurg* 86: 708–713
11. Majós C, Cucurella G, Aguilera C, Coll S, Pons LC (1999) Intraventricular meningiomas: MR imaging and MR spectroscopic findings in two cases. *AJNR* 20: 882–885
12. Burtscher IM, Skagerberg G, Geijer B, Englund E, Stahlberg F, Holtas S (2000) Proton MR spectroscopy and preoperative diagnostic accuracy: an evaluation of intracranial mass lesions characterized by stereotactic biopsy findings. *AJNR* 21: 84–93
13. Connelly A, Cross JH, Gadian DG, Hunter JV, Kirkham FJ, Leonard JV (1993) Magnetic resonance spectroscopy shows increased brain glutamine in ornithine carbamoyl transferase deficiency. *Pediatr Res* 33: 77–81
14. Negendank WG, Sauter R, Brown TR, et al (1996) Proton magnetic resonance spectroscopy in patients with glioma tumors: a multicenter study. *J Neurosurg* 84: 449–458
15. Wang Z, Sutton LN, Cnaan A, et al (1995) Proton MR spectroscopy of pediatric cerebellar tumors. *AJNR* 16: 1821–1833
16. Kugel H, Heindel W, Ernestus RI, Bunke J, du Mesnil R, Friedmann G (1992) Human brain tumors: spectral patterns detected with localized  $\text{H}-1$  MR spectroscopy. *Radiology* 183: 701–709
17. Poptani H, Gupta RK, Roy R, Pandey R, Jain VK, Chhabra DK (1995) Characterization of intracranial mass lesions with in vivo proton MR spectroscopy. *AJNR* 16: 1593–1603
18. Meyerand ME, Pipas JM, Mamourian A, Tosteson TD, Dunn JF (1999) Classification of biopsy-confirmed brain tumors using single-voxel MR spectroscopy. *AJNR* 20: 117–123
19. De Edelenyi FS, Rubin C, Estève F, et al (2000) A new approach for analyzing proton magnetic resonance spectroscopic images of brain tumors: nosologic images. *Nat Med* 6: 1287–1289
20. Grand S, Passaro G, Ziegler A, et al (1999) Necrotic tumor versus brain abscess: Importance of amino acids detected at  $^1\text{H}$  MR spectroscopy-Initial results. *Radiology* 213: 785–793
21. Preul MC, Caramanos Z, Collins DL, et al (1996) Accurate, noninvasive diagnosis of human brain tumors by using proton magnetic resonance spectroscopy. *Nat Med* 2: 323–325
22. Tien RD (1991) Intraventricular mass lesions of the brain: CT and MR findings. *Am J Roentgenol* 157: 1283–1290
23. Rauschning W (1994) Brain tumors and tumorlike masses: Classification and differential diagnosis. In: Osborn AG (ed) Diagnostic neuroradiology. Mosby, St Louis pp 422–436
24. Jelinek J, Smirniotopoulos JG, Prisi JE, Kanzer M (1989) Lateral ventricular neoplasms of the brain: differential diagnosis based on clinical, CT, and MR findings. *AJNR* 11: 567–574
25. Ursenius JP, Tuohimetsä S, Vainio P, Ala-Korpela M, Hiltunen Y, Kauppinen RA (1996) Automated classification of human brain tumours by neural network analysis using in vivo  $^1\text{H}$  magnetic resonance spectroscopic metabolite phenotypes. *NeuroReport* 7:1597–1600
26. Adamson AJ, Rand SD, Prost RW, Kim TA, Schultz C, Haughton VM (1998) Focal brain lesions: effect of single-voxel proton MR spectroscopic findings on treatment decisions. *Radiology* 209: 73–78
27. Castillo M, Kwock L, Mukherji SK (1996) Clinical applications of proton MR spectroscopy. *AJNR* 17: 1–15
28. Ross B, Michaelis T (1994) Clinical applications of magnetic resonance spectroscopy. *Magn Reson Q* 10: 191–247
29. Ott D, Henning J, Ernst T (1993) Human brain tumors: assessment with in vitro proton MR spectroscopy. *Radiology* 186: 745–752
30. Dowling C, Bollen AW, Noworolski SM, et al (2001) Preoperative proton MR spectroscopy imaging of brain tumors: correlation with histopathologic analysis of resection specimens. *AJNR* 22: 604–612
31. Kinoshita Y, Kajiwara H, Yokota A, Koga Y (1994) Proton magnetic resonance spectroscopy of brain tumors: an in vitro study. *Neurosurgery* 35: 606–614
32. Kinoshita Y, Yokota A (1997) Absolute concentrations of metabolites in human brain tumors using in vitro proton magnetic resonance spectroscopy. *NMR Biomed* 10: 2–12
33. Dean BL, Flom RA, Wallace RC, et al (1994) Efficacy of endovascular treatment of meningiomas: evaluation with matched samples. *AJNR* 15: 1675–1680
34. Bendszus M, Warmuth-Metz M, Burger R, Klein R, Tonn JC, Solymosi L (2001) Diagnosing dural metastases: the value of  $^1\text{H}$  magnetic resonance spectroscopy. *Neuroradiology* 43: 285–289
35. Shiino A, Nakasu S, Matsuda M, Handa J, Morikawa S, Inubushi T (1999) Noninvasive evaluation of the malignant potential of intracranial meningiomas performed using proton magnetic resonance spectroscopy. *J Neurosurg* 91: 928–934

**5. RESUMEN DE LOS TRABAJOS Y DISCUSIÓN GLOBAL**



### **5.1. Aspectos de los apartados de material y métodos de los artículos de trascendencia para valorar los resultados.**

Cabe considerar varias etapas entre la adquisición de los datos espectroscópicos (FID o free induction decay) y la clasificación de un determinado caso en un grupo tumoral en base a su patrón espectral. Parte de la discordancia entre los resultados obtenidos en diferentes trabajos puede ser explicada por los diferentes procedimientos utilizados en cada uno de estos pasos. Cabe destacar que en los tres trabajos que constituyen esta tesis se han utilizado procedimientos totalmente superponibles para cada uno de estos pasos, de manera que entre ellos únicamente ha variado la pregunta a responder y no la manera de procesar los datos espectroscópicos. Esto le confiere solidez a la valoración de la utilidad clínica de la ERM que constituye esta tesis.

Una vez obtenida la FID, la primera etapa consiste en el procesado de los datos con el objetivo de visualizar el espectro. En esta fase se aplican diferentes algoritmos para incrementar la resolución, mejorar la relación señal-ruido y se aplica la transformada de Fourier. También se aplican algoritmos para corregir la fase y la línea de base del espectro. El método ideal de preprocessado ha de incluir la menor manipulación posible por parte del operador y la utilización de los mismos algoritmos para evitar que los datos cuantitativos estén afectados de manera diferente por los procedimientos reseñados anteriormente. Para disminuir al máximo el efecto del operador en

esta tesis hemos calculado áreas de cada resonancia del espectro con un algoritmo que trabaja en el dominio del tiempo. De esta manera los procedimientos descritos anteriormente (algoritmos para incrementar resolución, para mejorar la relación señal ruido, para corregir la fase y la línea del espectro en el dominio de la frecuencia) no afectan y el procesamiento del espectro se ha realizado siguiendo los criterios citados anteriormente únicamente con fines de presentación.

Dado que los resultados obtenidos en la cuantificación de un espectro se dan en unidades relativas, es importante su normalización de cara a obtener cifras comparables entre casos diferentes. En esta tesis se ha utilizado un método innovador, que utiliza la fórmula “ $x = 100 \cdot x_i / (NACC^2 + Cr^2 + Cho^2)^{1/2}$ ” (siendo  $x_i$  el valor del área original de la resonancia a normalizar) para el procedimiento. Los métodos utilizados anteriormente han consistido en calcular relaciones entre resonancias (por ejemplo entre Cho y Cr, NACC y Cr...), entre la altura de una resonancia y la altura del global de puntos del espectro valorada en forma de la integración del mismo, y entre una resonancia y la resonancia del agua. La principal ventaja de los métodos que calculan relaciones entre resonancias radica en su simplicidad, mientras que el principal inconveniente es que ante un resultado determinado (p.e. aumento de la ratio Cho/Cr) no permite distinguir el origen del mismo (puede ser debido a aumento de Cho o descenso de Cr). Los métodos con valoraciones más globales, ya sea mediante la integración del área del espectro o la relación del metabolito con respecto al agua, obvian este inconveniente, dando una valoración más

absoluta, a costa de una mayor complejidad de la cuantificación. El método utilizado para esta tesis permite obtener una valoración global del espectro de una forma más sencilla, más fácil de aplicar en la práctica clínica, mediante la relación entre el área de una resonancia determinada y la suma de las tres resonancias predominantes del espectro.

El siguiente paso, una vez cuantificado el espectro y obtenidos valores comparables, es la clasificación en grupos. Diferentes grados de complejidad matemática se han utilizado para elaborar las herramientas para la clasificación, que se han llamado “clasificadores”. Para esta tesis se ha utilizado un método de clasificación no paramétrico basado en la distribución de los valores de las determinadas resonancias en cada grupo, y se han posicionado los valores de corte a nivel de los percentiles del 90%. También se trata de un método innovador, no utilizado previamente para clasificación de espectros, cuya principal ventaja es que no requiere asumir distribución normal de los valores. A pesar de que obtiene resultados de clasificación ligeramente inferiores a métodos descritos con anterioridad (p.e. con LDA – “linear discriminant analysis”), este método, al no requerir asumir una premisa no demostrada (distribución normal), debiera ser más robusto y producir mayor reproducibilidad de los resultados. Se ha puesto especial énfasis en que el método sea suficientemente manejable para poder ser actualizado fácilmente con casos nuevos, para poder ser optimizado por usuarios con diferente experiencia previa (sea por características técnicas de las secuencias u otros factores) y para ser optimizado para diferentes diagnósticos diferenciales.

Finalmente se deben comprobar los resultados obtenidos con el método. Para realizar este proceso de una forma fiable cabe dos opciones: a/reservar un grupo de casos no usados para elaborar los clasificadores y probar el clasificador con este grupo, que se denomina grupo de test o “test set”, y b/usar el método denominado “dejar uno fuera” o “leave-one-out” (Miller AJ). Este último método consiste en calcular los clasificadores varias veces, una para cada caso, incluyendo todos los casos excepto el que está siendo evaluado. La exactitud del método se evalúa clasificando el caso que ha sido dejado fuera. En los dos primeros trabajos de esta tesis se ha optado por el primer método, reservando un grupo de casos para ser utilizado como grupo de test. Consideramos que este método proporciona una validación más sólida de los resultados, ya que el grupo de entrenamiento del clasificador es totalmente independiente del grupo de test. En casos en que solo se dispone de un limitado número de casos, la aplicación del método de “dejar uno fuera” permite evitar el efecto negativo que tendría el incluir un caso extremo en un test set de dimensiones reducidas. En el tercer trabajo se utilizó este método (dejar uno fuera) dado que el número de casos en que se debía aplicar el clasificador era bajo ( $n=5$ ).

En resumen, existen tres rasgos comunes en los artículos de esta tesis que los caracterizan:

- La cuantificación mediante áreas integradas y normalización según la fórmula  $x= 100 \cdot x_i / (NACC^2 + Cr^2 + Cho^2)^{1/2}$ .
- La elaboración de un método de clasificación no paramétrico que utiliza los percentiles del 90% de determinadas resonancias.
- La utilización de grupos de test (test sets) para la comprobación de resultados (en los trabajos 1 y 2).

## 5.2. Discusión global de los tres artículos

En el primer artículo se abordó el tema de la clasificación de tumores cerebrales en los cinco grupos de mayor prevalencia en adultos: meningioma, astrocitoma de bajo grado, astrocitoma anaplásico, glioblastoma y metástasis. Para ello se incluyó 108 estudios de espectroscopia en 108 pacientes afectos de meningioma ( $n=29$ ), astrocitoma de bajo grado ( $n=15$ ), astrocitoma anaplásico ( $n=12$ ), glioblastoma ( $n=25$ ) y metástasis ( $n=27$ ). A parte de estos pacientes se incluyó un grupo de test de 25 casos compuesto por 8 meningiomas, 3 astrocitomas de bajo grado, 2 astrocitomas anaplásicos, 5 glioblastomas y 7 metástasis. El estudio estadístico detectó diferencias significativas entre grupos en ocho de las nueve resonancias evaluadas (Lip 0.9, Lip 1.3, Lact, Ala, NACC, Glx, Cr y Cho). La resonancia Lip 1.3 se mostró como la más característica del grupo de tumores de mayor grado (glioblastoma

y metástasis), mostrando diferencias altamente significativas con el resto de grupos tumorales ( $p<0,001$ ). Alfa resultó ser muy característica de meningioma, también con alta significación ( $p<0,001$ ). La comparación entre astrocitoma anaplásico y de bajo grado mostró diferencias significativas en Cr ( $p<0,01$ ) y Cho ( $p<0,05$ ). De acuerdo con estos resultados, se elaboró un algoritmo con estas cuatro resonancias para clasificar el total de tumores. En el primer paso el clasificador evaluaba la resonancia de Lip 1.3 para identificar glioblastoma y metástasis. En el segundo se evaluaba la resonancia de Alfa para identificar los meningiomas. Por último, el tercer y cuarto paso evaluaban Cr y Cho para separar meningioma, astrocitoma de bajo grado y astrocitoma anaplásico. Este algoritmo clasificó de forma satisfactoria 21 de los 25 casos incluidos en el test set (84%). En este artículo se evaluó también la diferenciación entre glioblastoma y metástasis. Ninguna resonancia del espectro mostró diferencias significativas entre estos dos grupos de tumores. Gly/ml fue la que mostró mayor capacidad para distinguir entre los dos grupos, con correcta clasificación de 36 de 48 tumores (4 tumores fueron excluidos de esta valoración debido a que el área del espectro en que se detecta la resonancia Gly/ml estaba artefactada) en el grupo de entrenamiento (75%), y 9 de 11 tumores (1 tumor fue excluido por no ser valorable el área en que se detecta la resonancia Gly/ml) en el grupo de test (82%).

Este primer trabajo permitió concluir que la información bioquímica sobre los tejidos que nos brinda la ERM  $^1\text{H}$  permite categorizar los grupos tumorales más frecuentes del SNC, y que usando un método relativamente sencillo de

clasificación se pueden obtener resultados satisfactorios para su aplicación en la práctica clínica. Una objeción es que, al igual que se ha constatado en estudio previos, los grupos glioblastoma y metástasis no mostraron diferencias significativas. No obstante, se consiguió una separación entre ellos razonablemente satisfactoria con la resonancia Gly/ml.

La siguiente pregunta a plantearse es que sucede con los grupos tumorales menos prevalentes. Este es el punto que desarrolló el segundo artículo. Para ello se evaluaron retrospectivamente 9 pacientes diagnosticados de tumor neuroectodérmico primitivo (TNEP), y se compararon sus características a las de 22 meningiomas, 12 astrocitomas de bajo grado, 8 astrocitomas anaplásicos, 23 glioblastomas y 21 metástasis. Las características del TNEP fueron la presencia de una prominente resonancia de Cho, superior a la de todos los otros grupos, con muy escasa resonancia de lípidos y baja NACC y Cr. Ala mostró valores significativamente menores que en el meningioma, pero algo superiores que en astrocitoma de bajo grado, anaplásico y metástasis. Se desarrollaron algoritmos para el diagnóstico diferencial entre TNEP y cada uno de los otros cinco grupos incluidos en el estudio, utilizando las 2 resonancias con mayores diferencias entre TNEP y el grupo a comparar. El sistema clasificador se validó utilizando un grupo test compuesto por 2 TNEP, 7 meningiomas, 3 astrocitomas de bajo grado, 4 astrocitomas anaplásicos, 2 glioblastomas y 6 metástasis. Los resultados obtenidos en esta evaluación fueron: 78% clasificaciones correctas, 9% procedimientos en que el sistema clasificador no fue capaz de sugerir un

diagnóstico, y 13% en que el diagnóstico sugerido fue incorrecto. Estos resultados son muy satisfactorios para el diagnóstico de un grupo tumoral tan poco frecuente como es el TNEP en adultos, y potencian la ERM como un método a ser utilizado ante la sospecha de un TNEP, para realizar el diagnóstico diferencial con otros grupos posibles. El método utilizado es de sencilla elaboración y abre la posibilidad de elaborar algoritmos similares para ser aplicados en el resto de tumores cerebrales de baja incidencia, de cara a ayudar en el diagnóstico diferencial con tumores más frecuentes en situaciones clínicas concretas.

El tercer trabajo pretende analizar la aplicación del método elaborado en el segundo trabajo en el diagnóstico diferencial entre los tumores del primer grupo. Este método mejoraría el diagnóstico en casos en que el estudio convencional permitiera excluir del diagnóstico diferencial algunos tumores. Para desarrollar el estudio se eligió un tipo de tumores, los meningiomas, que en la mayoría de casos presenta un aspecto característico (tumores extraaxiales con captación homogénea, implante dural y escaso/nulo edema en sustancia blanca), pero que en un número reducido de casos (14% en el estudio) pueden presentar un aspecto radiológico atípico, con captación heterogénea, implante dural dudoso y edema en sustancia blanca. En estos casos plantean diagnóstico diferencial con un grupo reducido de tumores. En el estudio se incluyeron 37 meningiomas, 15 astrocitomas de bajo grado, 14 astrocitomas anaplásicos, 30 glioblastomas y 34 metástasis. De los 37 meningiomas, 5 mostraron aspecto radiológico atípico (14%). Los algoritmos

producidos para el diagnóstico diferencial consideraban las tres resonancias con mayores diferencias entre meningioma y el grupo tumoral a comparar. En todos los algoritmos se incluyó Ala en el primer o segundo paso. Otras resonancias utilizadas fueron Lip 1.3, Cr, Cho y Glx. Con estas resonancias se obtuvo una clasificación correcta en 226 de 241 procedimientos testados por el método de “dejar uno fuera” (94%), inclasificable en 4 procedimientos (2%) e incorrecta en 11 procedimientos (4%). Los 5 meningiomas atípicos generaron 12 procesos de diagnóstico diferencial, siendo correcto el diagnóstico sugerido por los algoritmos en 10 casos (83%). El método descrito permite mejorar el procedimiento diagnóstico en los tumores más prevalentes del SNC cuando el diagnóstico diferencial puede ser acotado de forma fiable mediante el estudio de imagen.



## **6. CONCLUSIONES**



### **6.1. Conclusiones generales**

1. Los tumores cerebrales presentan patrones espectroscópicos determinados que pueden ser utilizados para identificar los grupos tumorales más frecuentes.
2. La información obtenida por medio de la ERM  $^1\text{H}$  puede ser aplicada en la práctica clínica para la aproximación diagnóstica de los tumores cerebrales con resultados satisfactorios.

### **6.2. Conclusiones específicas**

1. Los tumores cerebrales más frecuentes en el adulto (meningioma, astrocitoma de bajo grado, astrocitoma anaplásico, glioblastoma y metástasis) presentan diversas características propias, entre las que destacan:
  - a. Valores de Lip 1.3 superiores en glioblastomas y metástasis que en el resto de tumores.
  - b. Valores de Ala superiores en meningiomas que en el resto de tumores.

- c. Valores de Cho superiores en astrocitomas anaplásicos que en astrocitomas de bajo grado, y a su vez en meningiomas que en los otros grupos tumorales
  - d. Valores de Cr inferiores en astrocitomas anaplásicos que en astrocitomas de bajo grado, y a su vez en meningiomas que en los otros grupos tumorales
2. Mediante un algoritmo que considera la distribución de las diferentes resonancias en los diferentes grupos tumorales se consigue separar cuatro grupos tumorales (meningioma, astrocitoma de bajo grado, astrocitoma anaplásico y glioblastoma+metástasis) con buenos resultados (84% clasificaciones correctas).
3. El TNEP presenta un patrón espectroscópico característico consistente en presencia de Cho en cantidades superiores al resto de tumores estudiados, escasa cantidad de Cr y NACC, ausencia o escasa cantidad de Lip, y presencia de Ala en cantidad inferior a meningiomas pero algo superior a astrocitomas de bajo grado, anaplásico y metástasis.
4. La implementación de los hallazgos descritos en el punto anterior en un algoritmo para diagnóstico diferencial “dos a dos” entre TNEP y los tumores cerebrales más frecuentes, permite identificar los TNEP con

buenos resultados (78% clasificaciones correctas, 9% no clasificables y 13 % clasificaciones incorrectas).

5. Cuando se aplican los hallazgos diferenciales de los meningiomas en un algoritmo de diagnóstico diferencial se consigue distinguir satisfactoriamente entre meningioma y no-meningioma (94% clasificaciones correctas).
6. Los meningiomas de aspecto radiológico atípico pueden ser reconocidos satisfactoriamente con este procedimiento (83% clasificaciones correctas).



## 7. BIBLIOGRAFÍA



1. van den Boogaart A. Quantitative data analysis of in vivo MRS data sets. *Magn Reson Chem* 1997; 35: S146-S152.
2. Tzika AA, Cheng LL, Goumnerova L, et al. Biochemical characterization of pediatric brain tumors by using in vivo and ex vivo magnetic resonance spectroscopy. *J Neurosurg* 2002; 96: 1023-1031.
3. Kugel H, Heindel W, Ernestus RI, et al. Human brain tumors: spectral patterns detected with localized H-1 MR spectroscopy. *Radiology* 1992; 183: 701-709.
4. Alger JR, Frank JA, Bizzi A, et al. Metabolism of human gliomas: assessment with H-1 MR spectroscopy and F-18 fluorodeoxyglucose PET. *Radiology* 1990; 177: 633-641.
5. Ross B, Michaelis T. Clinical applications of magnetic resonance spectroscopy. *Magn Reson Q* 1994; 10: 191-247.
6. Behar KL, den Hollander JA, Stromski ME, et al. High resolution 1H NMR study of cerebral hypoxia in vivo. *Proc Natl Acad Sci USA* 1983; 80: 4945-4948.
7. Tallan HH. Studies on the distribution of N-acetyl-L-aspartic acid in brain. *J Biol Chem* 1957; 224: 41-45.

8. Howe FA, Barton SJ, Cudlip SA. Metabolic profiles of human brain tumors using quantitative in vivo <sup>1</sup>H magnetic resonance spectroscopy. *Magn Reson Med* 2003; 49: 223-232.
9. Murphy M, Loosemore A, Clifton AG, et al. The contribution of proton magnetic resonance spectroscopy (<sup>1</sup>HMR) to clinical brain tumour diagnosis. *Br J Neurosurg* 2002; 16: 329-334.
10. Ishimaru H, Morikawa M, Iwanaga S, Kaminogo M, Ochi M, Hayashi K. Differentiation between high-grade glioma and metastatic brain tumor using single-voxel proton MR spectroscopy. *Eur Radiol* 2001; 11: 1784-1791.
11. Kinoshita Y, Kajiwara H, Yokota A, Koga Y. Proton magnetic resonance spectroscopy of brain tumors: an in vitro study. *Neurosurgery* 1994; 35: 606-614.
12. Herminghaus S, Pilatus U, Moller-Hartmann W, et al. Increased choline levels coincide with enhanced proliferative activity of human neuroepithelial brain tumors. *NMR Biomed* 2002; 15: 385-392.

13. Shimizu H, Kumabe T, Shirane R, Yoshimoto. Correlation between choline level measured by proton MR spectroscopy and ki-67 labelling index in gliomas. AJNR Am J Neuroradiol 2000; 21: 659-665.
14. Yu X, Liu Z, Tian Z, et al. Stereotactic biopsy for intracranial space-occupying lesions: clinical analysis of 550 cases. Stereotact Funct Neurosurg 2000; 75: 103-108.
15. Alesch F, Pappaterra J, Tratting S, Koos WT. The role of stereotactic biopsy in radiosurgery. Acta Neurochirur Suppl (Wien) 1995; 63: 20-24.
16. Bernstein M, Parrent AG. Complications of CT-guided stereotactic biopsy of intra-axial brain lesions. J Neurosurg 1994; 81: 165-168.
17. Ott D, Henning J, Ernst T. Human brain tumors: assessment with in vitro proton MR spectroscopy. Radiology 1993; 186: 745-752.
18. Paulus W, Pfeiffer J. Intratumoral histologic heterogeneity of gliomas. A quantitative study. Cancer 1989; 64: 442-447.
19. De Edelenyi FS, Rubin C, Estève F, et al. A new approach for analyzing proton magnetic resonance spectroscopic images of brain tumors: nosologic images. Nat Med 2000; 6: 1287-1289.

20. Preul MC, Caramanos Z, Leblanc R, Villemure JG, Arnold DL. Using pattern recognition of in vivo proton MRSI data to improve the diagnosis and surgical management of patients with brain tumors. *NMR Biomed* 1998; 11: 192-200.
21. Dowling C, Bollen AW, Noworolski SM, et al. Preoperative proton MR spectroscopy imaging of brain tumors: correlation with histopathologic analysis of resection specimens. *AJNR Am J Neuroradiol* 2001; 22: 604-612.
22. Mittler MA, Walters BC, Stopa EG. Observer reliability in histological grading of astrocytoma stereotactic biopsies. *J Neurosurg* 1996; 85: 1091-1094.
23. Poptani H, Kaartinen J, Gupta RK, Niemitz M, Hiltunen Y, Kauppinen. Diagnostic assessment of non-neoplastic brain disorders in vivo using proton nuclear magnetic resonance spectroscopy and artificial neural networks. *J Cancer Res Clin Oncol* 1999; 125: 343-349.
24. Ursenius JP, Tuohimetsä S, Vainio P, Ala-Korpela M, Hiltunen Y, Kauppinen RA. Automated classification of human brain tumours by neural network analysis using in vivo  $^1\text{H}$  magnetic resonance spectroscopic metabolite phenotypes. *NeuroReport* 1996; 7: 1597-1600.

25. de Stefano N, Caramanos Z, Preul MC, Francis G, Antel JP, Arnold DL. In vivo differentiation of astrocytic brain tumours and isolated demyelinating lesions of the type seen in multiple sclerosis using  $^1\text{H}$  magnetic resonance spectroscopic imaging. *Ann Neurol* 1998; 44: 273-278.
26. Tate AR, Majós C, Moreno A, Howe FA, Griffiths JR, Arús C. Automated classification of short echo time in vivo  $^1\text{H}$  brain tumor spectra: a multicentre study. *Magn Reson Med* 2003; 49: 29-36.
27. Bruhn H, Frahm J, Gyngell ML, et al. Noninvasive differentiation of tumors with use of localized  $\text{H}-1$  MR spectroscopy in vivo: Initial experience in patients with cerebral tumors. *Radiology* 1989; 17: 541-548.
28. Gill SS, Thomas DG, Van Bruggen N, et al. Proton MR spectroscopy of intracranial tumors: In vivo and in vitro studies. *JCAT* 1990; 14: 497-504.
29. Luyten PR, Marien AJH, Heindel W, et al. Metabolic imaging of patients with intracranial tumors:  $\text{H}-1$  MR spectroscopic imaging and PET. *Radiology* 1990; 176: 791-799.
30. Wilken B, Dechent P, Herms J, et al. Quantitative proton magnetic resonance spectroscopy of focal brain lesions. *Pediatr Neurol* 2000; 23: 22-31.

31. Roda JM, Pascual JM , Carceller F, et al. Nonhistological diagnosis of human cerebral tumors by  $^1\text{H}$  magnetic resonance spectroscopy and amino acid analysis. *Clin Cancer Res* 2000; 6: 3983-3993.
32. Kaminogo M, Ishimaru H, Morikawa M, et al. Diagnostic potential of short echo time MR spectroscopy of gliomas with single-voxel and point-resolved spatially localised proton spectroscopy of brain. *Neuroradiology* 2001; 43: 353-363.
33. Negendank WG, Sauter R, Brown TR, et al. Proton magnetic resonance spectroscopy in patients with glial tumors: a multicenter study. *J Neurosurg* 1996; 84: 449-458.
34. Majós C, Cucurella G, Aguilera C, Coll S, Pons LC. Intraventricular meningiomas: MR imaging and MR spectroscopic findings in two cases. *AJNR Am J Neuroradiol* 1999; 20: 882-885.
35. Rand SD, Prost D, Haughton V, et al. Accuracy of single-voxel proton MR spectroscopy in distinguishing neoplastic from nonneoplastic brain lesions. *AJNR Am J Neuroradiol* 1997; 18: 1695-1704.
36. Chang L, Mc Bride D, Miller BL, et al. Localized in vivo  $^1\text{H}$  magnetic resonance spectroscopy and in vitro analyses of heterogeneous brain tumors. *J Neuroimaging* 1995; 5: 157-163.

37. McBride DQ, Miller BL, Nikas DL, et al. Analysis of brain tumors using  $^1\text{H}$  magnetic resonance spectroscopy. *Surg Neurol* 1995; 44: 137-144.
38. Ursenius JP, Kauppinen RA, Vainio PA, et al. Quantitative metabolite patterns of human brain tumors: detection by  $^1\text{H}$  NMR spectroscopy in vivo and in vitro. *JCAT* 1994; 18: 705-713.
39. Krouwer HGJ, Kin TA, Rand SD, et al. Single-voxel proton MR spectroscopy of nonneoplastic brain lesions suggestive of a neoplasm. *AJNR Am J Neuroradiol* 1998; 19: 1695-1703.
40. Cecil KM, Jones BV. Magnetic resonance spectroscopy of the pediatric brain. *Top Magn Reson Imag* 2001; 12: 435-452.
41. Davie CA, Hawkins CP, Barker GJ, et al. Serial proton magnetic resonance spectroscopy in acute multiple sclerosis lesions. *Brain* 1994; 117: 49-58.
42. Law M, Meltzer DE, Cha S. Spectroscopic magnetic resonance imaging of a tumefactive demyelinating lesion. *Neuroradiology* 2002; 44: 986-989.

43. Saindane AM, Cha S, Law M, Xue X, Knopp EA, Zagzag D. Proton MR spectroscopy of tumefactive demyelinating lesions. *AJNR Am J Neuroradiol* 2002; 23: 1378-1386.
44. Castillo M, Kwock L, Mukherji SK. Clinical applications of proton MR spectroscopy. *AJNR Am J Neuroradiol* 1996; 17: 1-15.
45. Castillo M, Kwock L. Proton MR spectroscopy of common brain tumors. *Neuroimaging Clin North Am* 1998; 8: 733-752.
46. Kinoshita Y, Yokota A. Absolute concentrations of metabolites in human brain tumors using in vitro proton magnetic resonance spectroscopy. *NMR Biomed* 1997; 10: 2-12.
47. Meyerand ME, Pipas JM, Mamourian A, Tosteson TD, Dunn JF. Classification of biopsy-confirmed brain tumors using single-voxel MR spectroscopy. *AJNR Am J Neuroradiol* 1999; 20: 117-123.
48. Fountas KN, Kapsalaki EZ, Gotsis SD, et al. In vivo proton magnetic resonance spectroscopy of brain tumors. *Stereotact Funct Neurosurg* 2000; 74: 83-94.
49. Tedeschi G, Lundbom N, Raman R, et al. Increased choline signal coinciding with malignant degeneration of cerebral gliomas: a serial proton

- magnetic resonance spectroscopy imaging study. *J Neurosurg* 1997; 87: 516-24.
50. Bulakbasi N, Kocaoglu M, Ors F, Tayfun C, Ucoz T. Combination of single-voxel proton MR spectroscopy and apparent diffusion coefficient calculation in the evaluation of common brain tumors. *AJNR Am J Neuroradiol* 2003; 24: 225-233.
51. Tien RD, Lai PH, Smith JS, et al. Single-voxel proton brain spectroscopy exam (PROBE/SV) in patients with primary brain tumors. *AJR Am J Roentgenol* 1996; 167: 201-209.
52. Arnold DL, Shoubridge EA, Villemure JG, Freindel W. Proton and phosphorus magnetic resonance spectroscopy of human astrocytomas in vivo: preliminary observations on tumor grading. *NMR Biomed* 1990; 3: 184-189.
53. Demarael P, Johannik K, Van Hecke P, et al. Localized H-1 NMR spectroscopy in fifty cases of newly diagnosed intracranial tumors. *JCAT* 1991; 15: 67-76.
54. van del Knaap MS, van der Grond J, van Rijen PC, et al. Age-dependent changes in localized proton and phosphorous MR spectroscopy of the brain. *Radiology* 1990; 176: 509-515.

55. Roser W, Hagberg G, Mader I, et al. Assignment of glial brain tumors in humans by in vivo  $^1\text{H}$ -magnetic resonance spectroscopy and multidimensional metabolic classification. MAGMA 1997; 5: 179-183.
56. Castillo M, Smith JK, Kwock L. Correlation of myo-inositol levels and grading of cerebral astrocytomas. Am J Neuroradiol 2000; 21: 1645-1649.
57. Maxwell RJ, Martínez-Pérez I, Cerdán S, et al. Pattern recognition analysis of  $^1\text{H}$  NMR spectra from perchloric acid extracts of human brain tumour biopsies. Magn Reson Med 1998; 39: 869-877.
58. Carpinelli G, Carapella CM, Palombi L, Raus L, Caroli F, Podo F. Differentiation of glioblastoma multiforme from astrocytomas by in vitro  $^1\text{H}$  MRS analysis of human brain tumors. Anticancer Res 1996; 16: 1559-1564.
59. Hanstock CC; Rothman DL, Howseman A, et al. In vivo determination of NAA concentration in the human brain using the proton aspartyl resonance (abstr). In: Book of abstracts: Society of Magnetic Resonance in Medicine 1989. Berkley, Calif: Society of Magnetic Resonance in Medicine, 1989; 442.

60. Lowry OH, Berger SJ, Chi M, et al. Diversity of metabolic patterns in human brain tumors. I. High energy phosphate compounds and basic composition. *J Neurochem* 1977; 29: 959-977.
61. Manton DJ, Lowry M, Blackband SJ, Horsman A. Determination of proton metabolite concentrations and relaxation parameters in normal human brain and intracranial tumors. *NMR in Biomed* 1995; 8: 104-112.
62. Opstad KS, Provencher SW, Bell BA, Griffiths JR, Howe FA. Detection of elevated glutathione in meningiomas by quantitative in vivo  $^1\text{H}$  MRS. *Magn Reson Med* 2003; 49: 632-637.
63. Kuesel AC, Sutherland GR, Halliday W, Smith ICP.  $^1\text{H}$  MRS of high grade astrocytomas: mobile lipid accumulation in necrotic tissue. *NMR Biomed* 1994; 7: 149-155.
64. Kimura T, Sako K, Gotoh T, Tanaka K. In vivo single-voxel proton MR spectroscopy in brain lesions with ring-like enhancement. *NMR in Biomed* 2001; 14: 339-349.
65. Sijens PE, Levendag PC, Vecht CJ, van Dijk P, Oudkerk M.  $^1\text{H}$  MR spectroscopy detection of lipids and lactate in metastatic brain tumors. *NMR in Biomed* 1996; 9: 65-71.

66. Sijens PE, Knopp MV, Brunetti A, et al.  $^1\text{H}$  MR spectroscopy in patients with metastatic brain tumors: a multicenter study. *Magn Reson Med* 1995; 33: 818-826.
67. Cho YD, Choi GH, Lee SP, Kim JK.  $^1\text{H}$ -MRS metabolic patterns for distinguishing between meningiomas and other brain tumors. *Magnetic Resonance Imaging* 2003; 21: 663-672.
68. Wang Z, Sutton LN, Cnaan A, et al. Proton magnetic resonance spectroscopy of pediatric cerebellar tumors. *AJNR Am J Neuroradiol* 1995; 16: 1821-1833.
69. Arle JE, Morriss C, Wang ZJ, Zimmerman RA, Phillips PG, Sutton LN. Prediction of posterior fossa tumor type in children by means of magnetic resonance image properties, spectroscopy, and neural networks. *J Neurosurg* 1997; 86: 755-761.
70. Tate AR, Griffiths JR, Martínez-Pérez I, et al. Towards a method for automated classification of  $^1\text{H}$  MRS spectra from brain tumours. *NMR Biomed* 1998; 11: 177-191.
71. Martínez-Pérez I, Moreno A, Alonso J, et al. Diagnosis of brain abscess by magnetic resonance spectroscopy. Report of two cases. *J Neurosurg* 1997; 86: 708-713.

72. Barba I, Moreno A, Martínez-Pérez I, et al. Magnetic resonance spectroscopy of brain hemangiopericytomas: high myoinositol concentrations and discrimination from meningiomas. *J Neurosurg* 2001; 94: 55-60.
73. Ernst T, Hennig J. Coupling effects in volume selective  $^1\text{H}$  spectroscopy of major brain metabolites. *Magn Reson Med* 1991; 21: 82-96.
74. Burtscher IM, Skagerberg G, Geijer B, Englund E, Ståhlberg F, Holtås S. Proton MR spectroscopy and preoperative diagnostic accuracy: an evaluation of intracranial mass lesions characterized by stereotactic biopsy findings. *AJNR Am J Neuroradiol* 2000; 21: 84-93.
75. Adamson AJ, Rand SD, Prost RW, Kim TA, Schultz C, Haughton VM. Focal brain lesions: Effect of single-voxel proton MR spectroscopic findings on treatment decisions. *Radiology* 1998; 209: 73-78.
76. Shimizu H, Kumabe T, Tominaga T, et al. Noninvasive evaluation of malignancy of brain tumors with proton MR spectroscopy. *AJNR Am J Neuroradiol* 1996; 17: 737-747.

77. Grand S, Passaro G, Ziegler A, et al. Necrotic tumor versus brain abscess: Importance of amino acids detected at 1H MR spectroscopy-Initial results. Radiology 1999; 213: 785-793.
78. Lehnhardt FG, Röhn G, Ernestus RI, Grüne M, Hoehn M. 1H- and 31P-MR spectroscopy of primary and recurrent human brain tumors in vitro: malignancy-characteristic profiles of water soluble and lipophilic spectral components. NMR Biomed 2001; 14: 307-317.
79. Castillo M, Kwock L, Scatliff J, Mukherji SK. Proton MR spectroscopy in neoplastic and non-neoplastic disorders. MRI Clin of North Am 1998; 6: 1-20.
80. Gotsis ED, Fountas K, Kapsalaki E, Toulas P, Peristeris G, Papadakis N. In vivo proton MR spectroscopy: The diagnostic possibilities of lipid resonances in brain tumors. Anticancer Res 1996; 16: 1565-1568.
81. Miller AJ, ed. Subset selection in regression. London. Chapman & Hall, 1990.
82. Zimmerman RA, Bilaniuk LT. Brain Tumors. In: Zimmerman RA, Gibby WA, Carmody RF, eds. Neuroimaging: clinical and phisical principles. New York, NY: Springer-Verlag, 1997; 1004-1009.

83. Osborn AG. Meningiomas and other non-glial neoplasms. In: Osborn AG, ed. Diagnostic neuroradiology. St Louis, Mo: Mosby, 1994; 613-620.
84. Meyers SP, Kemp SS, Tarr RW. MR Imaging features of medulloblastomas. AJR Am J Roentgenol 1992; 158: 859-865.
85. Bourgouin PM, Tampieri D, Grahovac SZ, Léger C, Del Carpio R, Melançon D. CT and MR imaging findings in adults with cerebellar medulloblastoma: Comparison with findings in children. AJR Am J Roentgenol 1992; 159: 609-612.
86. Koci TM, Chiang F, Mehringer CM, et al. Adult cerebellar medulloblastoma: imaging features with emphasis on MR findings. AJNR Am J Neuroradiol 1993; 14: 929-939.
87. Nelson M, Diebler C, Forbes WStC. Paediatric medulloblastoma: atypical CT features at presentation in the SIOP II trial. Neuroradiology 1991; 33: 140-142.
88. Tortori-Donati P, Fondelli MP, Rossi A, et al. Medulloblastoma in children: CT and MRI findings. Neuroradiology 1996; 38: 352-359.
89. Maleci A, Cervoni L, Delfini R. Medulloblastoma in children and in adults: a comparative study. Acta Neurochir (Wien) 1992; 119: 62-67.

90. Davis PC, Wichman RD, Takei Y, Hoffman JC Jr. Primary cerebral neuroblastoma: CT and MR findings in 12 cases. *AJNR Am J Neuroradiol* 1990; 11: 115-120.
91. Preul MC, Caramanos Z, Collins DL, et al. Accurate, noninvasive diagnosis of human brain tumors by using proton magnetic resonance spectroscopy. *Nat Med* 1996; 2: 323-325.
92. Carapella CM, Carpinelli G, Knijn A, Raus L, Caroli F, Podo F. Potential role of in vitro  $^1\text{H}$  magnetic resonance spectroscopy in the definition of malignancy grading of human neuroepithelial brain tumours. *Acta Neurochirur [Suppl] (Wien)* 1997; 68: 127-132.
93. Sutton LN, Wehrli SL, Gennarelli L, et al. High-resolution  $^1\text{H}$ -magnetic resonance spectroscopy of pediatric posterior fossa tumors in vitro. *J Neurosurg* 1994; 81: 443-448.
94. Connelly A, Cross JH, Gadian DG, Hunter JV, Kirkham FJ, Leonard JV. Magnetic resonance spectroscopy shows increased brain glutamine in ornithine carbamoyl transferase deficiency. *Pediatr Res* 1993; 33: 77-81.
95. Hochberg Y, Tamhane AC, ed. Multiple comparison procedures. New York. John Wiley & sons Inc, 1987.

96. Becker LE. Pathology of pediatric brain tumors. Neuroimaging Clin North Am 1999; 9: 671-690.
97. Brandes AA, Palmisano V, Monfardini S. Medulloblastoma in adults: clinical characteristics and treatment. Cancer Treatment Reviews 1999; 25: 3-12.
98. Rubinstein LJ. Embryonal central neuroepithelial tumors and their differentiating potential. A cytogenic view of a complex neuro-oncological problem. J Neurosurg 1985; 62: 795-805.
99. Rémy C, Arús C, Ziegler A, et al. In vivo, ex vivo, and in vitro one- and two-dimensional nuclear magnetic resonance spectroscopy of an intracerebral glioma in rat brain: assignment of resonances. J Neurochem 1994; 62: 166-179.
100. Kleihues P, Burger PC, Scheithauer BW. The new WHO classification of brain tumours. Brain Pathol 1993; 3: 255-268.
101. Bell JD, Brown JCC, Nicholson JK, Sadler PJ. Assignment of resonances for “acute-phase” glycoproteins in high resolution proton NMR spectra of human blood plasma. FEBS Letters 1987; 215: 311-315.

102. Lenkinski RE. MR spectroscopy: Clinical tool or research probe? (Revisited). *Acad Radiol* 2001; 8: 567-570.
103. Ginsberg LE. Radiology of meningiomas. *J Neurooncol* 1996; 29: 229-238.
104. Russell EJ, George AE, Kritcheff MD, Budzilovich G. Atypical computed tomographic features of intracranial meningioma. *Radiology* 1980; 135: 673-682.
105. Jelinek J, Smirniotopoulos JG, Prisi JE, Kanzer M. Lateral ventricular neoplasms of the brain: differential diagnosis based on clinical, CT, and MR findings. *AJNR Am J Neuroradiol* 1989; 11: 567-574.
106. Dean BL, Flom RA, Wallace RC, et al. Efficacy of endovascular treatment of meningiomas: evaluation with matched samples. *AJNR Am J Neuroradiol* 1994; 15: 1675-1680.
107. Bendszus M, Warmuth-Metz M, Burger R, Klein R, Tonn JC, Solymosi L. Diagnosing dural metastases: the value of  $^1\text{H}$  magnetic resonance spectroscopy. *Neuroradiology* 2001; 43: 285-289.
108. Shiino A, Nakasu S, Matsuda M, Handa J, Morikawa S, Inubushi T. Noninvasive evaluation of the malignant potential of intracranial

meningiomas performed using proton magnetic resonance spectroscopy. J Neurosurg 1999; 91: 928-934.